Mycobacterium tuberculosis ESX-5 Paralogs Modulate Macrophage Responses and Bacterial Metal Homeostasis

Austin Michael Haynes

A dissertation

submitted in partial fulfillment of the

requirements for the degree of

Doctor of Philosophy

University of Washington

2025

Reading Committee:

Thomas R. Hawn, Chair

David R. Sherman

Kevin B. Urdahl

Program Authorized to Offer Degree:

Department of Global Health

University of Washington

Abstract

Mycobacterium tuberculosis ESX-5 Paralogs Modulate Macrophage Responses and Bacterial Metal Homeostasis

Austin Michael Haynes

Chair of the Supervisory Committee:

Thomas R. Hawn

Department of Medicine, Division of Allergy and Infectious Diseases

and

Department of Global Health

Extended co-evolutionary history of humans and *Mycobacterium tuberculosis* (Mtb), the causative agent of TB disease, has led to an evolutionary arms race between host and pathogen. The processes by which the immune system recognizes and destroys invading pathogens has been extensively co-opted and subverted by Mtb via the evolution of specially adapted virulence effectors. Through a tightly orchestrated bacterial response, Mtb moves these effectors out of the bacterium and into the host cell interface. Traditional bacterial transport systems such as the generalized secretion (SEC) and twin arginine transport (TAT) systems move many effectors, however in Mtb,

Type-7 or “ESX” systems play an essential role in virulence processes. Of the five ESX systems in Mtb, some have experimentally defined roles in virulence. ESX-1 is essential for phagosome antagonism while ESX-3 sequesters iron from the host, an essential micronutrient. ESX-5 in contrast is poorly resolved despite secreting a large number of effectors (5-10% of Mtb coding capacity). Based on prior clinical, genetic, and lab-based studies, we hypothesize ESX-5 may play roles in virulence and nutrient acquisition. To date, limited functional work has been performed to fully elucidate functional roles for many ESX-5 secreted putative virulence factors.

In complement, the human immune system is persistently evolving in the face of extensive pathogen pressure. The historic and current burden of Mtb infection across modern hominids has pushed human populations to evolve strategies countering pathogens such as Mtb. While humans evolve substantially slower than their mycobacterial counterparts, there is evidence to suggest human populations are actively evolving mechanisms to counter Mtb infection resulting in resistance. Clinically, populations who resist TB infection via persistently negative testing (RSTRs) are being extensively studied to understand the complex genetic interplay resulting in presumed enhanced control of Mtb during early exposure. However, given the complexity of human genetics, the interplay of multiple genes and cell types, and the heterogeneity of Mtb infection itself, we still don’t mechanistically understand how RSTRs are able to remain Mtb negative compared to their susceptible counterparts (LTBI). As such we aimed to understand how the genetics of Mtb resistant populations (RSTRs) differ from susceptible individuals (LTBI), affording possible functional insight into resistance

processes. Ultimately, we aim to gain functional insight into both human and bacterial genetics to more clearly resolve early Mtb-Host interactions during early infection.

Initially, we performed a brief transcriptomic screen of RSTR and LTBI alveolar macrophages to explore the role of human genetics in altering transcriptional responses to early Mtb infection. We demonstrated that alveolar macrophages from these populations display similar but distinct responses. These transcriptional responses in RSTRs are marked by an increased inflammatory response to interferons relative to LTBI counterparts, which could possibly lead to enhanced control of Mtb. Subsequently we investigated the function of specific Mtb gene clusters during early primary macrophage infection. We independently deleted ESX-5a, ESX-5b, and ESX-5c, each containing a PE/PPE heterodimer and Esx heterodimer from the H37Rv strain of Mtb. We then examined the functional consequences of these deletions in macrophages, mice, and axenic bacterial culture. We initially observed that deletion of these gene clusters significantly alters cytokine levels of TNF, IL-6, and IL-1β in primary macrophages. Further analysis revealed this may be due to differential post-transcriptional or translational regulation of target cytokines, resulting in divergent cytokine profiles within infected macrophages. We next examined if this impact observed in human macrophages would impact the fitness of these strains in vivo where we observed early time point growth defects of our mutant strains tested in C57BL/6 mice. Subsequent transcriptome analysis revealed these gene clusters likely play a role in heavy metal response or homeostasis. Indeed, we demonstrated these gene clusters

are metal responsive and that their level of expression is correlated to cytokine response levels in primary human macrophages.

Together, these observations indicate that both human and bacterial genetics play a role in the outcome of early disease. Not only are these ESX-5 gene clusters involved in stimulating a cellular response in vitro and in vivo, but that these paralogs likely also play a dual role in heavy metal response. These suggest novel function for these previously undefined paralogs and highlight the importance of studying both bacteria and host concurrently to gain novel insight into host-pathogen interactions.

Table of Contents

Figure List

Acknowledgments

There are too many people to thank for the roles they've played in getting me to this point. It could quite possibly rival the length of this dissertation if I gave everyone the praise they deserved. So, we'll have to settle for these brief tributes to the people I couldn't have done this without.

To my parents – April and Michael. Thank you for your support over the years, instilling in me that education is a pathway forward and up. Thank you for sacrificing your time, money, and sleep throughout my childhood to ensure I had all the opportunity I could muster out of this world. There are many kids (here and abroad) who aren't afforded the same chances I had, simply because some aren't willing or able to make the sacrifices you made for me. While you may have not always understood this path in terms of where I was heading, you trusted me to get there, and you supported me while I did it.

To my sister – Sydney. Thank you for being my best friend and providing me the love and support you have throughout our childhood and adult life. We share a comradery and respect with one another that feels like home. I know you'll always be there for me, and I for you. That kind of unwavering support and closeness was essential for getting me here, through the dark. Also, I want you to appreciate my diligent use of the oxford comma throughout this body of work.

To my chosen family – Josh, Michael, Will, Olivia, Irene, Shannon, Shane, and JJ. You all represent more than friendship, you represent family. Few people are as fortunate as me to call one person, let alone a lengthy list of people "chosen family". You have all in some way shaped me to who I am today. You stood by me during my awkward and challenging moments of growth (still happening); you championed me during my periods of success and forward momentum (hopefully more to come). Maybe most importantly of all, you have always been there, accepting the true me regardless of how I'm able to show up, on a good day or a bad day. That kind of support truly cannot be understated. Without all of you I would not be the person I am today, let alone receiving this PhD. So, thank you for all of it.

To my colleagues who became my friends – Christine, Nathan, Josh, Nicole, and Mark. What a rare and wonderful shift that is. Moving from coworkers to true friendship isn't always easy, but I'm so glad we made that leap. I feel incredibly fortunate for the unique kinship and connection we've built, each of you bringing something distinct and meaningful into my life. Thank you not just for the camaraderie in the professional sense, but also laughter and growing friendship over the years. Thanks for allowing me to be part of your lives while also playing an important role in mine.

To my mentors, past and present – Lorenzo, Dave, Sheila, and Tom. I quite literally would not be here today, finishing a dissertation, without all of you taking a chance on me. I like to think I was a low-risk bet, but the truth is every undergrad who marches into a lab and asks to work there represents an incredible investment of time, energy, money, and mentorship. While its "part of the job" being in academia, not every faculty

member does it, and not every faculty member does it with as much vigor and care as you all. So, thank you for choosing to take the chance on me and for always being in my corner.

Chapter 1. Introduction

1.1 Mycobacterial distribution and Pathogen Evolution

Mycobacteria are a broad group of organisms belonging to the genus “Mycobacterium”. These organisms are characterized generally as non-motile, rod-shaped bacteria, with a complex lipid rich membrane ultrastructure containing many specialized lipids heterogeneously expressed across species, such as mycolic acids, lipoarabinomannan (LAM), phthiocerol dimycocerosate (PDIM), etc. (1). Due to the chemical nature of this cell wall, containing an extreme density of specialized lipids, these bacteria can be classified as neither gram positive or gram negative and as such are classified as acid fast (2,3). Mycobacteria can be found in almost every niche on Earth (4,5). It is believed that Mycobacteria as a genus arose approximately 150 million years ago (6,7) and initially filled environmental niches before developing pathogenic capabilities (4,5,7). This paradigm arises from recent research suggesting *Mycobacterium tuberculosis* (Mtb) and other obligate or opportunistic pathogenic mycobacteria (including other members of the *Mycobacterium tuberculosis* complex, the “MTBC”) arose more recently, somewhere between 70,000-10,000 years ago (8–10). The geographic distribution of human populations and the relative isolation of Mtb strains during human migration out of Africa also gave rise to distinct lineages of Mtb currently denoted L1 through L7, associated with distinct regions (8,11). New work examining Mtb genomes proposes the expansion of the historical lineage framework to include L8 and L9, emphasizing the nuance and challenge associated with classifying disease-causing mycobacteria (12).

Alternative competing hypotheses suggest a more recent evolutionary and expansion history of Mtb, placing the evolution of *Mycobacterium tuberculosis* sensu stricto in line with the neolithic era of human expansion, approximately 10,000 years ago to present (13). While the neolithic expansion of humans undoubtedly aided in the enhanced spread and dispersal of Mtb amongst human populations, strong genetic evidence argues against a neolithic origin of Mtb (8). Regardless, the current genetic and virulence characteristics defining Mtb lineages highlights the true breadth of heterogeneity found among human-Mtb interactions (14–16).

1.2 Human-Mtb Co-Evolution and the Current Human Burden of Disease

The co-evolution of Mtb and humans has resulted in a wide dispersal of the bacterium, with approximately 2 billion, or one quarter of the human population showing immunological evidence of infection at some point in their life (17–19). Most infections with Mtb (~90%) will result in presumed bacterial clearance, latent infection, or other sub-clinical forms of TB disease (20). At the time of infection, an individual possesses a 10% risk for progression to active disease over there, totaling 10-15 million cases of active TB disease annually (21). This results in about 1.5 million deaths per year, the largest cause of mortality from a single infectious agent (22,23). As mentioned above, there has been a long co-evolutionary period between Mtb and humans. This extended interaction period has not only provided pressure on Mtb to become a more efficient human pathogen, it has also provided significant pressure on human populations to counter, giving rise to populations of humans which appear to resist Mtb infection (also

called “resisters” (RSTR)) (24–28). Resisters are clinically characterize via a resistance to Interferon Gamma Release Assay (IGRA) and Tuberculin Skin Test (TST) conversion despite known Mtb exposure (28–30). Presumably, these populations rapidly clear Mtb upon deposition in the lung, preventing the development of systemic responses that we can measure using IGRA and TST. This complex infection dynamic has been difficult to characterize; the axis between bacterial virulence and human genetics in these populations is intricately linked resulting in subtle phenotypes and heterogeneous infection outcomes (31–35). Concurrently, the current gold standard tests make it challenging to differentiate incipient disease from uninfected (and possibly resistant) individuals (36). Additionally, previous exposure to Mtb, environmental mycobacteria, BCG vaccination, heterogeneous spread, and case indexing make the identification and specific classification of RSTRs challenging. Nevertheless, multiple studies have developed methods for countering confounding variable in the identification of RSTRs and demonstrated that individuals with RSTR and LTBI phenotypes exhibit distinct genetic and functional predispositions in their responses which may help explain how RSTR individuals remain persistently negative despite prolonged and intense exposure to Mtb (24–27,37–41). Specifically, the field has observed notable differences in the monocytic response to Mtb in these individuals, reflected in unique transcriptomic, epigenetic (methylation), and chromatin accessibility (ATAC-seq) profiles that may aid the innate immune system in more effectively clearing incipient infection (37,42). Nevertheless, a clear functional and mechanistic understanding of how innate cells from RSTRs promote Mtb clearance, and by extension effective Mtb resistance, remains undefined. Refining our understanding at the axis of human genetics, early

immunological responses, and bacterial effector function may allow for more effective and synergistic therapeutic deployment targeted at both human and pathogen, thus tipping the balance in favor of the host.

1.3 Therapeutic Treatment of Mtb and Vaccine Development

Treatment for Mtb is intensive and long lasting (43). Updated CDC recommendations state two preferred standard therapy regimens for drug-sensitive Mtb infection (44). Standard therapy originally consisted of 2HRZE/4HR or 2HRZE/7HR, a 6- or 9-month regimen of isoniazid, pyrazinamide, rifampin, and ethambutol (44). Recently updated CDC guidance alternatively recommends a four-month regimen of rifapentine, isoniazid, pyrazinamide, and moxifloxacin shortening treatment duration with observed non-inferior efficacy (43–45). Drug resistant Mtb is treated with a longer regimen of approximately 4-9 months utilizing variable combinations of first line therapeutics depending on resistance profiles of the bacteria (45). Failed treatment then turns to a subsequent ~18-month treatment period of personalized drug combinations, often comprised of second line drugs (45). Of importance to note, therapeutic regimens historically and geographically fluctuate depending on the locality where treatment is initiated and what is considered standard of care at the time (46). Despite the burden these regimens impose on patients, we still do not have an efficacious vaccine alternative (47). Currently, BCG is the only licensed Mtb vaccine, however, it is variably protective in adults and provides modest protection in children for all-cause mortality, including Mtb (47–56). The United Nations framework has outlined targeted goals for

the reduction of overall MTB burden in high risk, high burden settings (17,19,21,57,58). While we have made progress towards these goals, we have not achieved the targeted aims in reduction. Multiple factors have contributed to these missed targets such as the evolution of SARS-CoV-2 alongside the difficulty of developing efficacious Mtb vaccines, or deploying therapeutic intervention where it is needed (59–63). Greater understanding and resolution of the molecular and cellular interactions between Mtb and humans will allow us to design more effective chemotherapeutic treatments and vaccines that target effective correlates of protection, enabling us to meet reduction goals.

1.4 Cellular and Molecular Interactions Between Mtb and the Host

Initial deposition of Mtb into the alveolar space results in the uptake of these bacilli by alveolar resident cells (64). Most alveolar compartment cells are comprised of alveolar macrophages (AMs) which make up ~80-95% of the alveolar cell milieu (65–68). AMs are also the primary host cell for Mtb during early infection. During early deposition of Mtb into the alveolar compartment, AMs phagocytose Mtb and begin cellular processing to attempt clearance of the foreign material (64,69). Canonically, it is believed that alveolar macrophages skew anti-inflammatory relative to circulating macrophages and are ineffective at restricting Mtb growth or clearing the bacilli (70,71). This results in the potentiation of Mtb within alveolar macrophages prior to the recruitment of circulating hematopoietic-derived immune cells. Peripheral phagocytic cells such as monocyte derived macrophages (MDMs) and neutrophils can be recruited to the site of infection to aide in bacterial clearance (39,72–75). As infection progresses the adaptive immune

system is engaged where classical and non-classical T cells work together to activate phagocytes and generate a restrictive immune profile within cells harboring Mtb (39,72–75). This orchestration of the immune response during early infection is classically characterized by granulomatous formation in the alveolar space which contain bacilli within a defined region of the lung (76,77). Hallmark features of a granuloma often include a fibrotic cuff, leukocyte infiltrate at the core, and interspaced lymphocytes leading to an antimicrobial environment (64,76–78,78–81). This formation is associated with either bacterial clearance or latent infection due to the reduction in replicative bacilli (82,83). In cases where the immune system fails to clear the infection, Mtb often persists in the face of these antimicrobial pressures within the granuloma (76). Often, the granuloma will fail to sterilize, resulting in a quiescent infection and risk of subsequent active disease without intervening treatment (22,84–86). The reason alveolar macrophages and the broader immune response heterogeneously restrict Mtb is not entirely resolved. It is believed this is partially due to the permissive, anti-inflammatory nature of alveolar macrophages, in addition to the highly evolved immune evasion strategies Mtb deploys upon contact with phagocytes (87–90). Mtb secretes many virulence factors to the host cell interface which antagonize essential anti-microbial pathways, potentiating growth in a hostile immune cell. Namely, Mtb can block phagolysosomal maturation, inhibit phagosome acidification, and induce macrophage necrosis (91–94). While not an exhaustive list, these strategies serve as an example of how Mtb subverts what is otherwise a potent innate immune response. Critical to these strategies is Mtb's ability to escape the phagosome. Through one of its type seven

secretion systems (T7SS) known as ESX-1, Mtb perforates the phagosome, enabling cytosolic access to the bacilli and bacterial virulence effectors (95–97).

1.5 Type 7 Secretion Systems and their Expansion in Mtb

Bacterial secretion can broadly be categorized into eleven distinct types, denoted as T1SS-T11SS (98,99). Common secretion systems amongst many prokaryotes and specific eukaryotic organelles include the Sec and TAT system which are describes separately from the remining eleven systems (99,100). These systems are heterogeneously dispersed amongst prokaryotic groups, often enabling specific effector or virulence function. An example of specificity within secretion systems amongst prokaryotes is the almost exclusive association of type 7 (T7SS) with the actinobacterium phylum (101). Amongst the actinobacteria is the Mycobacterium genus, including Mtb. Type 7 systems are defined as inner membrane transporters, embedded within the cytoplasmic membrane of mycobacteria (102). They contain hexameric geometry within the inner membrane (trimer of dimers) and utilize ATP to secrete small, heterodimeric, pre-folded cargo into the pseudo-periplasm of mycobacteria (101,103). Beyond these conserved details, the type 7 systems have expanded within Mycobacteria to encompass five distinct transport systems containing high levels of genetic and structural conservation, but diverse mechanistic function (104). These systems provide an array of functions which is sometimes species dependent (105). It is believed these systems arose via genetic duplication events within ancestral mycobacteria resulting in a wide array of system combinations distributed across the

genus (104,106,107). Their heterogeneity across Mycobacteria leads to diverse and unique combinations of effector function, but importantly Mtb possesses all five with varying degrees of experimentally defined function within this organism. In addition to the ancestral ESX-4, the Mtb chromosome encodes ESX-1, ESX-2, ESX-3, and ESX-5 (101,102,108). Often, ESX-1 is associated with phagosome escape, ESX-3 associated with iron sequestration, ESX-4 secretes CpnT/TNT (a necrosis-inducing toxin-antitoxin heterodimer), and ESX-2/ESX-5 remain poorly defined (97,109). These systems carry out their evolved function via their secreted protein repertoire. These proteins often belong to the PE/PPE family and Esx heterodimer family which are typically encoded within the chromosomal regions also encoding the secretion machinery (101). Despite low resolution of function for ESX-2 and ESX-5, we do know ESX-5 is associated with pathogenic mycobacteria and has predicted virulence function for some of its secreted proteins (15,110–120).

1.6 ESX-5 Structure and Hypothesized Functions

The ESX-5 system is organized similarly to the other ESX systems in the Mtb chromosome (Figure 1.1) (121). The secretion channel is comprised of ESX Conserved Component (Ecc) proteins (101,121). These proteins comprise the structural components that form the secretion channel and catalyze the export of small, folded substrates such the ESX-5 dependent Esx and PE/PPE heterodimers. While seven of these small heterodimers are encoded within the chromosomal ESX-5 parent cluster, the ESX-5 secreted PE/PPE and Esx proteins are a large family dispersed throughout

the chromosome including the more recently expanded PE_PGRS and PPE_MPTR families (112,122). Ultimately, ESX-5 is predicted to secrete over 100 of these small pleomorphic proteins. Interestingly, a four gene cluster in the parent ESX-5 cluster comprised of EsxN, EsxM, PE19, PPE27 was duplicated three additional times in the Mtb chromosome resulting in paralogous clusters ESX-5a (PE8, PPE15, EsxI, EsxJ), ESX-5b (PE13, PPE18, EsxK, EsxL), and ESX-5c (PE32, PPE65, EsxV, EsxW) (123). The function of these paralogous clusters and the broader family of PE/PPE or Esx proteins is poorly defined, however there have been recent clinical and functional studies suggesting these clusters may play a role in virulence and are highly immunogenic (15,111,124). Work by Saelens et.al have shown that clinical strains of Mtb containing an intact EsxM gene show increased rates of extrapulmonary dissemination (111). Similarly, a study by Holt et. al showed that clinical lineage 2 isolates of Mtb contain polymorphisms in the EsxW gene that are associated with increased transmissibility in their Vietnamese cohort (15). These studies add rationale for understanding the molecular function of these effectors in the context of macrophage interaction and their role in Mtb physiology, independent of a host cell.

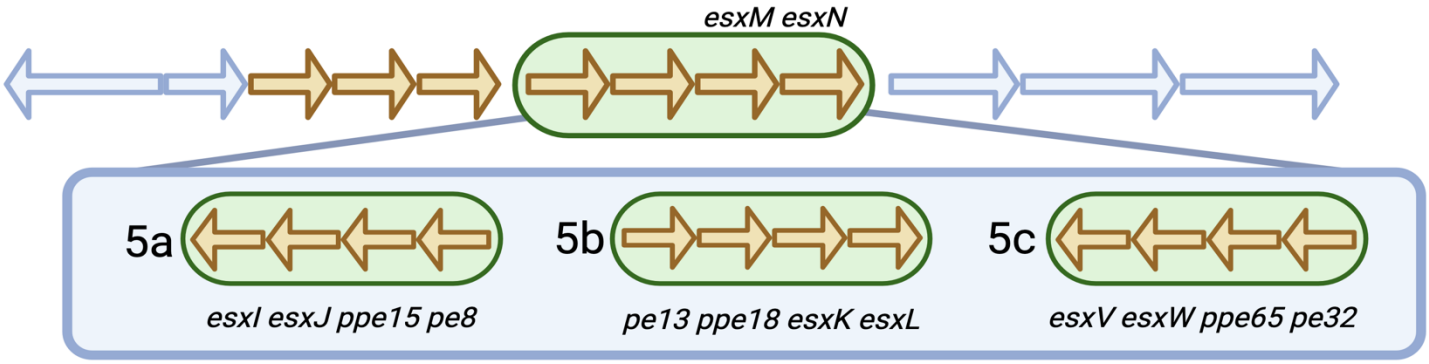

Figure 1.1 – Model diagram of ESX-5 genetic organization within Mtb. Blue arrows denote structural proteins that comprise the hexameric ESX-5 porin. Orange arrows represent the ESX-5 associated and secreted cargo comprised of *pe/ppe* and *esx* genes. Green circle enclosed around the four orange-gene cluster shows the genetic element that was duplicated three additional times and resulted in the three paralogous clusters, ESX-5a, ESX-5b, and ESX-5c shown expanded in blue box. These paralogs are genomically dispersed away from the parent gene cluster in the Mtb chromosome. Created in BioRender. Haynes, A. (2025) https://BioRender.com/9larwr6.

Chapter 2. Aims and Research in Context

The overarching goal of this research is to deepen our understanding of early molecular host–pathogen interactions during *Mycobacterium tuberculosis* (Mtb) infection. Via a more complete understanding of early host-pathogen interactions, we aim to aid in the downstream development of more efficacious therapeutic and preventative strategies. Tuberculosis remains a major global health burden, and despite advances in diagnostics and treatment, significant gaps remain in our understanding of how Mtb manipulates host responses in the earliest phases of infection. This project addresses these gaps by dissecting the role of host genetic variation in early transcriptional response to Mtb infection, primary macrophage phenotypic responses to Mtb strains carrying targeted deletions of genes of interest, and defining Mtb ESX-5 effector function via microbiologic approaches.

The first aim of this research is to investigate how human genetic variation contributes to differential responses during Mtb infection. By leveraging primary human cells from genetically diverse donors, we seek to identify host genetic factors that influence macrophage responsiveness and inflammatory signaling in the early stages of infection. This aim addresses the observation that susceptibility and disease progression during TB disease are not uniform across populations and may be partly explained by host-intrinsic factors.

The second aim focuses on characterizing the functional impact of ESX-5 paralog deletions on host macrophage responses in vitro. The ESX-5 secretion system exports a number of PE/PPE and Esx proteins, some of which are believed to modulate host immunity. We hypothesize that specific ESX-5 paralogs (ESX-5a, ESX-5b, and ESX-5c) influence macrophage activation and cytokine production to differentially shape the early response to infection. Using deletion mutants and primary human macrophages, we will define how these bacterial factors shape the host response during early infection.

Lastly, we aim to characterize how deletion of these ESX-5 paralogs perturbs bacterial regulatory networks and gene expression programs. Given the proposed functional ties between ESX systems and Mtb physiology, we hypothesize that loss of individual paralogs may lead to compensatory changes in transcriptional networks, secretion profiles, or metabolic pathways. Through transcriptomic analysis, we will map these perturbations to better understand how Mtb adapts. Collectively, this work integrates host and bacterial perspectives to provide a more complete understanding of early infection events that could be exploited for new interventions.

Chapter 3. Characterizing Transcriptional Responses of RSTR Alveolar Macrophages to Mycobacterium tuberculosis Infection

**This chapter was submitted in full as a manuscript: "*Alveolar macrophage transcriptional signatures associated with resistance to TST/ IGRA conversion following *Mycobacterium tuberculosis* exposure" Haynes AM, et.al, 2025

3.1 Introduction

Mycobacterium tuberculosis (Mtb) is an aerosol-borne bacterium of which one quarter of the human population demonstrates immunological evidence of exposure (125–127). While asymptomatic tuberculosis infection (also called latent TB infection (LTBI)) is the most common outcome, a proportion will progress to active disease which causes significant mortality, totaling near 1.5 million deaths per year (125–128). The wide dispersal of Mtb is often attributed to its tight co-evolution with humans, making Mtb extremely well-adapted to its niche (129–134). By some estimates, co-evolution has been occurring for nearly 70,000 years resulting in an intricate interaction web of numerous cell types and profiles of Mtb throughout the course of infection (31–35). This results in a complex infection dynamic that has been difficult to characterize. Interestingly, this co-evolutionary period has also driven the development of human populations which appear to resist Mtb infection (also called "resisters" (RSTR)), presumably through rapid clearance of the bacterium upon deposition in the lung(25,29,30,35).

RSTR populations are clinically characterized by remaining durably negative for Mtb infection via Interferon Gamma Release assay (IGRA) and Tuberculin Skin Test (TST) despite exposure to Mtb (28–30). Several previous studies have shown that RSTR and LTBI individuals display genetic and functional predispositions in their response to Mtb, which could help explain how RSTR individuals are able to remain durably negative in the face of prolonged heavy exposure (24–27,37–41). Monocytes from RSTRs have unique cellular profiles as measured via RNA-seq, methylation, and ATAC-seq differentiating their gene expression from LTBI monocytes (37,42) . Despite these observations, a clear mechanistic understanding of how myeloid-lineage cells differ in response to Mtb infection, and thus result in clearance, is elusive.

The initial interaction of Mtb with human immune cells predominantly occurs in the lung where Mtb is phagocytosed by alveolar macrophages (AMs) (128,135). These AMs make up approximately 80-95% of the immune cell milieu of the alveolar space (128,136). Not only do these macrophages possess a distinctive cellular origin, in contrast with other canonical myeloid-lineage cells which originate via hematopoiesis, AMs also display a divergent cellular profile. Compared to MDMs, AMs have a milder inflammatory response, likely due to the need to balance constant airway exposure to antigen, clearance of microbes and debris, while also avoiding destructive inflammatory recruitment in the airway (137–140). Previous studies demonstrated that AMs display unique Mtb-induced expression profiles compared to other macrophage subtypes (27,70,141,142). Integrating the unique profiles of AMs with RSTR status represents a

novel opportunity to understand how this first-line cell differs between LTBI and RSTR individuals as well as to its circulating monocyte-derived counterparts.

Herein we test the hypothesis that AMs have differential RNA expression profiles from other myeloid lineage cells derived from the RSTR cohort and that transcriptional AM profiles will differ between RSTR and LTBI individuals at baseline and during *in vitro* Mtb infection.

3.2 Methods

3.2.1 Human Subjects

HIV-negative individuals from the Uganda household contact study were recruited for this study as described previously (29,37,143). In brief, individuals with culture-positive pulmonary tuberculosis (TB) were recruited as part of the Kawempe Community Health Study in Kampala, Uganda from 2002 to 2012 as previously described. Household contacts of index cases were initially followed for 2 years with serial tuberculin skin test (TST) monitoring. A subset of individuals was retraced from 2014 and 2017 and re-assessed by TST as well as IFNγ release assays (IGRA) for another 2 years. Individuals were also re-assessed via IGRA at the time of bronchoscopy 0 to 5 years after retracing. Individuals were classified as concordant negative resisters (RSTR) or concordant positive latent tuberculosis infection (LTBI). At time of re-tracing, all participants were HIV-negative and gave updated written informed consent which was approved by the institutional review boards of their associated institution. For minors

(age <18 years in Uganda), informed consent was obtained from a legal parent or guardian with concurrent assent obtained from the minor. An Mtb-infected monocyte dataset was used for comparison which was derived from cryopreserved peripheral blood mononuclear cells (PBMC) from a subset of these retraced individuals (29). All methods of this study were approved by Makerere University, CWRU, and the University of Washington institutional review boards (IRB).

3.2.2 Bronchoscopy and BAL fluid processing

Bronchoscopies were performed as described previously(136). All BAL collection was performed under topical anesthesia via a trans-nasal approach in the bronchoscopy unit at Naguru Hospital, Kampala, Uganda. Before each procedure, participants received aerosolized 2% lidocaine and gargled several times with 2% lidocaine solution for 30 seconds. Topical anesthesia of the nasal passage was performed using 2% viscous lidocaine jelly applied with cotton applicators. Further local anesthesia was provided by topical application of 1 to 2ml aliquots of 1% or 2% lidocaine to the airways via the bronchoscope. Participants received supplemental oxygen (2 l/min) via nasal cannula and all vital signs were monitored during bronchoscopy. Bronchoalveolar lavage was performed by wedging the tip of the bronchoscope in a subsegment of the right middle lobe or lingua. Aliquots of 30 ml of ambient temperature sterile normal saline solution (up to a total of 240 ml) were instilled into the airway and gently aspirated using a 60 ml syringe. We then collected the lavage fluid and pelleted at 300g for 10 minutes at room temperature. Cells from the same donor were pooled and enumerated via trypan blue. One-half of each sample was washed x2 with C10 medium (see media make-up in

‘Media and reagents’) and spun at 300xg for 10 minutes to pellet the cells. The pellet was then solubilized in 1mL of Invitrogen Trizol reagent (Waltham, MA) and stored at -80 C for downstream extraction (labeled “BALC (BAL cell)- Fresh” (Figure 1, Supplemental Table 1). The other half of each sample, washed x2 with HBSS (without calcium or magnesium), pelleted as described, and then resuspended in a freeze medium. Cells were then slowly frozen to -80C using an isopropanol freeze chamber to achieve -1C/min. The following day, vials were moved to liquid nitrogen for long-term cryogenic storage and transfer to Seattle (labeled “BALC cryopreserved”).

3.2.3 Media and reagents

Collected BAL cells were washed using C10 medium consisting of RPMI 1640 (containing 1% HEPES and 0.5% Penicillin/Streptomycin v/v) supplemented with 10% fetal bovine serum (FBS). Thawed AMs were cultured in RPMI-10 which consists of RPMI 1640 medium (Gibco, Waltham MA) with 10% FBS (Atlas Biologicals (Fort Collins CO)), along with macrophage colony stimulating factor (M-CSF) (PeproTech, Cranbury NJ) at 50ng/mL. For mycobacterial culture, bacteria were grown in 7H9 base medium supplemented with Glycerol, ADC, and Tween 80 at final concentrations of 0.2%, 10%, and 0.05% respectively. Sautons medium used for washing mycobacteria is a basal medium composed of 4.0 grams of L-asparagine, 0.5 grams of $MgSO_4$, 0.5 grams of K_2HPO_4, 0.1 milliliters of a 1% $ZnSO_4$, 2.0 grams of citric acid, and 0.05 grams of ferric ammonium citrate into 1 liter of water. Tween 80 and Glycerol were added at the same concentration as for 7H9.

3.2.4 Bacterial cultivation

Virulent Mtb, strain H37Rv (gift of Dr. David Sherman), was grown in 7H9 broth according to previously outlined protocols. In short, a frozen 1mL stock of Mtb H37Rv was thawed to room temperature. This stock was then inoculated into supplemented 7H9 medium as outlined in media section. This culture was grown to an OD of ~1.0 before being back diluted to an OD 0.2. The culture was then outgrown overnight to an OD of 0.4, washed with Sautons medium x2, and resuspended at an OD of 1.0 in Sautons medium and frozen at -80C. Frozen, Sautons washed H37Rv was then thawed and used with a standard OD conversion factor to infect AMs at a multiplicity of infection of 1.0.

3.2.5 Infection of alveolar macrophages with Mtb

Cryogenically preserved AMs were removed from liquid nitrogen tanks and thawed using a gentle swirling motion in a 37C water bath. Once the vial was almost fully thawed, the vial was removed and 1mL of RPMI-10 was slowly added to bring up the temperature of the stock while diluting the DMSO. This mixture was then slowly added to 5mL of pre-warmed RPMI-10 medium in a sterile 50mL falcon tube. The cells were then spun at 500xg for 5 minutes and washed x2 using RPMI-10 before plating into a non-tissue culture treated dish and incubated with a penicillin-streptomycin solution for 4 hours. The monolayer was then washed 6x with a 1x HBSS solution and rested overnight in RPMI-10. The following day, cells were collected and viability enumerated using trypan blue. Cells were plated into a 24-well tissue culture dish at a concentration

of 2E5 cells per well and rested overnight in 1mL of RPMI-10 with M-CSF (labeled “AM thaw”, Figure 1, Supplemental Table 2). The following day cells were infected with Sautons washed Mtb H37Rv at an MOI of 1.0. Briefly, after inoculation, plates were spun at 500xg for 5 minutes at room temperature to bring bacteria into contact with the cell monolayer. After brief centrifugation, cells were returned to a 5% CO2 incubator. After 6 hours, supernatant was removed and the cell monolayer for each sample was dissolved using 1mL of Trizol reagent (ThermoFisher, Waltham, MA).

3.2.6 Cellular processing and RNA extraction

RNA was isolated from Trizol samples according to the manufacturer’s protocol. Briefly, 0.2mL of chloroform was added to the 1mL Trizol sample and shaken vigorously. The samples were then spun at 12,000xg for 15 minutes to isolate aqueous and organic phases. Aqueous phase from each sample was isolated and mixed 1:1 with 100% ethanol then added to a respective RNeasy mini column (Qiagen, Hilden Germany). From here, manufactures protocol for RNeasy was performed, including on-column DNase treatment to remove genomic DNA. Total RNA was eluted using RNase free water with RNA quality and concentration evaluated using nanodrop.

3.2.7 RNA sequencing

RNA was processed for sequencing using SMARTseq for cDNA generation (Takara). Sequencing libraries were constructed using the NexteraXT DNA sample preparation kit (Illumina, San Diego CA) to generate Illumina-compatible barcoded libraries. Libraries

were pooled and quantified using a Qubit Fluorometer (Life Technologies, Waltham MA). Sequencing of pooled libraries was carried out on a NextSeq 2000 sequencer (Illumina, San Diego CA) with paired-end 50-base reads, using a NextSeq P3 sequencing kit (Illumina, San Diego CA) with a target depth of 5 million reads per sample. Base calls were processed to FASTQs on BaseSpace (Illumina, San Diego CA), and a base call quality-trimming step was applied to remove low-confidence base calls from the ends of reads. The FASTQs were aligned to the GRCh38 human reference genome using STARv.2.4.2a, and gene counts were generated using htseq-count.

3.2.8 Transcriptomic and Bioinformatics analysis

QC and metrics analysis was performed using the Picard family of tools (v1.134). Briefly, libraries were assessed by total aligned sequences, median coefficient of variation (CV) coverage, and principal component analysis (PCA) of log2 counts per million (CPM) counts (Sup Figure 1A-1D). All libraries passed median coefficient of variation filters (CV < 1). For BALC-Fresh libraries (N = 23 RSTR, 26 LTBI), 1 RSTR library was removed as a PCA outlier (> 3 standard deviations away from the mean on PC1 or PC2) and 3 RSTR libraries were removed for patients who converted IGRA at the time of bronchoscopy. This resulted in 45 libraries (N = 19 RSTR, 26 LTBI) for analysis. For AM-Thaw libraries (N = 12 RSTR, 9 LTBI), libraries with < 1 million aligned sequences (N = 1 RTSR, 1 LTBI) or that were PCA outliers (N = 1 RSTR, 1 LTBI) were removed. In addition, 2 AM-Thaw RSTR donors were determined to have potential media contamination. Since it could not be determined if media samples were

contaminated or switched with Mtb samples, these donors were removed. In total, 6 donors were removed during QC, which resulted in 30 libraries (N = 8 RSTR, 7 LTBI, media and Mtb) for AM-Thaw analysis. Independently within each experiment, pass-filter libraries were then filtered to genes with at least 0.5 CPM in at least 2 libraries and trimmed means of M (TMM) plus voom log2 CPM normalized.

We then assessed which covariates to include in our analytic model by assessing Akaike information criterion (AIC) values. When compared to an unadjusted model with no covariates, an absolute delta in AIC (|dAIC|) of >6 is considered significant change in fit, 2 < |dAIC| < 6 is considered moderate change in fit, and |dAIC| < 2 is considered no change in fit. Based on these criteria for the BALC-fresh dataset, we selected a model of RSTR vs LTBI corrected for median CV, sex, age, and Mtb exposure risk score(144). For the AM-thaw dataset, we selected a model of the interaction of RSTR/LTBI with Mtb stimulation (RSTR:Mtb) corrected for median CV and sex. After model selection for both datasets, differentially expressed genes (DEGs) were examined to identify condition specific gene expression profiles in both datasets (FDR < 0.2). Further analysis consisted of performing pathway enrichment approaches, including gene set enrichment analysis (GSEA) of covariate corrected model estimates (fold changes) against the Broad Molecular Signatures database (MSigSB) Hallmark gene sets (FDR < 0.3)(145). For quality control, we measured whole transcriptome correlation between donors used in both arms of this study to determine intra-individual variation. R^2 values were high (>0.83) and indicated minimal intra-individual variation at a global gene expression level

despite differences in cell composition and experimental conditions including cryopreservation, and overnight culture in media prior to infection (**Figure 3.1**).

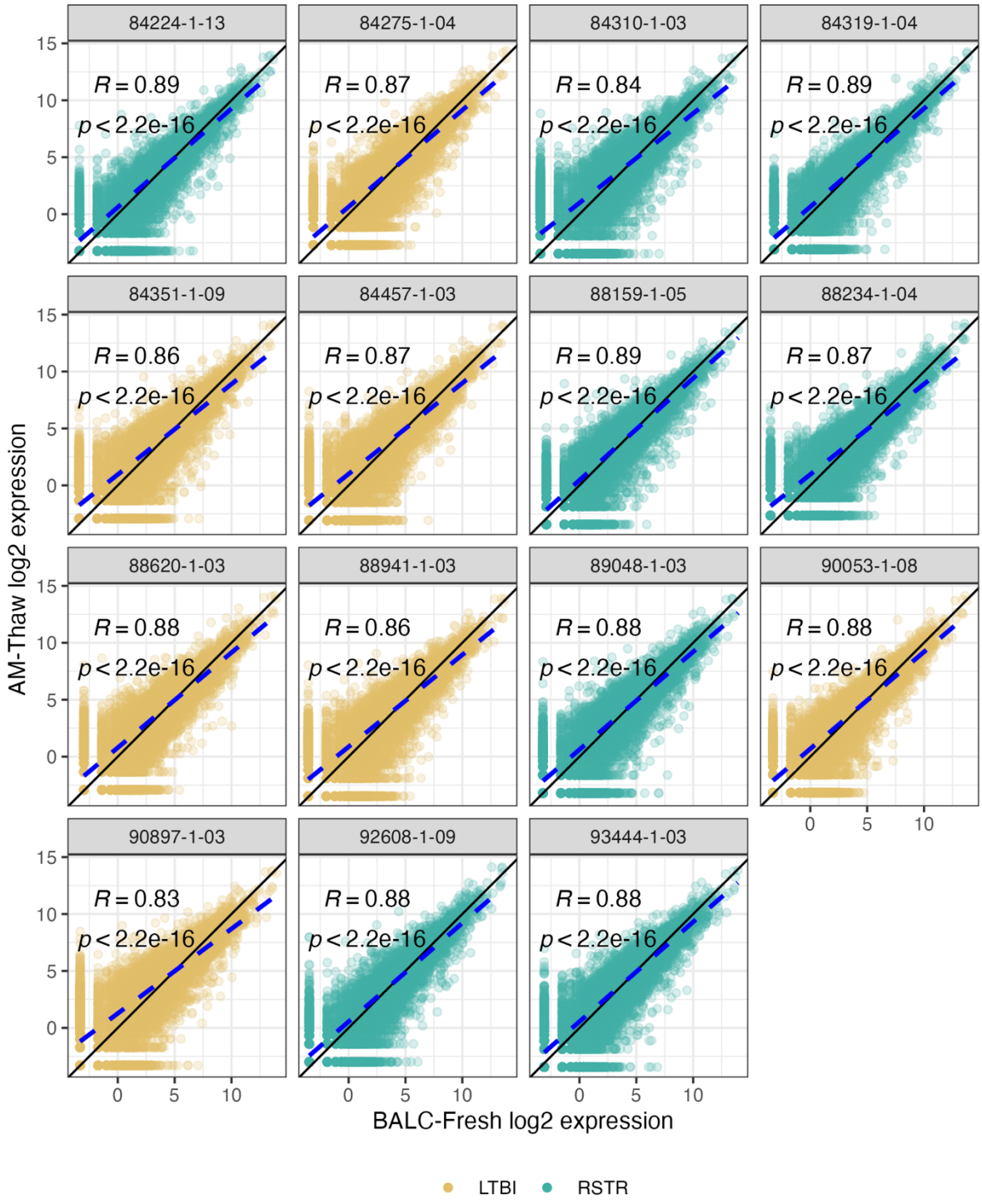

Figure 3.1– Transcriptome correlation analysis. Correlation graphs of the expression profiles from pass-filter donors used across both datasets. Linear regression was used to identify R^2 values across expression profiles in donors from "BALC- Fresh" dataset and "AM-thaw" dataset. BALC-Fresh X axis, AM-thaw on Y axis. Each dot represents log 2 normalized expression of a gene from the corresponding dataset. Black line indicates

perfect correlation; blue dashed line represents actual correlation between datasets. Individual donors (RSTR or LTBI) are stratified by color. Average R^2 value is 0.87, minimum 0.83. Correlation regression determined minimal impact of cell processing variables on expression profiles across cohorts.

3.3 Results

3.3.1 Basal alveolar macrophage transcriptional profiles differ in RSTR and LTBI groups

To investigate whether RSTR and LTBI alveolar macrophages have different transcriptional profiles, we performed RNA sequencing on freshly isolated BAL cells ("BALC-fresh") (Figure 3.2A). After assessing covariates in model fitting with stepwise feature selection via impact on AIC values, the final model included median CV, sex, age, and Mtb exposure risk score (Figure 3.3A-C). Among 19 RSTR and 26 LTBI individuals, we did not detect any differentially expressed genes in this analysis (FDR <0.2) (Figure 3.2B). GSEA analysis revealed 13 differentially expressed gene sets between RSTR and LTBI groups at FDR <0.3 and five with increased stringency of FDR <0.1 (Figure 3.2C). Twelve of the 13 gene sets were negatively enriched in the RSTR group while "E2F targets" was positively enriched in the RSTR group (Figure 3.2C). The leading-edge genes that belong to the E2F gene set included 46 targets, the majority (32 of 46) of which strongly interacted in the STRING protein-protein database (Figure

3.2D). These data suggest that RSTR and LTBI AMs have divergent basal gene expression.

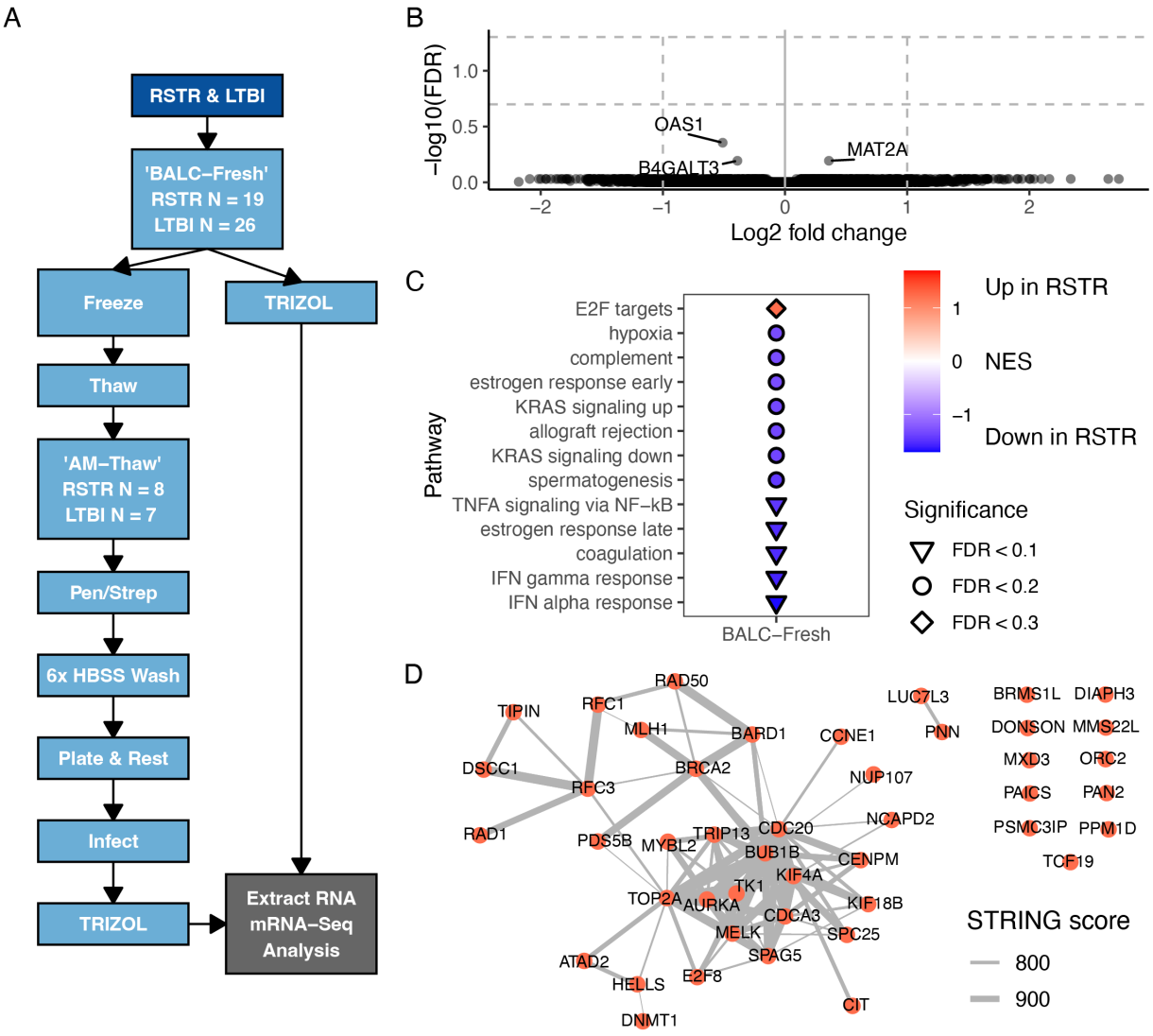

Figure 3.2 – BALC-Fresh alveolar macrophage transcriptional profiles at baseline. 3.2A. Flow chart of cell processing. After BAL, cells were isolated from the BAL and split into two cell fractions. One fraction was immediately preserved in Trizol solution ("BALC-Fresh"). The other fraction was cryopreserved and shipped to Seattle. Cells ("AM-Thaw") from this fraction were thawed, rested, and washed to purify AMs (~80-95% of BALC-Fresh fraction), then infected with Mtb (H37Rv). Infected cells were then solubilized with Trizol. All fractions then underwent RNA extraction and bulk cell mRNA sequencing. Sample numbers indicate pass-filter samples in the final analyses. 3.2B. Volcano plot of RSTR versus LTBI DEG analysis of BALC-Fresh dataset. Y axis depicts -Log10 FDR values indicating significance of RSTR vs LTBI. X axis depicts the Log2 fold change. Plot indicates no genes reach our significance criterion of FDR<0.2 and Log2FC > (+/- 1) with

the top 3 genes labeled. 3.2C. Differentially enriched gene sets via GSEA in RSTR vs. LTBI BALC-Fresh dataset (enrichment of RSTR relative to LTBI). Y axis labels show Hallmark gene sets and X axis label depicts analyzed group (BALC- Fresh). Dot color indicates normalized enrichment score (NES) (red= positively enriched, blue= negatively enriched in RSTR). Shape of the dots indicate significance level at FDR cutoffs of 0.1, 0.2, 0.3, and non-significant (NS) > 0.3. 3.2D. String protein-protein interaction network of "E2F targets" leading-edge genes (N = 46, 1 DEG not found in STRING database). Each node represents a gene and lines depict combined STRING score of the corresponding nodes. Only scores > 700 are shown.

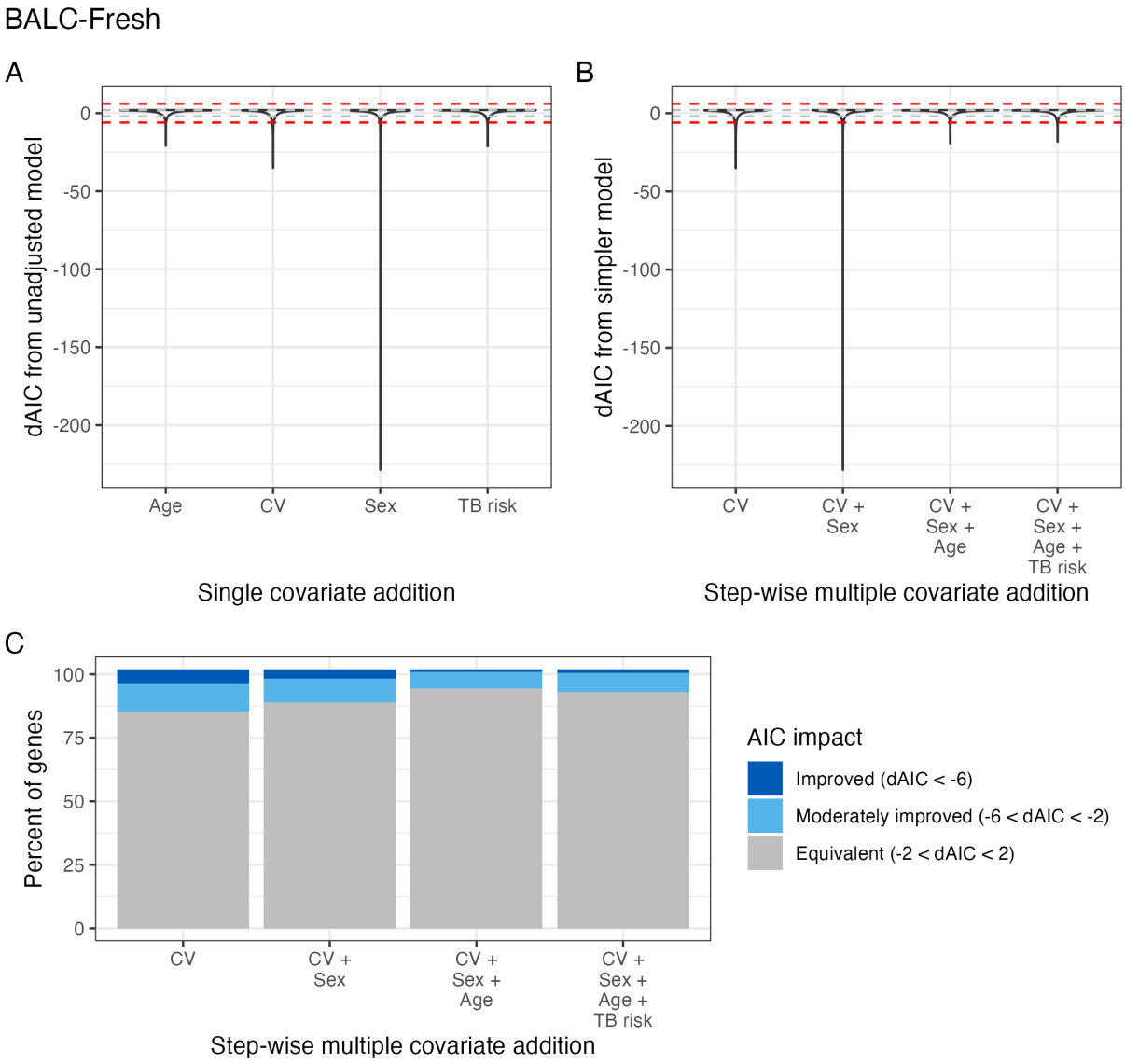

Figure 3.3 – Model fitting of RSTR versus LTBI "BALC-fresh" dataset. 3.3A. Impact of single covariates on AIC compared to an unadjusted model. Y axis depicts the delta AIC (dAIC) relative to an unadjusted model, and X axis depicts the model being tested. 3.3B. Graph depicts dAIC values of stepwise additions of covariates. Y axis depicts the

dAIC relative to the one covariate simpler model. X axis depicts the model being tested with stepwise addition of covariates from left to right. 3.3C. Percent of genes better or worse fit by stepwise addition models. Bar graph depicts model impact on percent of genes. Color coordinates dAIC bins for significant change in fit (|dAIC|>6), moderate change in fit (2 < |dAIC| < 6), and no change in fit (|dAIC| < 2). Warm colors indicate worse fit and cool colors indicate better fit with the addition of the covariate shown. The final model was RSTR vs LTBI corrected for median coefficient of variation (CV), sex, age, and Mtb exposure risk score as all covariates improved model fit without worsening fit for any genes.

3.3.2 Mtb infection drives differential responses in RSTR and LTBI alveolar macrophages

With a subset of the cohort (N=7 LTBI, N=8 RSTR), we examined gene expression under Mtb and media stimulation conditions in alveolar macrophages which were cryopreserved and then thawed prior to infection (“AM-thaw” dataset). Using the same model fitting approach, we selected a model that corrected for median CV and sex as covariates in this analysis (**Figure 3.4A-B**). We also tested an equivalent model to BALC-Fresh for direct comparison (**Figure 3.4C**). However, we observed significantly worse AIC values (dAIC > 6) when performing this analysis and opted to utilize a best fit model.

AM-Thaw

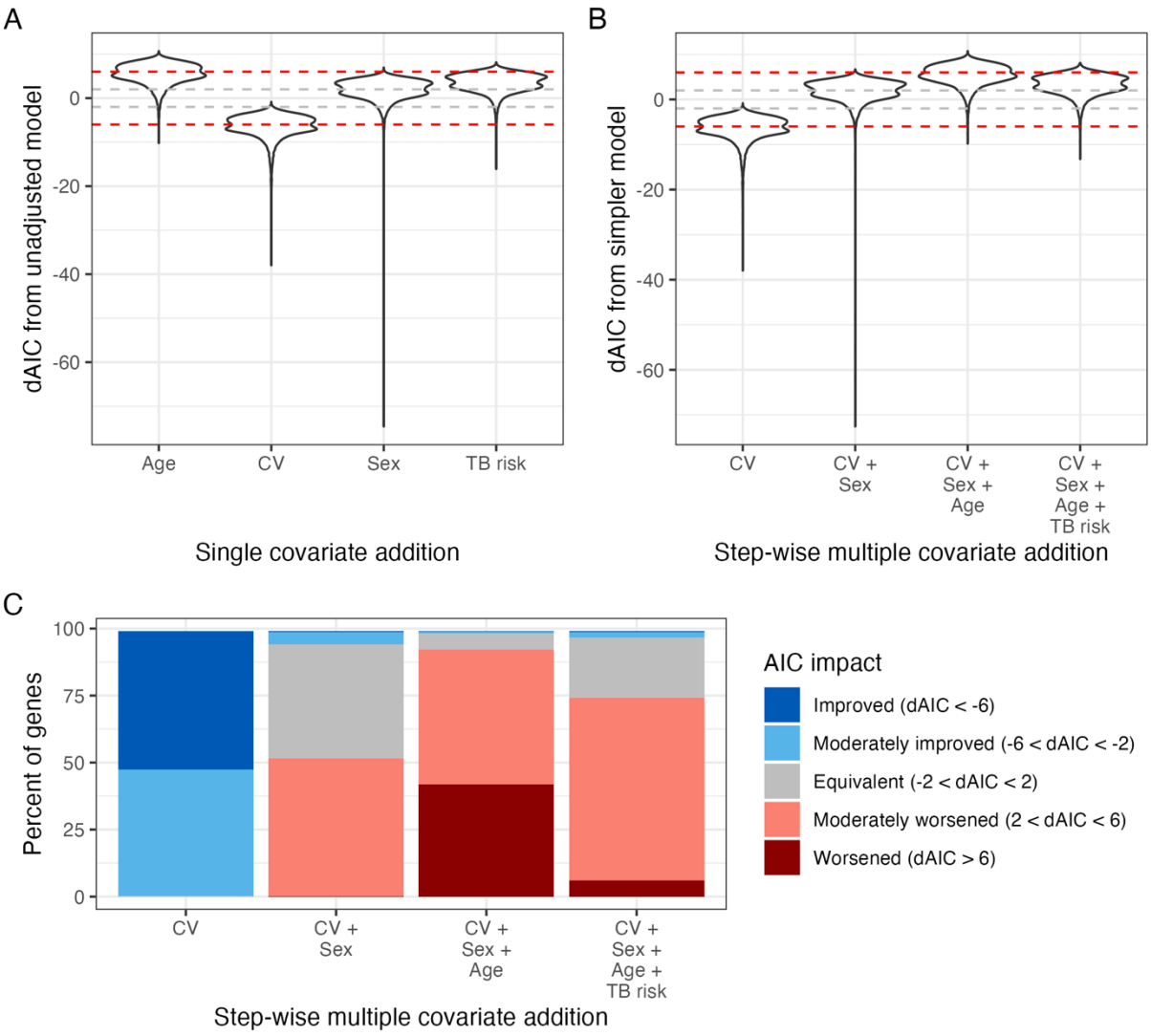

Figure 3.4 – Model fitting of RSTR versus LTBI "AM-thaw" dataset. 3.4A. Impact of single covariates on AIC compared to an unadjusted model. Y axis depicts the delta AIC (dAIC) relative to an unadjusted model, and X axis depicts the model being tested. 3.4B. Graph depicts dAIC values of stepwise additions of covariates. Y axis depicts the dAIC relative to the one covariate simpler model. X axis depicts the model being tested with stepwise addition of covariates from left to right. 3.4C. Percent of genes better or worse fit by stepwise addition models. Bar graph depicts model impact on percent of genes. Color coordinates dAIC bins for significant change in fit (|dAIC|>6), moderate change in fit (2 < |dAIC| < 6), and no change in fit (|dAIC| < 2). Warm colors indicate worse fit and cool colors indicate better fit with the addition of the covariate shown. The final model was the interaction of RSTR status and Mtb infection corrected for median coefficient of variation (CV) and sex as age and Mtb exposure risk score significantly worsened fit for some genes.

We detected 5338 DEGs when comparing Mtb-infected to the media condition (FDR <0.2, Figure 3.5A, 3.5B). When comparing the RSTR and LTBI groups, we identified 37 DEGs with no or similar responses to Mtb infection in RSTR and LTBI (FDR<0.2, Figure 3.5A). Applying a log 2-fold change >1/<-1 threshold decreases this to 7 DEGs more highly expressed in RSTR and

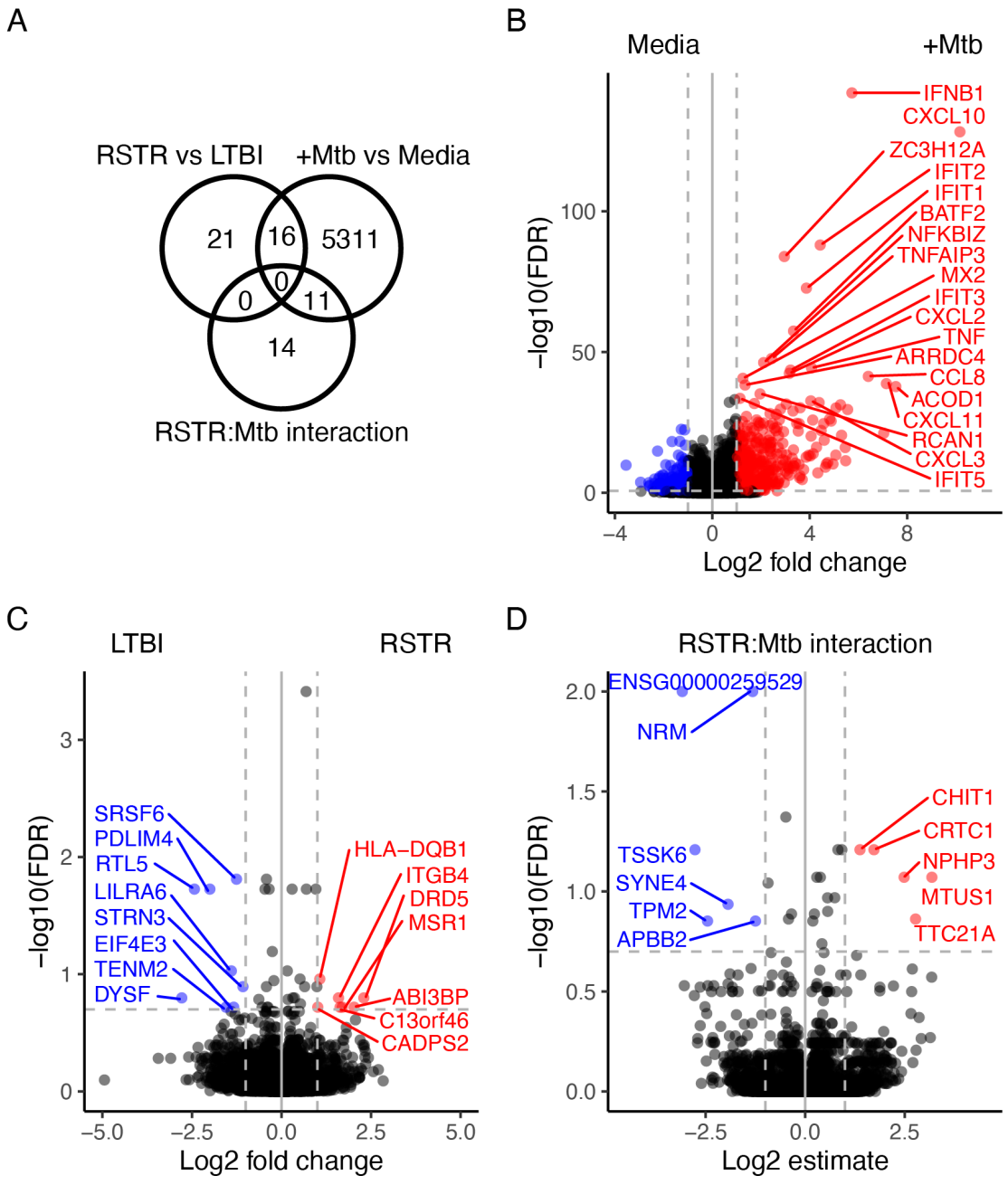

Figure 3.5 – AM-Thaw basal and Mtb-infected alveolar macrophage transcriptional profiles. 2A. Venn diagram of DEGs in the AM-thaw dataset. DEGs for each comparison are shown (FDR <0.2) with +Mtb vs media, RSTR vs LTBI, and the RSTR: Mtb interaction term. 2B. DEG volcano plot by Mtb infection condition. Figure 2C. DEG volcano plot by RSTR versus LTBI status. Figure 2D. DEG volcano plot by RSTR:Mtb interaction term. 2B-2D. Volcano plots depict differential gene expression per variable, all significant genes labeled on plots. Y axis depicts -Log10 FDR values indicating significance level, X axis depicts the Log 2-fold change in expression. Dotted lines denote thresholds of FDR < 0.2 and log2-fold change < -1 or > 1.

8 DEGs more highly expressed in LTBI individuals (Figure 3.5C). Finally, utilizing the interaction term (RSTR:Mtb), we identified 25 DEGs with different Mtb responses in RSTR vs LTBI (FDR<0.2, Figure 3.5A). Applying a log 2-fold change >1/<-1 threshold decreases this number to 11 total DEGs (Figure 3.5D).

Using GSEA, we found two gene sets in the Mtb infection and two in the media condition that were downregulated in RSTR compared to LTBI groups (FDR<0.3, media condition: TNF signaling via NF-kB, Inflammatory response; Mtb condition: Hypoxia, estrogen response early Figure 3.6A). Four gene sets were positively enriched in the RSTR group upon Mtb stimulation (Interferon gamma response, interferon alpha response, inflammatory response, allograft rejection) (Figure 3.6A). Notable leading-edge targets in this “inflammatory response” gene set contain TNF superfamily members and upstream potentiators of ROS and iNOS activity (TNFSF10, TNFSF9, TNFAIP6, NOD2, NLRP3, IL-6, IL-18, etc.).

We also compared GSEA results from the media arms of the two datasets, despite different features (cell ratios, fresh vs cryopreservation with thaw and isolation). The majority (N=11 of 14) of the gene sets significant in the media conditions shared

concordant directionality between RSTR and LTBI, although only one was statistically significant for both experiments (Hallmark TNF signaling via NF-kB) (FDR <0.3) (Figure 3.6A, 3.6B). Three had discordant directionality (Hallmark coagulation, interferon alpha response, and estrogen response late) although all failed to reach significance in our AM-thaw group (Figure 3.6B). Together, these results indicate shared expression profiles despite differing conditions of the experiments. In addition, these data suggest that Mtb induces differential gene expression in RSTR and LTBI AMs.

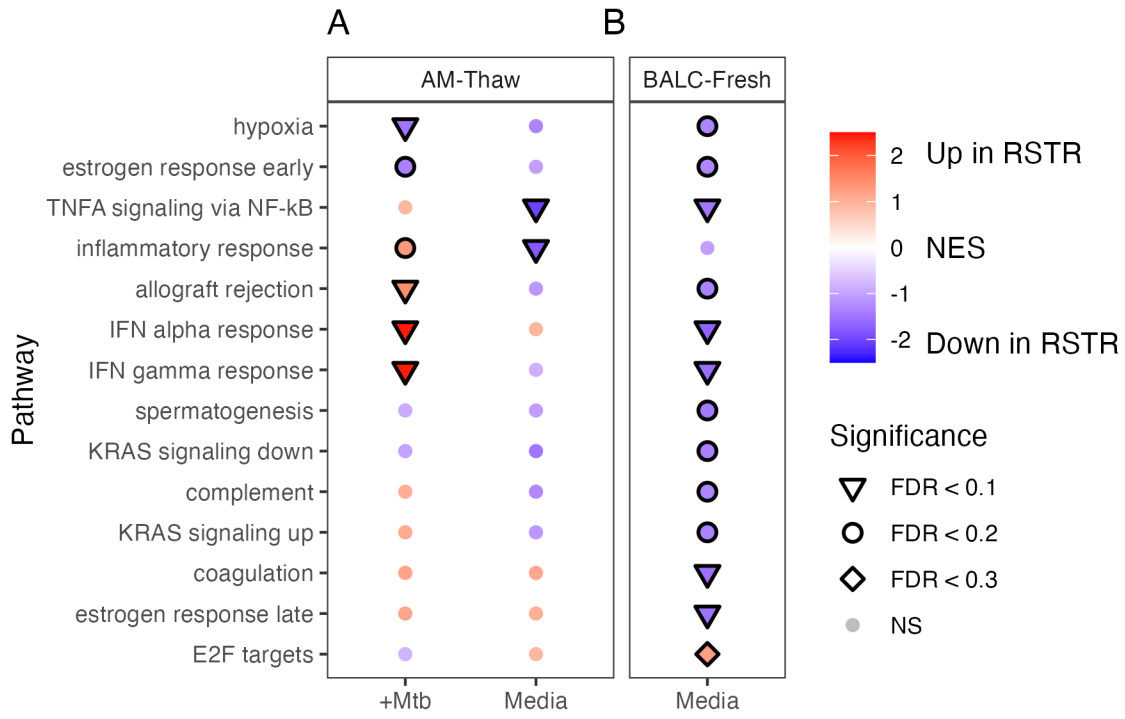

Figure 3.6 – Gene set enrichment results across AM-Thaw and BALC-Fresh. 3.6A. AM-Thaw and 3.6B. BALC-Fresh GSEA. 3.6A-3.6B. Gene sets significant in AM-Thaw and/or BALC-Fresh are shown (FDR<0.3). Y axis displays Hallmark gene sets and X axis depicts cellular cohort and Mtb condition. Dot color indicates normalized enrichment score (NES) (red= positively enriched, blue= negatively enriched in RSTR). Shape of the dots indicate significance level at FDR cutoffs of 0.1, 0.2, 0.3, and non-significant (NS) > 0.3.

3.3.3 RSTR versus LTBI expression profiles in AMs are distinct and partially cell-specific compared to peripheral blood monocytes

We next compared RSTR vs LTBI AM profiles to our previously published peripheral blood monocyte signatures, which included similar media and infection conditions from the same Ugandan cohort (37). When comparing RSTR versus LTBI DEG profiles, we did not detect overlapping DEGs between the “AM-thaw” and monocyte datasets for either RSTR vs LTBI or the RSTR:Mtb interaction term. GSEA profile comparisons between the media conditions of the “AM-thaw” and monocyte datasets revealed 11 overlapping gene sets with concordant negative directionality (downregulated in RSTR compared to LTBI)(37). Of these, only one gene set reached significance in both cell types and was also concordantly significant in BALC-Fresh (FDR <0.1 for TNFa signaling via NF-kB) (Figure 3.6A, Figure 3.7). No positively enriched gene sets were significant and concordant between these media groups though E2F showed concordant directionality without consistent significance. The Mtb infection arms of the AM-Thaw and monocyte studies share one significant positively enriched gene set in RSTRs (inflammatory response, AM-Thaw FDR<0.3, monocyte FDR<0.1 from the original study(37)) (Figure 3.6A, Figure 3.7). Several Mtb induced gene sets (N=3) have significant discordant directionality between these datasets (Allograft rejection, IFN gamma response, hypoxia) and six others were discordant with varied significance. Together, these data suggest that Mtb-induced AM RSTR versus LTBI transcriptional profiles are different and partially cell-specific when compared to monocytes.

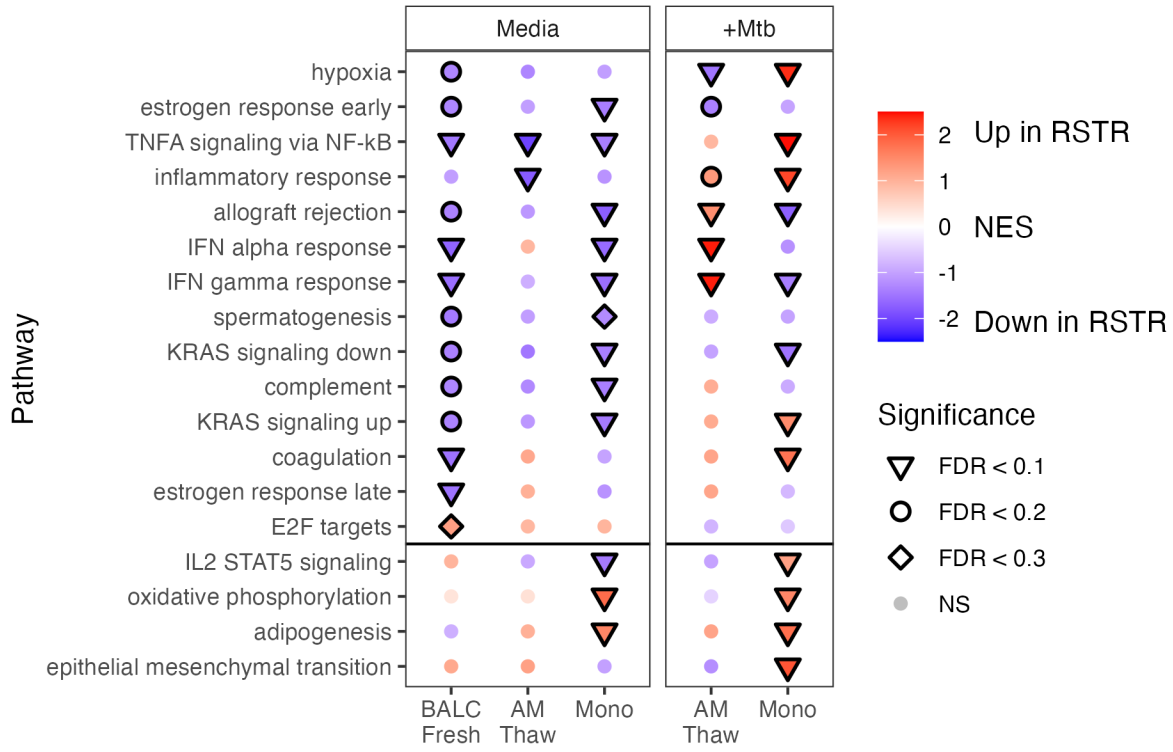

Figure 3.7 – Comprehensive GSEA results for AM-Thaw, BALC-Fresh, and Monocytes across Media and Mtb+ conditions. Gene sets significant in AM-Thaw and/or BALC-Fresh (FDR<0.3) as well as those significant in the original monocyte analysis (FDR<0.1) are shown (37). Y axis displays Hallmark gene sets in the same order as Figure 3 with monocyte significant only gene sets added at the bottom separated by a horizontal line. X axis depicts cellular cohort and Mtb condition. Dot color indicates normalized enrichment score (NES) (red= positively enriched, blue= negatively enriched in RSTR). Shape of the dots indicate significance level at FDR cutoffs of 0.1, 0.2, 0.3, and non-significant (NS) > 0.3.

3.4 Discussion

In this study, we found differential AM responses when comparing RSTR and LTBI individuals at baseline and in response to Mtb infection. In addition, the AM RSTR-specific data included new significant genes and pathways compared to previous observations in monocytes from the same cohort.

A central paradigm of AM immunology is an anti-inflammatory predisposition (137,139,146) with a decreased ability to clear Mtb or restrict growth (70,135). Although the RSTR AM transcriptional profile is less inflammatory than LTBI at baseline, we observe this profile shifts under Mtb infection conditions with upregulation of inflammatory responses relative to LTBI. The leading-edge genes in these inflammatory pathways include pathogen recognition receptors (NOD2, NLRP3, TLRs, etc.), cytokines, and cytokine receptors. Together, this suggests RSTR AMs more potently activate canonical inflammatory responses upon Mtb stimulation compared to their LTBI counterparts. This could enable RSTR AMs to more effectively control Mtb during initial contact and early infection. The upregulation of inflammatory responses also indicates the activation of antimicrobial processes essential in the control of Mtb, such as ROS generation, iNOS transcription, and TNF synthesis (147–149). Interestingly, we also observed monocytes from the same cohort show an upregulation of the Hallmark Inflammatory Response gene set, suggesting efficient proinflammatory upregulation may be a conserved RSTR Mtb response among different cell types that aid in Mtb clearance. Despite overlaps, these cell types also display a divergent IFN response signature. Interestingly, AMs from this cohort display an enrichment for IFNγ and IFNα responses due to Mtb stimulation in RSTR compared to LTBI. The directionality of these signatures is surprising given the clinical definition of groups in this cohort is based on LTBI IGRA positivity/RSTR IGRA negativity to Mtb-specific antigen stimulation. IFNγ activates macrophage antimicrobial profiles and enables restriction of Mtb growth(39,150–156). A possible model is that RSTR AMs are genetically programmed to

respond to IFNγ more robustly, which may promote early bacterial clearance before T-cell responses develop. Others have shown non-RSTR AMs are hyporesponsive to IFNγ, in agreement with an anti-inflammatory paradigm but possibly highlighting a RSTR response difference (157). The source of this IFNγ could arise from airway resident innate-like immune cells (e.g. DURTs, NKTs, ILC1s) rather than classically restricted $\alpha\beta$ T-cells (158–163). Interestingly, recent single-cell RNAseq data from an alternative RSTR cohort (in persons living with HIV (PLWH)) has shown innate-like, polyfunctional lymphocytes express an IFNγ profile in RSTR BAL, supporting our hypothesized model of RSTR AM responses to a local IFN source (27).

We also identified AM-specific RSTR gene sets and pathways that were not present in previous analyses of peripheral blood monocytes. The upregulation of E2F targets within the RSTR cohort AMs at baseline implicates a novel pathway in the functional predisposition of RSTR AMs to clear Mtb rapidly. E2F regulates cell cycle progression and may also play a central role in programmed cell death (164–166). The mechanism of cell death may impact control of Mtb. For example, apoptotic cell death leads to restriction of Mtb growth, while necrotic and pyroptotic cell death may potentiate cell-to-cell spread (167–169). A possible model is that RSTR AMs may be poised at baseline towards E2F-dependent apoptotic cell death that favors control of Mtb. Rapid induction of inflammatory profiles alongside restrictive cell death mechanisms may prevent the establishment of Mtb in the airway and subsequent recruitment of peripherally derived immune responses.

Our study has several limitations. First, environmental exposures (e.g. cooking smoke exposure, pollution) are important variables that impact AM cellular responses and are difficult to control in experimental design. Second, the sample size is small due to the challenges of obtaining BALs and epidemiologically defining RSTRs. Despite the small sample size, we were able to detect differences in our primary comparisons. Finally, additional variables in the Mtb infected arm of this study, such as cryopreservation, thaw, and use of M-CSF, could impact our results. Despite these conditions, we observed a high intra-donor correlation between the RNA-Seq profiles of AMs examined after immediate processing versus delayed with cryopreservation. These comparisons increase our confidence that technical issues are not confounding the results.

In summary, we discovered transcriptional differences from AMs of RSTR and LTBI individuals. Previous studies examining RSTR status in this cohort has focused on peripheral monocytes with epigenetic and transcriptional profiling along with genetic data to determine differences between RSTR and LTBI individuals(26,37,38,42,143). The current study illustrates the importance of studying cell-type specific mechanisms including the central role of AMs in TB pathogenesis.

3.5 Acknowledgements

We thank the individual study participants of the Kawempe Community Health Study, study coordinators and the clinical and research staff including LaShaunda Malone, Keith Chervenak, Marla Manning, Dr. Mary Nsereko, Dr. Moses Joloba, Hussein

Kisingo, Sophie Nalukwago, Dorcas Lamunu, Deborah Nsamba, Annet Kawuma, Saidah Menya, Joan Nassuna, Joy Beseke, Michael Odie, Henry Kawoya, Shannon Pavsek, Dr. E. Chandler Church, Anna Duewiger and Dr. Bonnie Thiel.

Chapter 4. Exploration of the ESX-5a, ESX-5b and ESX-5c Paralogs in the Context of Human Macrophage Infection

**This chapter was submitted in part as a manuscript: "ESX*-5 Deletions in *Mycobacterium tuberculosis* Alter Macrophage Cytokine Signaling, *In Vivo* Virulence, and Bacterial Heavy Metal Response" Haynes AM, et.al. 2025

4.1 Introduction

Pathogenic mycobacteria have co-evolved with their respective hosts for thousands of years (2,7,170). Arguably, the most prolific mycobacteria to cause disease in humans is *Mycobacterium tuberculosis* (Mtb). By some estimates, Mtb infects one quarter of the human population and causes approximately 1.5 million deaths per year (7,17,18,21,171). This tight co-evolution has facilitated the development of many antagonistic mechanisms that potentiate bacterial survival and spread in the face of an extensively developed and effective human immune system. Specifically, Mtb can block phagolysosomal maturation, inhibit phagosome acidification and induce macrophage necrosis, among other processes (92–94,172–174,174,175). The molecular innerworkings of how Mtb carries out many of its virulence functions are not fully described, particularly during early infection when the bacillus is phagocytosed by macrophages (76,77,89). A more complete understanding of the interplay between bacterial effectors and human macrophages will allow us to better design intervention strategies aimed at reducing burden of disease. To do this we need better definition of the Mtb antagonistic landscape.

The many specialized mechanisms evolved in Mtb for subverting antimicrobial pathways and persisting within phagocytes are often carried out by secreted virulence effectors (91,92,176,177). Mtb moves these effectors to the host cell interface where they antagonize cellular processes. The movement of these virulence factors is critical, with Mtb encoding numerous bacterial secretion systems on its chromosome. Namely, the general secretion (SEC), twin arginine translocation (TAT), and type seven secretion systems (T7SS)(100,101,103,178). In Mtb, T7SS are also called ESX systems. Specifically, Mtb encodes five, denoted ESX-1 through ESX-5 (101). Combined, these systems secrete roughly 5-10% of Mtb encoded proteins (102,179–181). Many have predicted or bona fide virulence function, such as ESX-1 via CFP-10 and ESAT-6 (97,182,183). Others, like ESX-5, are more sparsely defined.

ESX-5 secretes many Proline-Glutamic Acid (PE), Proline-Proline-Glutamic Acid (PPE), Esx, PE-Polymorphic GC-Rich Repetitive Sequence (PE_PGRS), and PPE- Major Polymorphic Tandem Repeat (PPE_MPTR) proteins (184–186). Together, these families comprise >100 proteins and are extensively expanded in Mtb (112,122,187). Functional characterization is lacking for most. Many of these effectors are thought to be involved in immune subversion, nutrient acquisition, membrane structuring, and virulence (93,108,116,117,122,188,189). Despite a paucity of defined function for most of these proteins in Mtb, recent clinical studies have implicated small paralogous ESX-5 secreted clusters in virulence, transmissibility, and immune recognition (15,111,124,190). These paralogs are each comprised of a four gene cluster and called ESX-5a, ESX-5b, and ESX-5c respectively. While these previous studies have provided an intriguing rationale

for follow up, notably absent from many is a functional reason for why these clusters may play a role in Mtb virulence or transmissibility.

Together, these gaps and early functional studies prompted us to investigate the role of these paralogs during human macrophages infection. Leveraging a well-defined lab strain of Mtb (H37Rv) we targeted all three paralogs for deletion, creating three knockout strains called ΔESX-5a, ΔESX-5b, and ΔESX-5c. We then queried differential responses to the knockouts during infection to begin understanding the role these proteins play during infection. The data generated herein will be key to more completely understanding the early interaction and impacts Mtb has on proinflammatory responses, possibly facilitating more efficacious vaccine or therapeutic design.

4.2 Methods

4.2.1 Ethics and Biosafety Precautions

All experiments performed within the scope of this study utilized primary human monocyte derived macrophages (MDMs) from healthy human donors in the Seattle area. All cells originate from Bloodworks Northwest and are deidentified prior to receipt. No IRB is required to perform studies with these cells. All experiments performed with live, virulent, Mtb were performed in an accredited BSL-3 at the University of Washington School of Medicine campus utilizing validated containment protocols to ensure biological safety.

4.2.2 Media

Media used throughout experiments consists of RPMI-10 (RPMI 1640 medium (Gibco, Carlsbad, CA) with 10% fetal bovine serum (Atlas Biologicals, Fort Collins, CO), along with macrophage colony stimulating factor (M-CSF) (Pepro Tech, Carlsbad, CA) at 50ng/mL. For cell culture of Huh7 cell lines, complete DMEM was used. This media was comprised of 90% DMEM (Gibco (Carlsbad, CA) and 10% fetal bovine serum (Atlas Biologicals (Fort Collins, CO). For mycobacterial culture, bacteria were grown in 7H9 base medium supplemented with Glycerol, ADC, and Tween 80 at final concentrations of 0.2%, 10%, and 0.05% respectively. Sautons medium used for washing mycobacteria is a basal medium composed of 4.0 grams of L-asparagine, 0.5 grams of $MgSO_4$, 0.5 grams of K_2HPO_4, 0.1 milliliters of a 1% $ZnSO_4$, 2.0 grams of citric acid, and 0.05 grams of ferric ammonium citrate into 1 liter of water. Tween 80 and Glycerol were added at the same concentration as for 7H9.

4.2.3 Bacterial Cultivation

H37Rv wildtype Mtb used in our laboratory was a gift from Dr. David Sherman. H37Rv pNIT was received from Drs. Christoph Grundner and Andrew Frando from Seattle Children's Research Institute (SCRI). All knockout strains (ΔESX-5a, ΔESX-5b, and ΔESX-5c) are descended from the H37Rv pNIT wildtype strain of Mtb. Complementation strains are decedents of their respective knockout parent strain. See full list of strains

below. All strains were cultured the same way unless otherwise described. To culture these Mtb strains, a frozen stock was removed from our -80C Freezer in our BSL-3 suite. The stock was thawed to room temperature and added to 4mL of 7H9-GAT comprised of 7H9 base along with 0.2% Glycerol (**G**), 10% ADC supplement (**A**) and 0.05% Tween 80 (**T**). Appropriate selection was added if required. Strains were cultured shaking and vented until OD reached ~0.8-1.0, then back diluted to OD 0.1, and outgrown to mid-logarithmic phase growth before using in downstream assays.

4.2.4 Mtb Gene Expression Quantitation

To quantify Mtb target gene expression we performed a TaqMan (Life Technologies, Waltham MA) based gene expression assay approach. We resuspended bacterial targets in 1mL of Trizol and transferred to Lysing Matrix B tubes (MP Biomedicals, Santa Ana CA). We then homogenized the sample using a 6500rpm, 30 second protocol on a beadruptor (Omni International, Kennesaw GA) followed by a 30 second incubation on ice. This was repeated x3 to ensure complete lysis of the bacteria and RNA liberation. RNA was then isolated using the manufactures isolation protocol for Trizol. Isolated RNA was subsequently quantified on a nanodrop (ThermoFisher, Waltham MA). This RNA was then input into a cDNA generation protocol using a high-capacity cDNA reverse transcription kit (Life Technologies, Waltham MA). Resulting cDNA was used in a TaqMan, probe-based gene expression assay. Briefly, target probe sets were added to cDNA along with an endogenous control probe set targeting sigma factor A (SigA). Quantitative PCR (qPCR) was performed to get Ct values of each target in multiplexed

samples. Relative quantitation was performed using the ΔΔCt method and converted to fold change expression relative to control for the target of interest (191).

4.2.5 Genomic DNA Extraction from Mtb

Genomic DNA was extracted from Mtb via a crude lysate method. Cultures of desired strains were grown to an optical density of 1.0 as described. One mL of culture was then pelleted at 14,000 rpm for 10 minutes and resuspended in 500uL of molecular water. These resuspensions were then boiled at 95 C for 30 minutes to inactivate and lyse bacteria. After 30 minutes, the lysates were pelleted again to remove insoluble debris. The aqueous fraction was then filtered through a 0.22-micron Polyether Sulfone (PES) filter unit for additional purification. Purified, water soluble DNA was then used for downstream, DNA-based applications.

4.2.6 CFU Quantitation of Mtb Growth

Colony forming unit assays were performed according to our standard protocol. Initially cells were infected as described in Macrophage infection method. Briefly, MDMs were infected at desired MOI and spun at 500g for 5 minutes. After desired time point of infection (72 hours for replication or 4 hours for uptake), media was removed from the monolayers, and the cells were washed using RPMI-10 and then lysed using 200uL of a 1% Triton X-100 solution in water. This constitutes our 0 dilution. The lysate was then serially diluted 10-fold in 7H9-GAT containing tween to break up bacterial clumps. At

each serial dilution, 20uL of the previous was moved into 180uL of fresh 7H9-GAT for a final dilution range of 10^{-1} to 10^{-6} for all samples. 100uL of the 10^{-3} through 10^{-5} was plated on 7H10 agar plates and dried at room temperature. Plates were outgrown for ~2 weeks and colonies enumerated. Back calculation was performed to determine the original CFU number in each condition. Replicates were averaged to generate intra-condition variability.

4.2.7 pNIT Allelic Exchange

Recombineering was performed using RecET mediated homology directed exchange as described previously. Briefly, we PCR amplified 500 base pair homology arms flanking our Mtb genome regions of interest. We subsequently generated a PCR product of a hygromycin resistance marker under control of a strong mycobacterial promotor. Concurrently, we linearized our destination plasmid pUC19 within the MCS using a single restriction enzyme coupled with dephosphorylation using Quick CIP (New England Bio Labs, MA). Once all linear products had been generated, we purified all constructs using a combination of gel (Qiaquick Gel Extraction) and PCR reaction clean up (Qiaquick PCR Purification) methods (Qiagen, Hilden Germany). After linear DNA products had been generated in sufficient purity and quantity, we performed an InFusion reaction (Takara Bio) as described by the manufacturer. Fused product was then used to transform Stellar Competent Cells (Takara Bio, Japan) followed by an overnight outgrowth on LB agar. Colonies were isolated and the contained plasmids amplified before validation using whole plasmid sequencing. Successful recombinants were

subsequently midi prepped using the NucleoBond Xtra Midi kit (Macherey-Nagel, Germany). From this stock construct, our linear exchange fragment was amplified using PCR with primers flanking the 5' and 3' ends. We then purified the exchange product using the Qiaquick Gel Extraction (Qiagen, Hilden Germany) and quantified knockout template quantity using nanodrop. After generating pure exchange constructs, we then used standard MTB electroporation protocols to introduce the exchange construct. Initially we induced the expression of the gp130 and 131 genes within Mtb H37Rv containing the pNIT plasmid, using Isovaleronitrile (sigma Aldrich, Saint Louis MO). We then made these recombinogenic bacteria electrocompetent via pelleting and successive washing using a chilled 10% glycerol solution three times. The final pellet is resuspended in 3mL (10% initial culture volume) 10% glycerol. 400uL of competent cells were added to a 2mm gap cuvette (BioRad, Hercules CA) along with ~1 microgram of pure gene exchange template. These mixtures were electroporated using a standard Mtb pulse of 2.5 kV, 1,000 Ω, and 25 μF. Bacteria were immediately recovered into 5mL of 7H9-GAT overnight. The following day recovered bacteria were concentrated via centrifugation and plated onto 7H10 agar plates with Hygromycin selection. Outgrowth was allowed to proceed for a maximum of 5 weeks. Colonies were selected and screened using molecular and phenotypic methods to ensure proper knockout.

4.2.8 Complementation Vector Cloning

Complementation cloning was performed using the pTEC15 plasmid (Gift of Dr. Rafael Hernandez). Complementation constructs were generated using a serial cloning

method. First, the pTEC15 plasmid was reengineered for Bleocin resistance by inserting a Bleocin resistance gene under control of the Mtb HSP60 promoter, destroying the original resistance marker. The resulting construct was named pTEC15 ZeoR and sequence verified via whole plasmid sequencing. Next, pTEC15 ZeoR was linearized using the EcoRV restriction site (New England Bio Labs, MA), destroying the mWasabi reporter marker. Insertion DNA was amplified using sequence specific primers containing 15 base pair homology arms flanking the EcoRV restriction site used. Insertion DNA and linear vector were then ligated using homology directed recombination with the InFusion system (Takara Bio, San Jose CA). These plasmids were then validated using whole plasmid sequencing. Properly assembled plasmids were then amplified and purified using the NucleoBond Xtra Midi Kit (Macherey-Nagel, Germany).

4.2.9 Macrophage generation and column isolation

Human peripheral blood mononuclear cells (PBMC) were obtained from Bloodworks Northwest as discarded byproduct from blood donation. We obtain leukocyte reduction system (LRS) cones that remove leukocytes during blood donation and extracted cells from this cone via standard Ficoll gradient isolation as described elsewhere. Isolated PBMC are stored in liquid nitrogen at 50E6 cells per vial until use. To generate macrophages, a PBMC stock was drawn from liquid nitrogen storage and thawed in a 37C water bath using a gentle swirling motion until only a small piece of ice was remaining. One milliliter of complete RPMI medium containing 10% FBS (RPMI-10) was

added to the stock to bring up temperature while concurrently diluting DMSO of the freeze media. This mixture was then added to 5mL of RPMI-10 and pelleted at 500g for 5 min. The cells were washed twice using RPMI-10 before final resuspension in RPMI-10 in a non-tissue culture treated petri dish. Macrophage colony stimulating factor (M-CSF) was added to this dish at a final concentration of 50ng/mL. Cells were incubated for 5-7 days at 37C and 5% CO2. At the end of incubation, macrophages were harvested by manual scraping and isolation via CD14+ affinity isolation using the MACS column separator according to manufacturer's protocol (Miltenyi Biotec, Germany). Cells were then plated at varying densities for desired assay and rested overnight at 37C, 5% CO2, before infection the following day.

4.2.10 Macrophage infections

Macrophage infections were carried out according to our labs standard protocol. Initially, cells were plated at necessary concentrations as described before. Concurrently, bacteria were cultured as outlined above. At the time of infection, bacterial culture was harvested via centrifugation (4000 rpm, 5-10 min) and washed twice with Sautons medium. The cultures were then resuspended in 2.5mL of Sautons medium and enumerated using OD600 absorbance and a standard conversion factor of 5E8 CFU/mL at OD600 of 1.0. After enumeration, necessary volumes of the bacterial suspensions were diluted into RPMI-10 to achieve the necessary MOI for the experiment. This media was then used to exchange the media on the macrophages. To bring bacteria into contact with cells rapidly, an optional spin at 500g for 5 minutes can be performed.

Macrophages were then returned to incubation for downstream assay specific timepoints.

4.2.11 Macrophage Fractionation

Cells were fractionated to collect paired secreted and cellular fractions from the same sample and query cellular cytokine concentrations. Cells were infected as described. At the time of harvest, cellular supernatants were collected and filtered in a 0.22-micron PVDF low protein binding filter plate for removal from the BSL-3. For the residual monolayer, it was washed x2 with 1x HBSS to remove any residual supernatant. Following wash, the monolayer was lysed using the following protocol. A 100uL aliquot of a 1% Triton x-100 in water solution (containing protease and phosphatase inhibitors) was added to each well. The plates were incubated at RT for 10-20 minutes to allow for complete lysis. The lysate was then agitated using a multichannel pipette to ensure complete lysis before filtration in a 0.22-micron low protein binding filter plate. Filtered fractions were then removed from the BSL-3 and used for downstream assays.

4.2.12 MG132 treatment

MG132 proteasome inhibitor was purchased from Millipore-Sigma (Burlington MA) as a lyophilized powder. 1mg of MG132 was resuspended at 10mM final stock concentration using 210µL of Dimethyl Sulfoxide (DMSO) as an organic solvent. For use in infections, the 10mM stock was diluted to a final concentration of 10µM by diluting 1uL of stock

solution per 1000uL of final media volume (1:1000 Dilution). Media was then exchanged onto cells at the start of Mtb infection and remained for 24 hours.

4.2.13 Acidic Phagosome Staining

LysoTracker Deep Red (L12492) (ThermoFisher, Waltham MA) was used to selectively label acidified compartments within cells. Macrophages were column isolated as described and plated at 5E5/well of a 96 well tissue culture treated plate. These cells were rested overnight and infected with H37Rv or knockout strains at an MOI of 1.0. Infection was carried out for four hours before adding LysoTracker at a final concentration of 100nM. LysoTracker treatment was run for two hours followed by a media exchange with RPMI-10. Treated cells were then measured via Mean Fluorescence Intensity (MFI) at 647nm excitation and 668nm emission using a BioTek Cytation 5 (Agilent, Santa Clara CA).

4.2.14 Enzyme Linked Immunosorbent Assay (ELISA)

DuoSet (R&D Systems, Minneapolis MN) enzyme linked immunosorbent assay (ELISA) was performed on isolated cell fractions, either secreted or cellular. Both fractions were treated the same during the protocol. Briefly, capture antibodies for a target analyte were plated on a ½ area 96 well plate and incubated sealed at room temp (RT) overnight to allow for antibody adherence to the plate. The following day, plates were

washed using 1X PBST to remove the primary antibody solution. Reagent diluent (1%BSA PBS solution) was added to each well for one hour at RT to allow for blocking. Following blocking, plates were washed x3 with PBST then sample added to respective wells at a 1:5 dilution with reagent diluent and incubated for 2 hours at RT. Concurrently, a standard analyte was added to its respective plate to generate a standard curve. Plates were then washed x5 with PBST and detection antibody was added to all wells, including standard analyte wells which was followed by a 1-hour incubation at RT. The plate was then washed x5 with PBST and Streptavidin HRP was added to each well for 20 minutes. Following this, the plates were washed again x5 with PBST and developed with a TMB substrate for 15 minutes and stopped with a 2N sulfuric acid. Plates were immediately read at 450nm absorbance.

4.2.15 Cellular RNA Isolations and Gene Expression Quantitation

To quantify gene expression of target genes in macrophages we performed probe-based gene expression assay approach. Initially, cellular RNA was isolated using a Trizol isolation technique. We resuspended cell monolayers in 1mL of Trizol. RNA was then isolated using the manufactures isolation protocol. Isolated RNA was subsequently quantified using nanodrop. This RNA was then input into a cDNA generation protocol using a high-capacity cDNA reverse transcription kit (Life Technologies, Waltham MA). Resulting cDNA was used in a probe-based, junction spanning, gene expression assay reaction to quantify transcript levels. Briefly, target-specific probe sets were used along with an endogenous control probe targeting human GAPDH (IDT, Coralville IA).

Quantitative PCR (qPCR) was performed to get Ct values of each target in multiplexed samples. Relative quantitation was performed using the ΔΔCt method and converted to fold change expression relative to control for the target of interest (191).

4.2.16 Interferon Beta Reporter Assay

Initially, supernatants from infected macrophages (containing IFNβ) were used to treat a transgenic Huh7 cell line with an IRF3-linked IFNAR. A 1:10 dilution of Macrophage output supernatants were diluted with complete DMEM. Within the Huh7 cell line, binding of IFNAR to IFNβ then leads to the downstream transduction of IRF3 to the MX1 promoter element. MX1 activation leads to the expression of Gaussia luciferase (gLuc). Gaussia luciferase is then secreted by these cells into the supernatant. After 24 hours of IFNβ stimulation on this transgenic cell line, supernatants were collected. These supernatants then mixed 1:1 with a coelenterazine substrate (ThermoFisher, Waltham MA) to measure luminescent signal.

4.2.17 LEGENDplex Cytokine Analysis

Staining was performed according to the manufactures protocol with a custom analyte panel (LEGENDplex, BioLegend CA). As outlined, supernatants were isolated from infected cells and filtered. These supernatants were then added to a bead mixture containing capture beads for our target analytes. These were then washed and bound by a secondary antibody for target detection. A fluorescent reporter was then conjugated

for detection via flow cytometry. Flow analysis resolved analyte bead populations based on color and bead size. Results were analyzed using BioLegend software where standard curves were calculated for respective analytes.

4.2.18 Phospho-eIF2 Alpha Western Blots

Western blots were performed as standard. Initially, macrophages were plated at a concentration of ~2E6 cells per well of a 6 well tissue culture dish. These cells were then infected with respective strains (H37Rv or ΔESX-5c) for 24 hours at an MOI of 5. The following day protein lysates were generated by removing the culture media and lysing cells in 45µL 1x RIPA Buffer (Millipore-Sigma, Burlington MA) containing complete protease and phosphatase inhibitors (Roche, Basel Switzerland). Lysates were then added to 15µL of 4x LDS buffer (ThermoFisher, Waltham MA) and boiled at 100C for 30 minutes. Proteins were then run on a gradient Bis-Tris polyacrylamide gel and transferred to a PVDF membrane using standard transfer approaches. Actin and p-eIF2a were targeted on separate blots using respective antibodies. Of note, only ABCAM anti-p-eIF2a (ab32157) has worked for us to detect this target. Targets were then developed using cell signaling signal fire ECL reagent (Danvers, MA) and imaged on a LICOR C-DiGit chemiluminescent imager (LICOR, Lincoln NE).

4.2.19 Caspase -1 Activity

Caspase activity was measured using a Caspase-Glo 1 Inflammasome Assay (Promega, Madison WI). Kit instructions were followed to measure the caspase activation upstream of IL-1β cleavage. Briefly, cells were infected with Mtb populations as outlined. We then added our detection substrate to the cells and measured luminescence using a Cytation 5 plate reader (Agilent, Santa Clara CA). Luminescent signal specific to Casp-1 activity was determined via the inclusion of a control inhibitor to identify background Caspase activity for apoptosis-linked caspases.

4.3 Results

4.3.1 In Silico Analysis of Exchange Regions

We sought to delete these paralogous structures (ESX-5a, ESX-5b, and ESX-5c) from the Mtb genome using a recombineering method that relies on the RecET enzymes of the CheC9 Mycobacteriophage under control of a synthetic, nitrile-responsive promoter. Via this method we were able to target the three discrete regions of the Mtb genome with high specificity. By designing exchange constructs with 500 base pair homology arms flanking the region of interest, we enhance specificity barring any homologous structures flanking these regions. All three paralogs were screened via *in silico* analysis for up and downstream genetic motifs that could interfere with the specific targeting of the exchange constructs. We identified an insertion element flanking the ESX-5b and ESX-5a loci. Specifically, we identified an IS1081 transposase flanking ESX-5b. There are 7 additional annotated IS1081 elements in the Mtb genome. To avoid any possibility

that alternative IS1081 elements interfere with allelic exchange efficiency, we designed the knockout template to remove this vestigial transposase along with the ESX-5b cluster. IS1650 flanks the ESX-5a cluster but only repeats once in the Mtb chromosome and as such we attempted allelic exchange without the removal of this transposase to minimize off target perturbations to the genome.

A

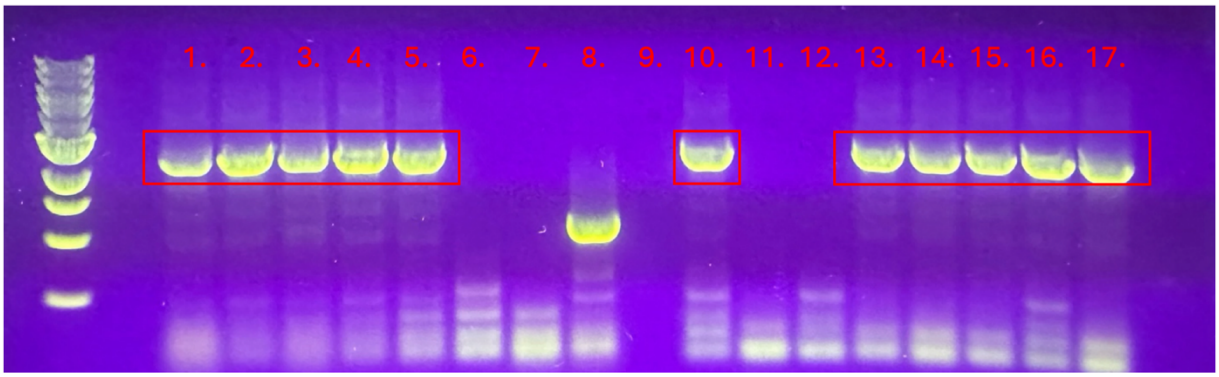

B

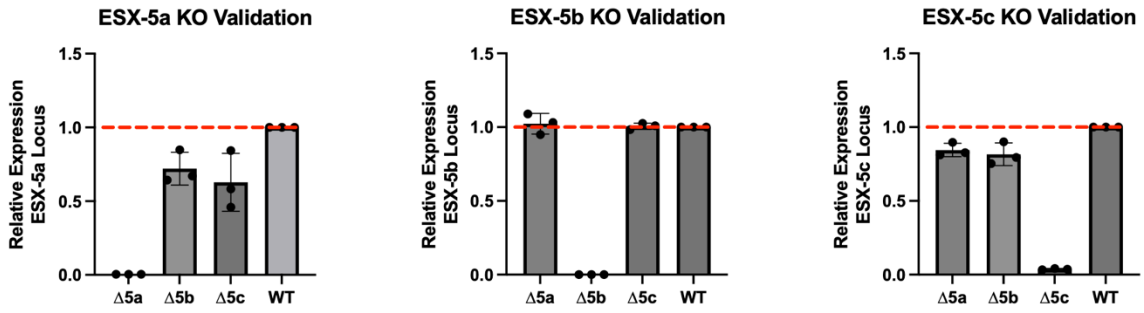

Figure 4.1 – Validation of ESX-5 Paralog Deletions via PCR and qPCR Amplification. 4.1A. PCR Gel Image for Hygromycin cassette amplification. Sixteen total clones were tested for Hygromycin cassette insertion via gene amplification, numbers indicate gel lane and target (1-5 = Δ5a, 6-8 & 10-12 = Δ5b, 13-17 = Δ5c), red boxes indicate amplification fragment of ~2200 base pairs corresponding to insert gene length and successful recombination. 4.1B. qPCR of deleted gene targets. Bar graph depicts fold change expression (y axis) of ESX-5a, ESX-5b, and ESX-5c gene cluster expression in respective deletion mutants (x axis). Title indicates gene target being measured, red dotted line indicates wildtype expression level for a given gene target. Analysis run in triplicate, error bars denote standard deviation of the mean.

4.3.2 Validation of Paralog Knockouts Demonstrates Deletion of Gene Regions.

To verify the complete removal of these loci from their respective parent strain we deployed concurrent, orthogonal approaches. Phenotypic analysis showed that primary colonies that were picked and expanded in selective rich broth grew normally, indicating a high degree of hygromycin resistance not found in the parental strain used to generate knockouts. We collected genomic DNA from these strains and designed several PCR reactions to amplify target regions in these knockouts. Ultimately, we designed a PCR reaction that amplified the Hygromycin resistance marker. Only clones with successful integration of the exchange template should amplify the hygromycin marker (**Figure 4.1A**). We demonstrated most of our phenotypically resistant clones also yield strong bands at ~2200 base pairs of length, corresponding to the length of the promoter and gene region of the hygromycin resistance cluster. To negate any risk that we amplified residual exchange template DNA, we also queried gene expression of the target clusters using TaqMan probes (Applied Biosystems, Waltham MA). Given these structures are operonic in nature and therefore polycistronic, we designed probes targeting coding regions of genes that have low homology with other genes in the Mtb chromosome, ensuring specificity. Quantitative PCR revealed our target genes were indeed bordering at or near undetectable (**Figure 4.1B).** Lastly, we sanger sequenced the junctions of our target regions to ensure the chromosome was altered at the desired position. By designing primers that flank upstream of the target regions and sequencing into the knockout region we were able to show the presence of the hygromycin resistance cassette where the original paralogs would be

(sequencing data not shown). With this successive validation approach, we were confident in the removal of these gene clusters from Mtb.

4.3.3 Paralog Knockouts Display Intact Replication Phenotypes in Human Macrophages and Rich Broth

With the putative role of these clusters being involved in virulence, we also tested if the deletion of these clusters alters the ability of macrophages to clear these bacteria relative to WT. As mentioned, innate macrophage responses will fail to restrict Mtb without T cell help via IFN-gamma activation. To test if these mutants are attenuated, we performed a CFU assay based on a 72-hour infection model where we let bacteria replicate within cells prior to cell death and lysis. Across six donors, we observed no difference in replication for all strains (**Figure 4.2A**). This result indicates there are no macrophage specific attenuations we introduced to these bacteria via these paralog deletions. Additionally, we assessed growth of these strains in 7H9 rich broth and showed no difference in growth for wildtype and knockout strains across ten independent growth experiments (**Figure 4.2B**). Together these data indicate these deletions impart no growth defect or attenuation in either macrophages or rich broth environments.

4.3.4 Lysotracker Staining of Acidified Organelles Demonstrates ESX-5c Dependent Reduction at Early Infection Time Points.

Previous studies have demonstrated that Mtb antagonizes the phagosome(91,129,133). Not only does Mtb escape this organelle, but it is also able to exclude key maturation moieties that facilitate the destruction of cargo and promote acidification. The prevention of acidification is key to Mtb surviving long enough to potentiate infection to the next cell. We know from previous work that ESX-1 is essential for phagosomal antagonism and tested phagosome acidification levels using our mutants to determine if there were any ESX-5 dependent impacts on acidified compartments. We tested early phagosome acidification levels looking at mean fluorescence intensity using lysotracker red four hours post infection. We reasoned this is early enough to see if there are direct impacts on Mtb's ability to subvert maturation processes but avoid potentially confounding late-stage maturation events such as autophagosome formation. We observed little difference in the MFI level of acidified compartments across three biological donors and strain conditions; however, we did see small differences. Notably, in two of our three donors we observed ∆5c mutant infected cells contain a lower level of acidified compartments relative to H37Rv infected. The other two mutants were not significantly different (**Figure 4.2C**).

4.3.5 Proinflammatory Cytokine Profiles are Strongly Reduced in Macrophages During Paralog Knockout Infections.

By removing these loci from Mtb, we generated a tool for interrogating early human macrophage responses to H37Rv Mtb in the absence of these clusters. Initially, we performed profiling experiments to characterize differences in the cellular response of

macrophages to these different strains. We reasoned that the putative role of these genes as virulence factors could lead to an impact on early macrophage responses. A 24-hour infection revealed that these primary human MDMs synthesize significantly reduced proinflammatory cytokine profiles when infected with our deletion strains (**Figure 4.2D**). Wildtype H37Rv induced levels of cytokine synthesis similar to what we've seen previously (**Figure 4.2D**). Restoration of locus expression via a trans-acting complementation approach completely restored wildtype levels of expression, in some cases inducing higher than wildtype expression levels (**Supplemental Figure 4.1A-C**). Importantly, mutant strains also do not appear to differentially impact cell viability (**Supplemental Figure 4.2**)

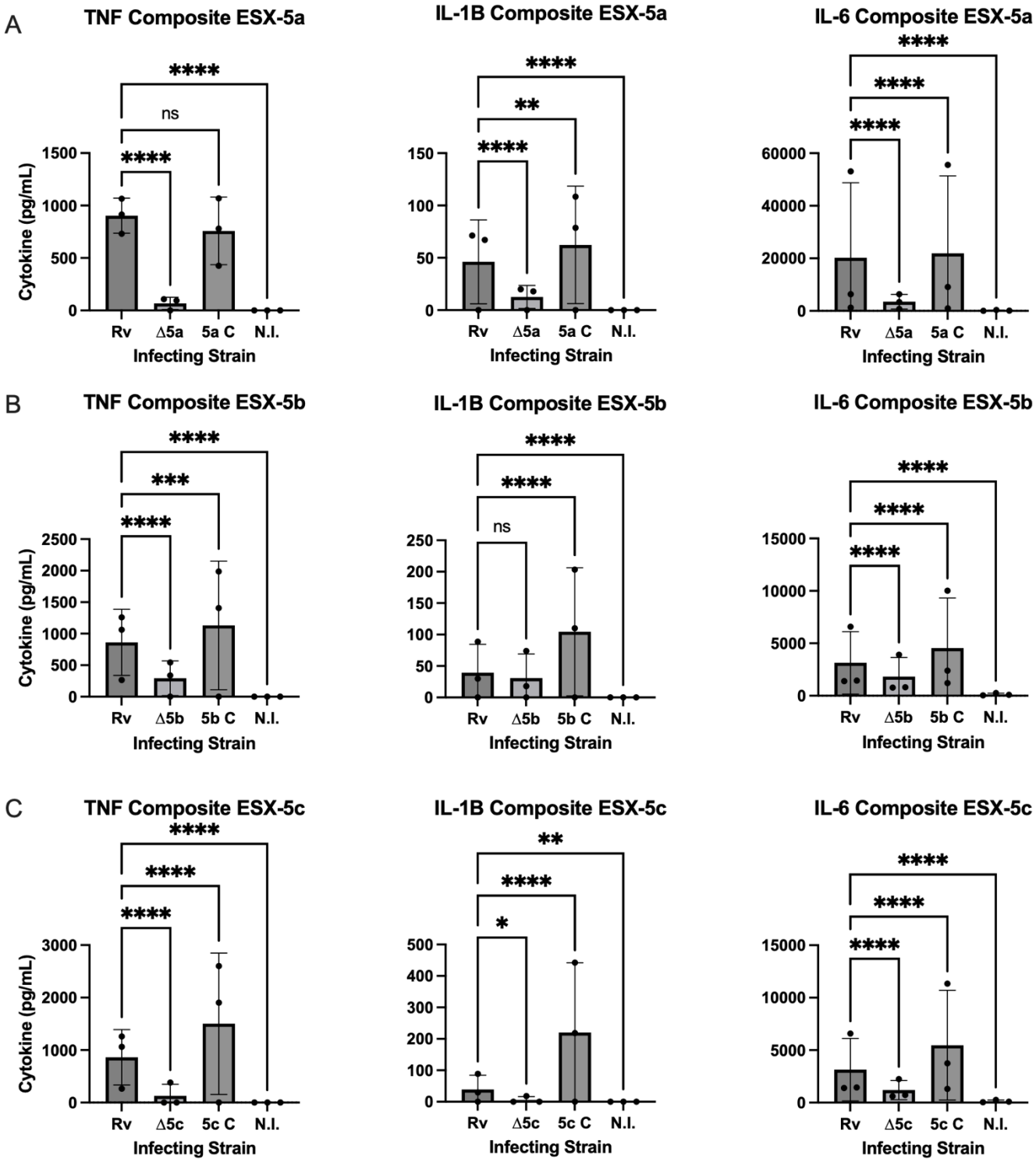

Supplemental Figure 4.1 – Complementation of paralogs ablates deletion phenotype. SF4.1A. Graphs display TNF, IL-6 and IL-1β levels across H37Rv (Rv), Δ5a, Δ5a complement (5a C), and not infected control (N.I.). SF4.1B. Graphs show same comparison but for Δ5b and 5b complement (5b C). SF4.1C. Graphs show same

comparison but for Δ5c and 5c complement (5c C). SF4.1A-C. Bar charts show expression levels for respective cytokines within a given comparison of a deletion mutant and its complement strain. For all graphs, y axis denotes concentration of the cytokine in picograms/milliliter while x axis shows the infecting strain used. Each condition was performed with N=3 biological donors in a minimum technical triplicate. Statistics for all graphs calculated using two-way ANOVA with a post-hoc T-test and Dunnett correction for multiple comparisons (95% Confidence interval, p≤0.05). Error bars show standard deviation around the mean.

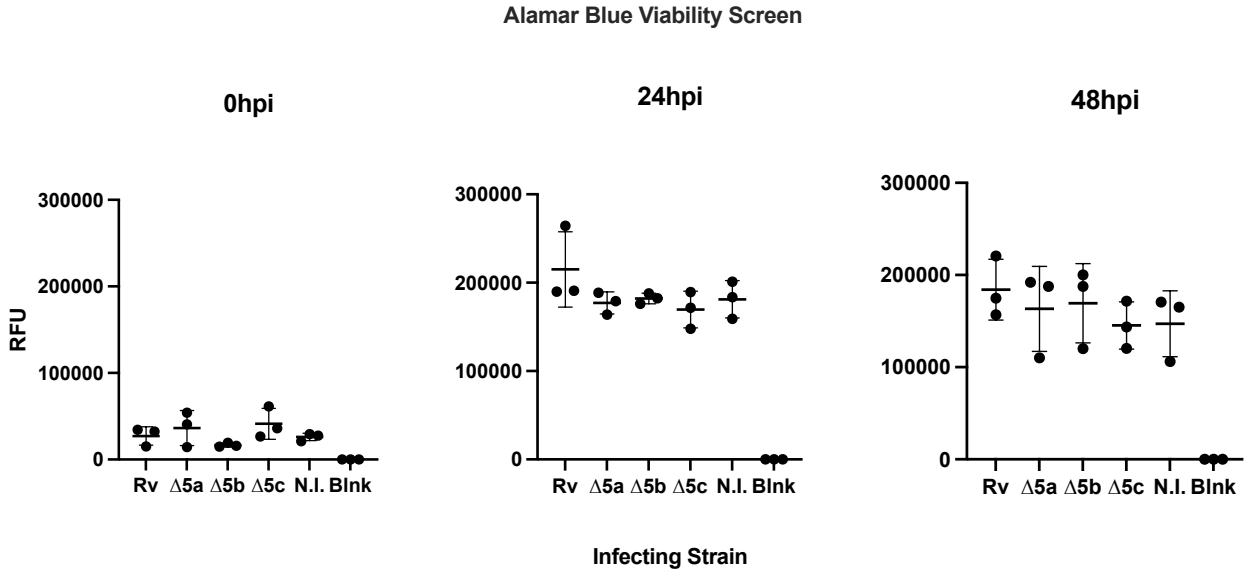

Supplemental Figure 4.2 – Macrophage cell health is not ESX-5 dependent during in vitro infection. Dot plots display the RFU measurement (y-axis) from cells treated with Alamar Blue and infected with varying strains of Mtb (x-axis, N.I. = uninfected, blnk = media only). Graphs depict respective time point measurements evaluating accumulated level of reduced Alamar Blue (saturation reached at 24hpi, decay observed at 48hpi). Error bars show standard deviation of the mean.

4.3.6 Bacterial viability is required for impact on cytokine synthesis

Despite wildtype levels of RNA induction, we wanted to validate that the mutations we generated did not alter the ligand-receptor interaction landscape of these strains in a way that reduces cytokine output via reduced receptor engagement. Additionally, to shed light on whether the cytokine effect we observe is due to an active process or a

static change in these bacteria we performed an infection of MDMs with fixed and inactivated bacteria. The fixation of all strains using 4% paraformaldehyde, coupled with extensive washing, allows for us to determine if the viability state of these bacteria impacts our observed cytokine phenotype. Once bacteria were inactivated, we infected MDMs as described and collected the secreted fraction for analysis via ELISA. Results demonstrate that the viability of the bacteria is essential for the cytokine suppression effect we observe with our knockout mutants. Specifically, we see across donors there is no reduction in the levels of secreted cytokine detectable in the mutant infected condition relative to wild type (**Figure 4.2E**). This result indicates that the effect we observe is likely due to an active process within these bacteria and is not due to an intrinsic or passive effect we have generated via the knockouts. Taken together these data suggest that not only are the effects specific to the knockouts, but that the viability state of these bacteria is essential for the phenotype, implying an active process altering the cytokine profile.

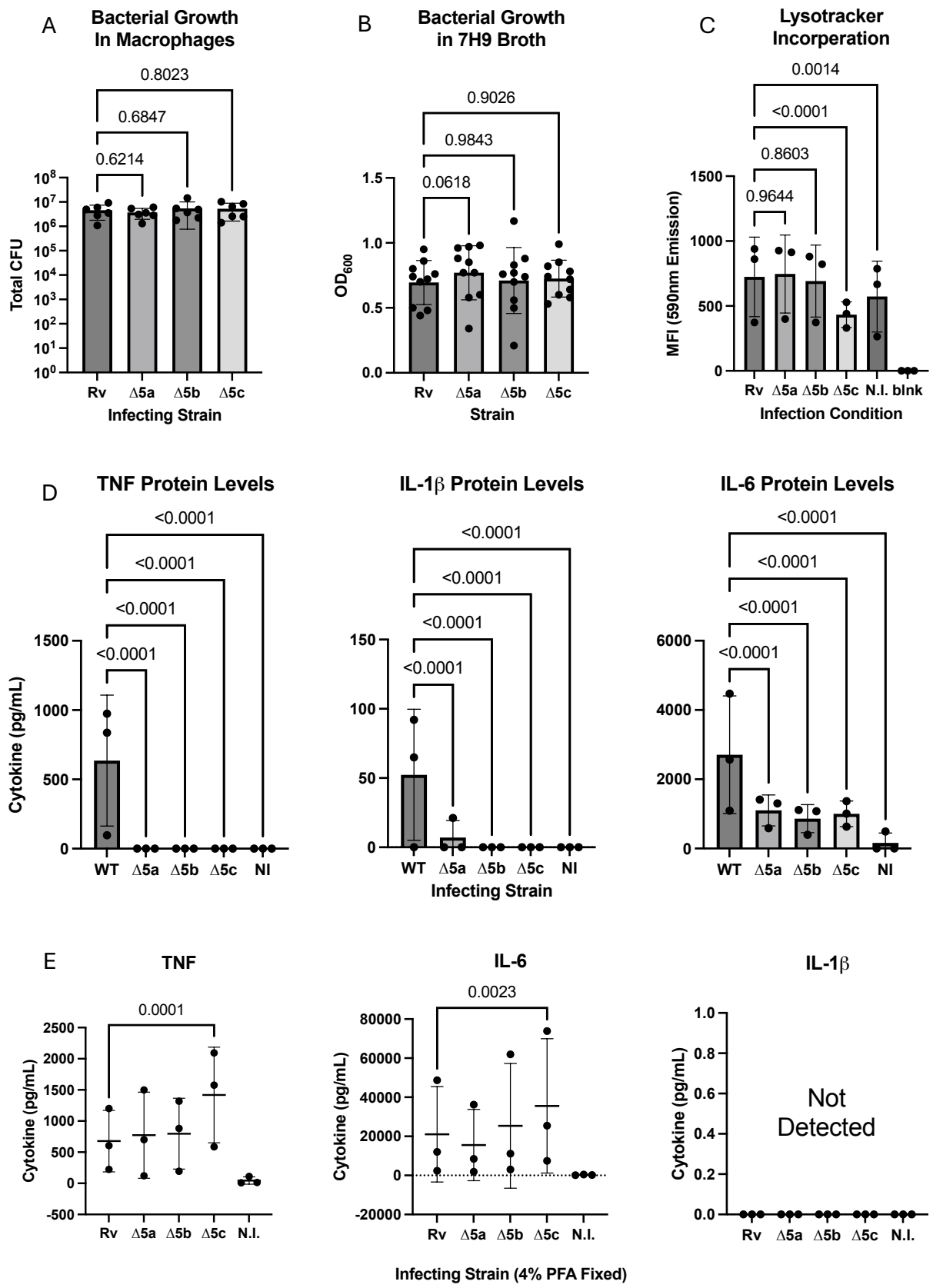

Figure 4.2 – ESX-5 paralog deletion mutants induce differential inflammatory

profiles in infected monocyte-derived macrophages. *4.2A. Mutations do not impact bacterial fitness in macrophages.* Bar chart displays 72hr replication rates via CFU recovered from N=6 infected donors. X axis displays infecting strain, y axis displays CFU recovered in Log10 scale. *4.2B. Knockout growth is not attenuated in broth culture.* Bar chart displays broth replication levels for all knockout and wildtype strains. X axis displays strain and y axis displays OD600 as a measure of growth. Statistics calculated on N=10 replicate values using one-way ANOVA with a post-hoc T-test and Dunnett correction for multiple comparisons (95% Confidence interval, $p \leq 0.05$). Error bars show standard deviation around the mean. *4.2C. Mutations may alter bacterial interaction with acidic organelles.* Bar chart displays acidic organelle staining in macrophages 6 hours post infection (6hpi). Infecting strain is on the x axis ("N.I." is uninfected control, "No LT" is no lysotracker control) and mean fluorescence intensity on the y axis. Dots represent N=3 biological donors run in technical triplicate. *4.2D. Mutants induce altered cytokine profile.* Bar charts each depict proinflammatory cytokine (TNF, IL-1B or IL-6) abundance after Mtb infection. For each bar chart y axis represents the protein level for a respective target in picograms per milliliter. Infecting Strain condition is displayed on the x axis. Dots represent N=3 distinct donors run in minimum of technical triplicate. *4.2E. Bacterial inactivation restores cytokine production.* Dot plots show cytokine protein level (TNF, IL-6, IL-1β) from cells infected with 4% PFA inactivated strains. Y axis shows respective cytokine in picograms per milliliter, x axis shows the strain used for infection along with the uninfected control (N.I.). All dots for a given column represent an individual biological donor run in minimum technical triplicate. 4.2A,4.2C-E. Statistics calculated using two-way ANOVA with a post-hoc T-test and Dunnett correction for multiple comparisons (95% Confidence interval, $p \leq 0.05$). Error bars show standard deviation around the mean.

4.3.7 Bacterial Uptake is not differential between strains

To understand if cytokine decreases spanning cytokine classes is due to a reduction in bacterial uptake and therefore less signal transduction, we performed an experiment comparing phagocytosis rates of the WT strain to our mutants. Cells were infected at an MOI of 1 for ~4 hours to allow for phagocytosis to occur (192). As performed for replication assays, we deployed a CFU readout to enumerate phagocytosed bacteria. Media was removed and the monolayers were washed to remove extracellular bacteria. Monolayers were lysed and bacteria plated. We observed that there are no strain-dependent differences in the number of bacteria phagocytosed at this early time point.

On a donor-by-donor basis, all three donors showed no significant difference, and this trend held when donors were analyzed as composite (**Figure 4.3A**) via two-way ANOVA with post hoc T-test (95% CI, P≤0.05, Dunnett correction).

4.3.8 RNA induction at early and medium timepoints is not impacted

The generation of robust cytokine responses is due in part to the initiation of signaling cascades, which drive the expression of pro inflammatory transcripts. Uptake is no different between these strains, indicating the level of inflammatory stimulus delivered to cells is not divergent between mutants and wild type bacteria. To determine if the transduction of inflammatory signals by TLR's, CLR's, and other receptors leads to an altered RNA landscape responsible for decreased cytokine output, we performed quantitative PCR (qPCR) looking at transcripts for IFNβ, IL-1β, TNF, and IL-6. Infected cells were harvested at 6 hours post infection using 1 mL of Trizol reagent before extracting total RNA from the sample. Subsequent cDNA generation and qPCR analysis revealed there is no difference between the amount of proinflammatory cytokine transcript within cells across paired WT and mutant conditions. Timepoint and MOI variables alter RNA levels but do not change significance levels between comparable groups. Composite analysis across N=3 biologically independent donors shows no difference reaching significance between the groups (**Figure 4.3B)**. A partial analysis of RNA profiles at 24-hour post infection revealed levels stay similar in the conditions we examined, never reaching significant differences between strain groups (**Supplemental Figure 4.3**).

4.3.9 Protein is not trapped within the cellular compartment

Previously, it has been demonstrated that other pathogenic Mycobacteria can antagonize the export of protein as a way of subverting immune responses and signaling between cells. By preventing the translocation of peptides into the endoplasmic reticulum (ER), *Mycobacterium abscessus* effectively shuts down protein export (193–195). We reasoned that Mtb could also possess mechanisms that antagonize proper localization or secretion of proteins, effectively trapping protein cellularly. To test this we fractionated cells, first collecting the secreted fraction then the paired cellular lysates using a gentle lysis reaction. We detected the same phenotype we observed previously with decreased secreted proinflammatory output from MDMs infected with any of our knockout mutants (**Figure 4.3C**). Additionally, we observed in cellular fractions that this phenotype is consistent in conditions where cytokines were detectable (IL-1β, IL-6) (**Figure 4.3C**). The absence of increased cellular cytokine indicated to us that these targets are likely not retained within the cellular fraction. However, we also reasoned that cellular retention may subject proteins to proteasomal degradation before the timepoint we analyzed. To ensure excess protein was not degraded in the cytosol before collection at 24hpi, we treated cells with a proteasome inhibitor (MG132) at the time of infection and performed an identical fractionation experiment. With or without this inhibitor, cellular lysates and supernatants display the same phenotype of reduced cytokine across all conditions (**Figure 4.3C-4.3D**). Together these data suggest that regulation of cytokine production likely occurs upstream of

protein synthesis, via translational antagonism or target-specific post transcriptional regulation.

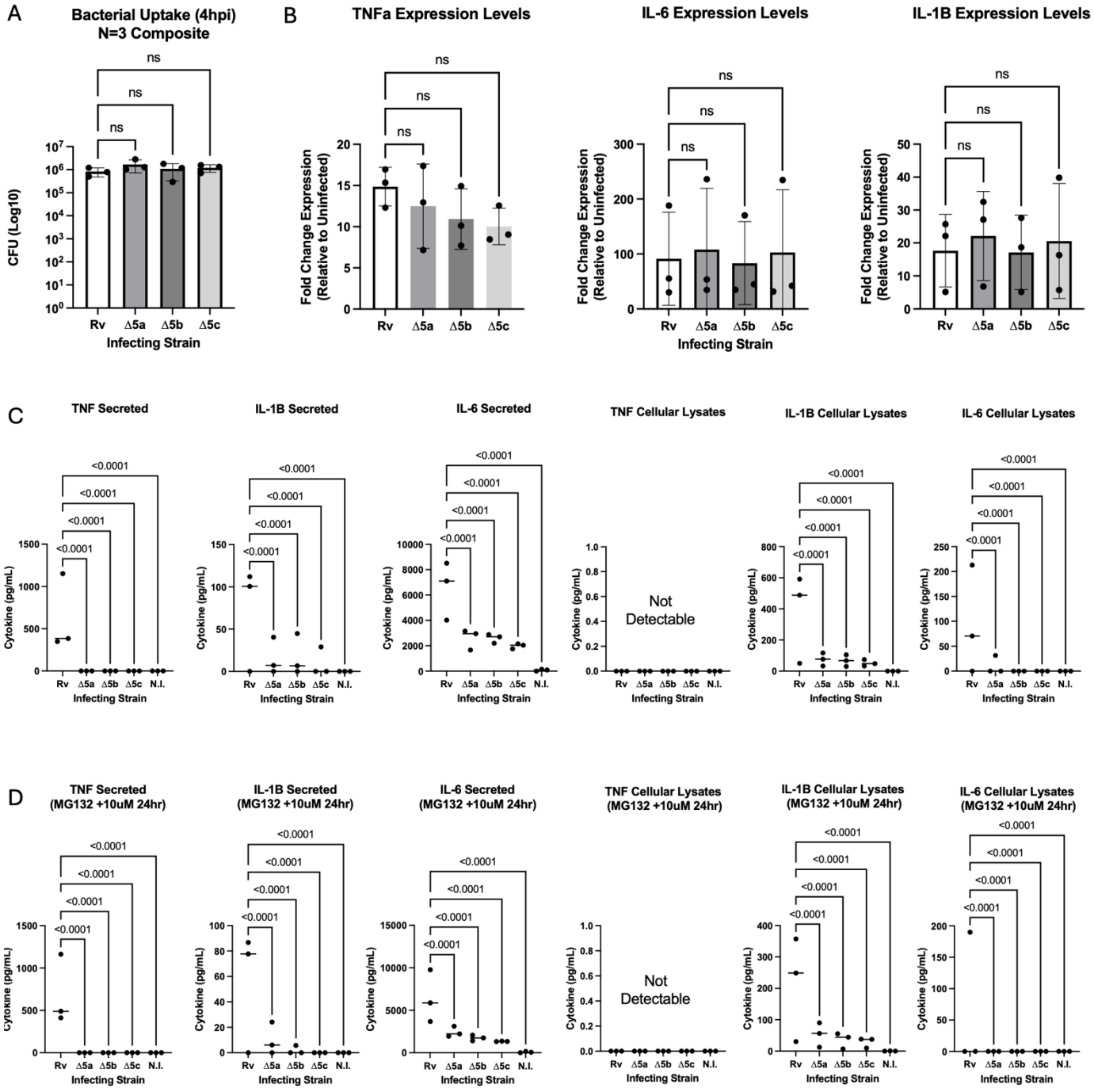

Figure 4.3 – Paralog deletions alter cytokine levels upstream of protein export but leave early cellular responses intact. 4.3A. Bacterial uptake is unchanged across mutant strains. Bar plot display 4-hour phagocytosis levels measured via CFU. X axis displays the respective strain used for infection (MOI 1) and y axis displays total CFU returned from a given infection in Log10 format. Individual dots by column represent the spread of three donors run in technical triplicate. 4.3B. RNA induction is comparable across strains. Bar charts represent the relative expression of target transcripts (TNF, IL-

6, and IL-1β) across infection conditions. For all graphs, x axis denotes the strain used for the infection (MOI 5), y axis shows the fold change expression of the respective target gene relative to uninfected cells. Dots represent the spread of N=3 distinct donors run in technical singlet. 4.3C. Cytokine is not retained with the cellular fraction of infected cells. Dot plots represent the cytokine levels (TNF, IL-6, IL-1β) for either secreted or cellular (internal) fractions of infected cells denoted by graph title. Y axis shows the quantity of target cytokine across conditions in picograms per milliliter while x axis shows the respective strain used for infection (MOI 5). N.I. is uninfected control. Dots represent individual donors run in technical triplicate. 4.3D. Proteasome inhibition does not rescue cytokine production. Dot plots display same data as 4.3C graphs but display cytokine production for respective conditions under the treatment of cells with 10μM MG132 to inhibit proteasome function. 4.3A-4.3D. Statistics for all analyses generated using two-way ANOVA with post-hoc T-test and Dunnett correction for multiple comparisons (95% confidence interval, p≤0.05). Error bars show standard deviation around the mean.

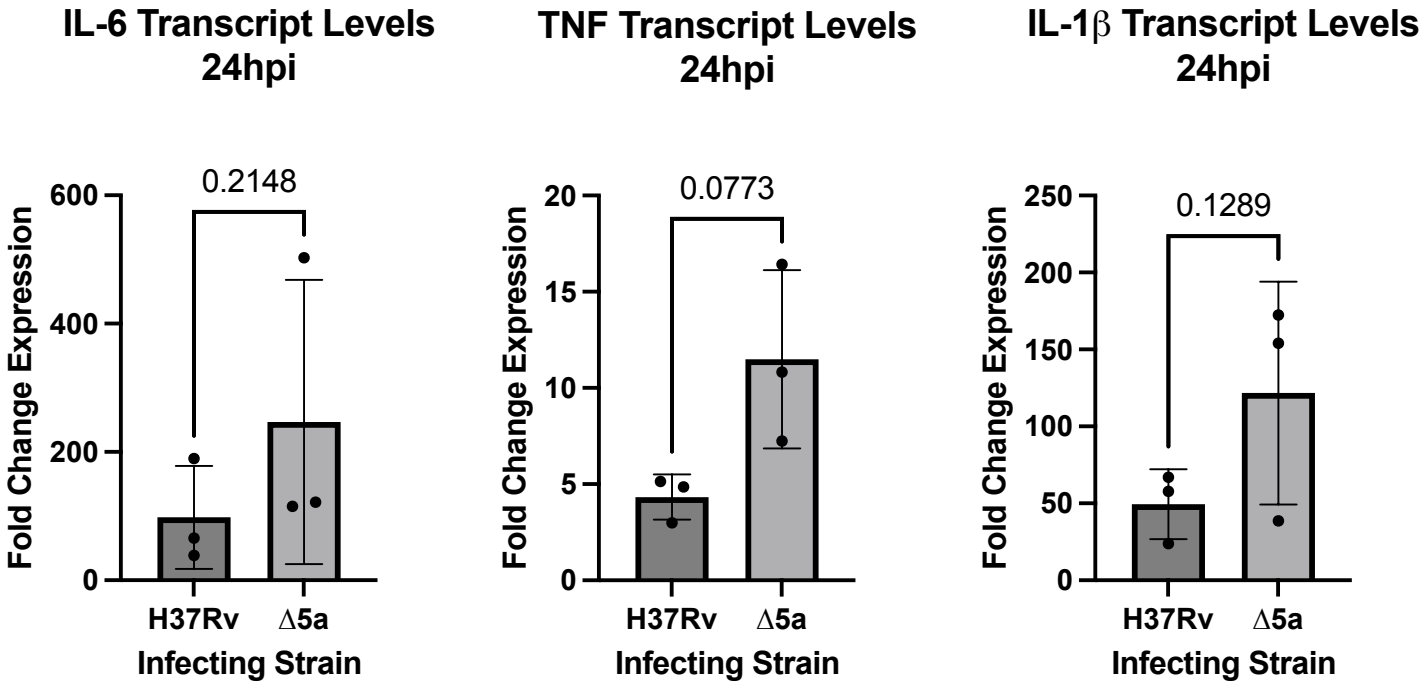

Supplemental Figure 4.3 – ESX-5 and macrophage 24-hour cytokine mRNA expression. SF4. RNA induction is non-significant across wild type and Δ5a mutant at 24hrs post infection. Bar charts represent the relative expression of target transcripts (TNF, IL-6, and IL-1β) across infection conditions. For all graphs, x axis denotes the strain used for the infection, y axis shows the fold change expression of the respective target gene relative to uninfected cells after 24 hours of infection. Dots represent the spread of N=3 distinct donors run in technical singlet. Statistics for all analyses generated using paired, two-tailed T-test (95% confidence interval, p≤0.05). Error bars show standard deviation of the sample mean.

4.3.10 Proinflammatory Cytokine Reduction is Class Spanning, Impacting Interferon Beta

To gain additional cellular insight into the impact mutant infection has on cellular cytokine outputs, we queried the Type-I Interferon response in these infected macrophages, specifically interferon beta (IFNβ). To test this, we deployed a cellular reporter-based approach. Direct measurements via capture ELISA were also performed but failed to resolve reliable concentrations. As seen with other cytokines, IFNβ levels were significantly reduced across various infectious doses with any of our three mutant strains as compared to wildtype (**Figure 4.4A)**. This result is interesting given the difference of IFNβ induction and synthesis pathways compared to alternative cytokines in macrophages. Specifically, we know Mtb signals through nucleic acid sensing toll like receptors (TLR's) to trigger IFNβ induction within macrophages. This is divergent from interleukins and TNF, suggesting a mechanism of regulation that is shared between these classes.

4.3.11 Extended cytokine analysis reveals differential impact on alternative Mtb induced macrophage cytokines

The reduction of cytokine level in both secreted and cellular fractions in conjuncture with normal levels of transcript suggest post-transcriptional or translational levels of regulation governing the observed cytokine phenotype. We reasoned that a broader

examination of cytokines at the protein level could provide insight into how extensive the effect is and afford possible insight into co-regulatory networks of cytokines that have been studied in the past (196–198). To discern between these mechanisms, we deployed several orthogonal approaches to determine the breadth of impact on cytokine families. We reasoned that spanning effects for all Mtb inducible cytokine would point towards a global level of regulation, such as translation antagonism, whereas discrete reduction for specific cytokine species would indicate transcript level regulation. To begin testing this, we examined an additional five cytokine targets, four via orthogonal approaches. We first leveraged our standard ELISA approach to investigate the levels of IL-8 (CXCL8), a highly expressed macrophage cytokine. As expected, we observed highly detectable IL-8 in infected and uninfected macrophages indicating a high baseline for this target, even in uninfected cells. Comparing mutant vs. wildtype cytokine induction levels, we observed that ΔESX-5a, ΔESX-5b, and ΔESX-5c elicit comparable levels of IL-8 to wildtype in macrophages (**Figure 4.4B**). This result suggests certain cytokine species may be differentially regulated. However, because this cytokine is already potently expressed, possibly obscuring Mtb-dependent effects, we aimed to find additional targets that display this trend. Accordingly, we used a LEGENDplex (BioLegend, San Diego CA) bead-based array to examine four additional cytokines (CCL3, CCL4, CCL5, and GM-CSF) that were previously shown to be expressed in macrophages during Mtb infection (199). Applying this approach to five independent donors (N=5) we demonstrated three additional cytokines (CCL3, CCL5, and GM-CSF) match prior trends of reduction under knockout infection (**Figure 4.4C).** Notably, CCL4 (known as MIP-1β) displayed no difference between strains, much like IL-8. We

observed CCL4 is highly inducible during MTB infection, but variable across donors in terms of magnitude (**Figure 4.4C**). To account for this high degree of variability we normalized the concentration values using a log transformation, which better allows us to fit the assumptions of our statistical test and reduce large outlier impact. We observed uninfected macrophages produce very low levels of CCL4 at baseline (~10-50 pg/mL, **Figure 4.4C**), indicating CCL4 is a highly inducible target during Mtb infection and is robustly divergent from other targets in showing no impact by infecting strain. Together, this differential regulation of specific transcript species possibly indicates target-specific mechanisms influencing the levels of cytokine synthesized during mutant infection of MDMs. However, CCL4 and IL-8 levels do not recapitulate any previously known co-regulatory networks that would provide insight into the cellular mechanism producing this phenotype.

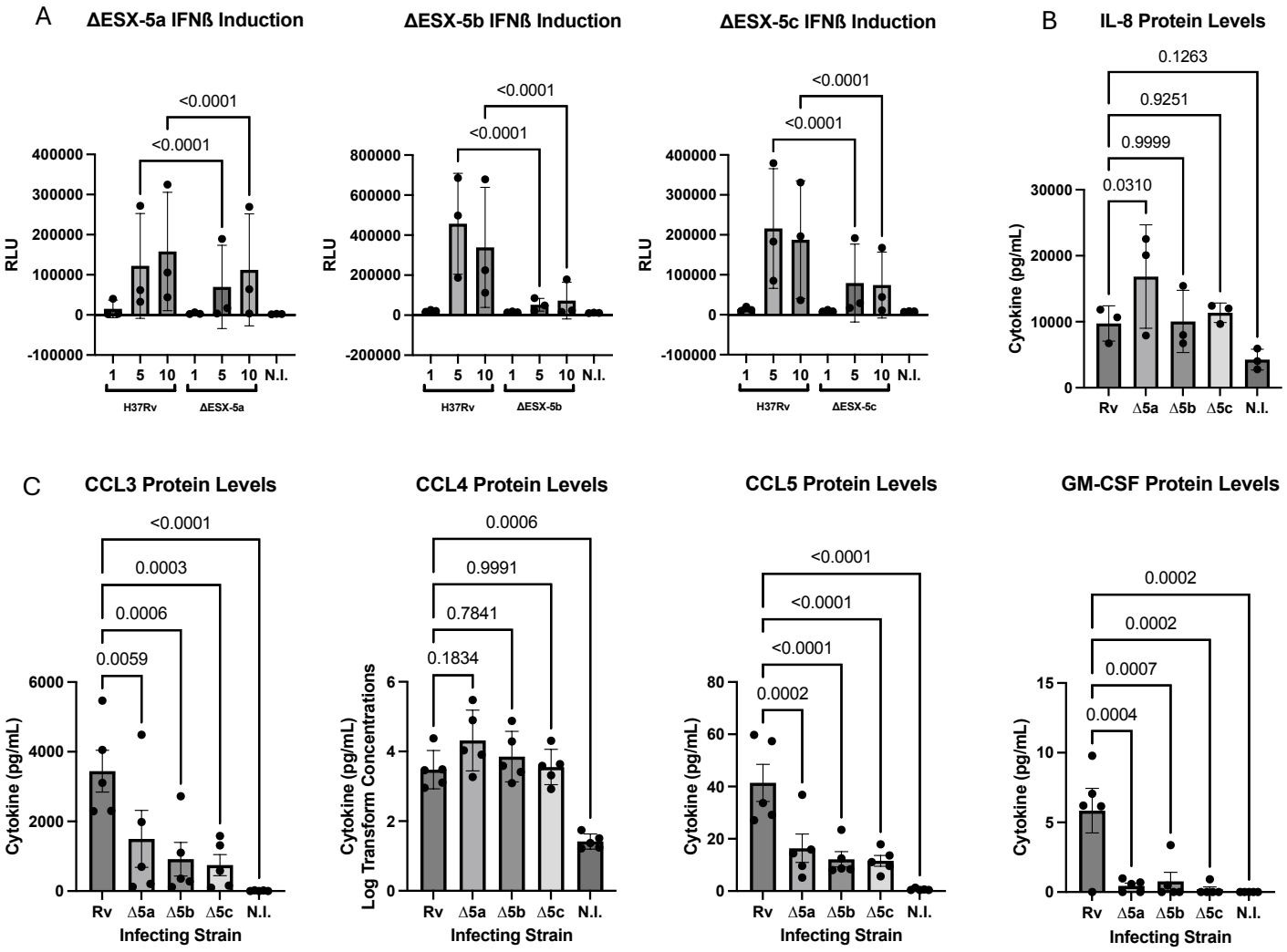

Figure 4.4 – ESX-5 regulates Mtb-induced signaling in macrophages with cytokine specificity *4.4A. ESX-5 and IFN-beta*. Bar charts show the level of interferon beta (IFN-β) across a bacterial dose curve comparing wildtype and a respective knockout strain. X axis for all plots displays the infecting strain and respective bacterial dose (MOI) along with the uninfected control (N.I.). Y axis shows relative luminescence units (RLU) for amount of reporter produced in response to IFNβ levels for that condition. Dots for every group represent N=3 donors run in technical triplicate. *4.4B. IL-8 levels are unaffected by ESX5 deletion mutants*. Bar chart shows the level of IL-8 expression across infection. Y axis shows concentration in picograms per milliliter while x axis shows infecting strain along with N.I. (uninfected control). Dots for every group represent N=3 donors run in technical triplicate. *4.4C. Chemokines display heterogenous reduction profile.* Bar charts display protein levels for four distinct chemokines and cytokines across infection conditions. Y axis shows cytokine concentrations in picograms per milliliter and x axis shows the infecting strain. CCL4 shows log transformed concentrations on y axis due to abnormal data across infection conditions (negative Shapiro-Wilk normality test). Dots represent N=5 biological donors run in technical singlet. 4.4A-C. Statistics for all analyses generated using two-way ANOVA with post-hoc T-test and Dunnett correction for multiple comparisons (95% CI, p≤0.05). Error bars show standard deviation around the mean.

4.3.12 Micro RNA Analysis of Mtb Infected Cells to Define Changes in the Micro RNA Landscape

It has been demonstrated previously that Mycobacteria induce potent and differential micro-RNA profiles in phagocytes. Given the role of miRNA profiles in post-transcriptionally shaping the protein response to infection, we examined the miRNA profile of cells infected with our mutants vs H37Rv to understand the possible roll miRNAs may contribute to our cytokine effect. Leveraging a direct probe hybridization approach called nCounter (Nanostring, Seattle WA), we measured the levels of ~800 biologically active and functional miRNA species across an N=3 donor set in response to wildtype and knockout infection. We initially set a threshold (inclusion ≥50 probes per sample) to remove lowly or inconsistently detected targets. This resulted in 130 detected targets meeting inclusion criteria **(Figure 4.5A)**. Of these targets, one probe showed a trending difference across infecting strains (hsa-miR-4454+hsa-miR-7975) with all three mutants eliciting more expression of this target compared to H37Rv infected cells and the Rv vs. ∆5c comparison approaching significance (**Figure 4.5B**). Human miR-4454 has been previously suggested to regulate NFkB (200). Together, these analyses indicate our knockout strains elicit a highly similar but slightly distinct miRNA profile as compared to H37Rv which may play a role in our cytokine effect via post-transcriptional regulation.

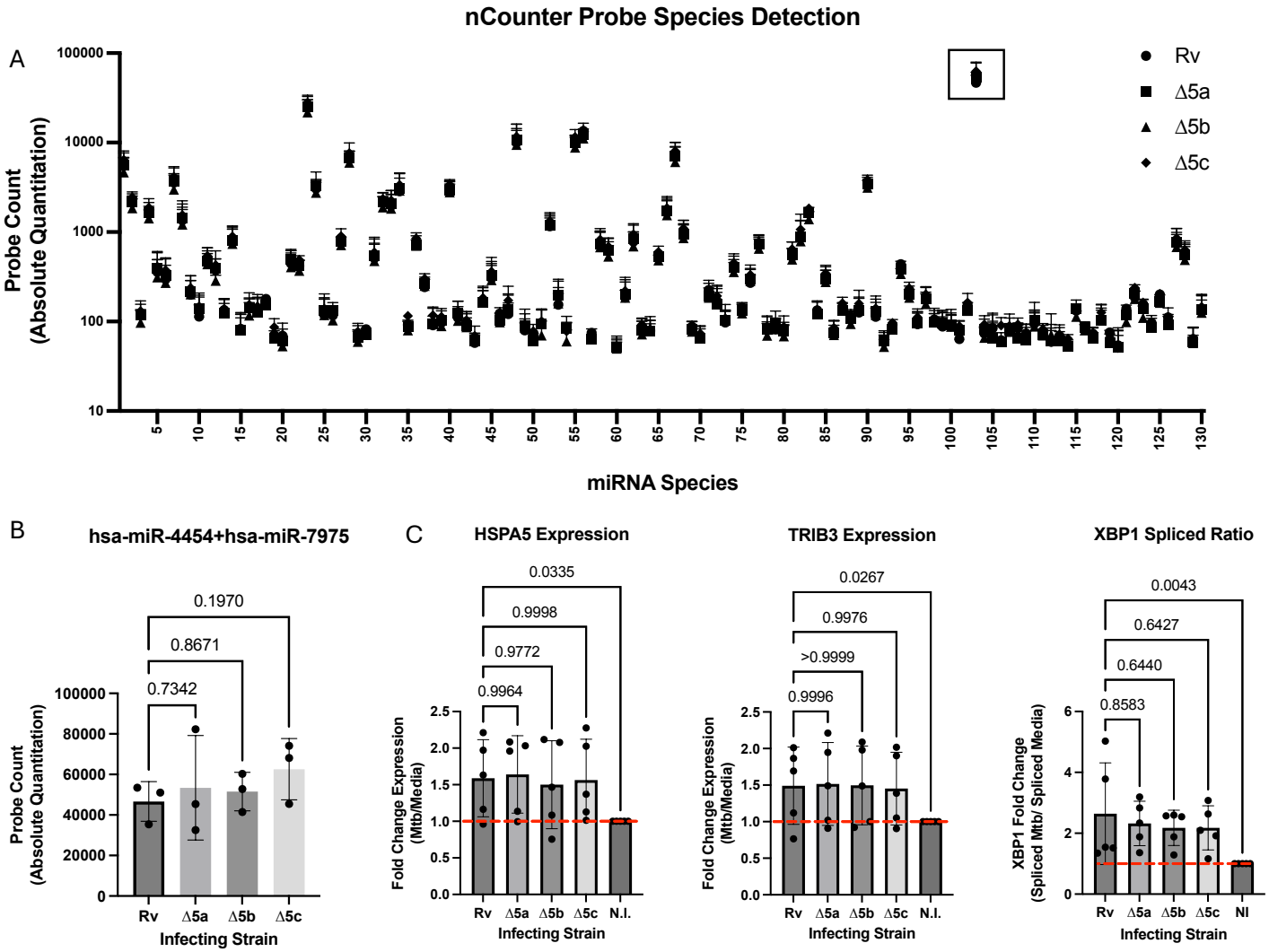

Figure 4.5 –miRNA and UPR responses are not ESX-5 dependent. *4.5A. Dot plot shows quantitation levels of Mtb inducible microRNA species in human macrophages using nCounter absolute quantitation.* Y axis shows the absolute number of probes detected while x axis shows respective microRNA species assigned by number (1-130). The included miRNA data has been baseline subtracted to remove lowly detected or inconsistently detected probe sets (removal of 697 probes). Dot shape correlates with respective strain used for infection within a given microRNA target (Circle = H37Rv, Square = Δ5a, Triangle = Δ5b, and Diamond = Δ5c). Black square represents highest abundance probe set detected for all samples, hsa-miR-4454+ hsa-miR-7975. All samples were run in biological triplicate for all strains. Error bars show standard deviation around the mean of N=3 samples per condition. *4.5B. Bar chart shows probe count across strains for probe target hsa-miR-4454+ hsa-miR-7975.* Y axis shows absolute probe count and x axis shows the infecting strain used. Dots represent individual biological donors (N=3) run in technical triplicate for each infection. *4.5C. Bar chart shows levels of*

respective UPR and ISR targets HSPA5, TRIB3, and spliced XBP1, respectively. Y axis represents fold change gene expression of the target over the control (Uninfected control). X axis shows the infecting strain used for given samples (N.I. is uninfected control cells). Red line denotes baseline expression across targets. Dots are representative of N=5 biological donors run in technical singlet for HSPA5 and TRIB3 while technical duplicate for XBP1. 4.5B-C. Error bars show standard deviation of the mean. Statistics for all analyses generated using two-way ANOVA with post-hoc T-test and Dunnett correction for multiple comparisons (95% CI, p≤0.05).

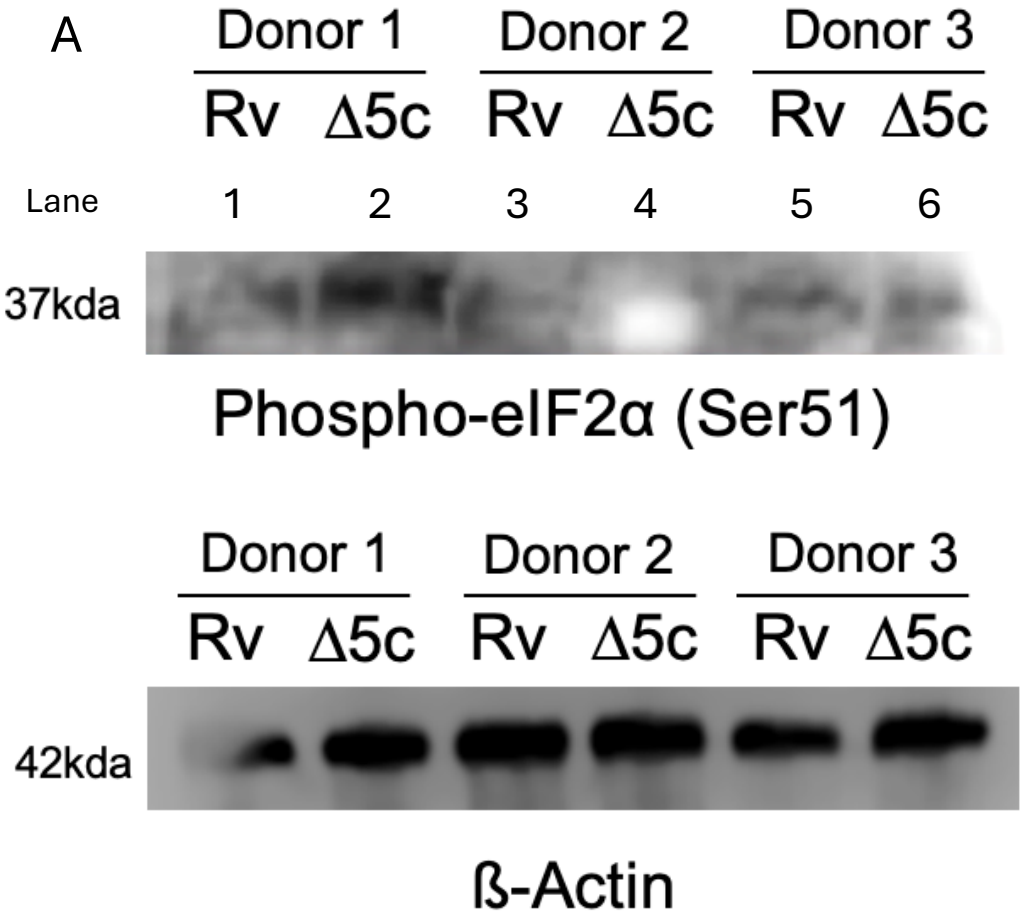

Supplemental Figure 4.4 – Western blot of phospho- eIF2α (Ser51) in ESX-5 paralog mutant infected cells. SF4.2. Blot shows the levels of detectable p-eIF2α (Ser51) and control ß-Actin across lanes 1-6. Lanes 1-2 shows protein from donor one, lanes 3-4 show donor 2, and lanes 5-6 show donor 3. Lanes 1,3, and 5 show H37Rv infected conditions while lanes 2,4, and 6 show Δ5c infected conditions.

4.3.13 Cellular Stress Levels are Equivalent Across Mutant and Wildtype Infections

Concurrently, we queried the levels of cellular stress these mutants elicit in macrophages. It has been described previously that Mtb induces the integrated stress response (ISR) and unfolded protein response (UPR) which alter the translational landscape when activated. We initially observed cells infected with our mutant strains display no change in the levels of HSPA5 or TRIB3 expression in addition to similar levels of XBP1 splicing during early infection (**Figure 4.5C**). These targets are downstream of UPR and ISR induction indicating activation of these pathways is similar across strains. Additionally, we observed that cells infected with our mutants display comparable levels of phospho-eIF2a (**Supplemental Figure 4.4**) which is a central mediator within the ISR and UPR pathways. From this we hypothesized cell stress mechanisms may be equivalent or marginally impacted between different strains. However, even small changes in the activation of the UPR and ISR pathways can lead to translational impacts within target cells. We tested whether inhibition of these pathways using pharmacological approaches would restore wildtype levels of cytokine synthesis. We initially targeted the three main transducers of the UPR (IRE1a, ATF6, and PERK) using 4μ8c, Ceapin-A7, and GSK2606414, respectively (Selleck Chemicals, Houston TX). Using ISRIB (Selleck Chemicals, Houston TX), we also directly inhibited the phosphorylation of eIF2a, preventing the development p-eIF2a mediated translational alterations broadly in these cells. We infected these pre-treated cells with our H37Rv and knockout strains to evaluate cytokine responses. Untreated cells displayed expected responses with reduced cytokine output in the mutant infection

conditions (**Figure 4.6A-C**). Inhibitor treatment displayed marginal but heterogeneous impacts across the cytokines we examined, however nearly all conditions tested displayed a phenotype matching untreated cells indicating UPR/ISR inhibition does not restore wildtype levels of cytokine secretion (**Figure 4.6A-C**). One exception is the IL-6 levels induced in 4μ8c treated cells infected with Δ5a and WT (**Figure 4.6B**). This comparison shows similar levels of cytokine; however, this response is largely driven by 2/5 donors that are outliers (>1SD above mean). Together these data indicate cell stress is modestly activated within these macrophages, but this activation is not differential across strains and is likely not the dominant underlying mechanism driving observed cytokine reduction phenotypes.

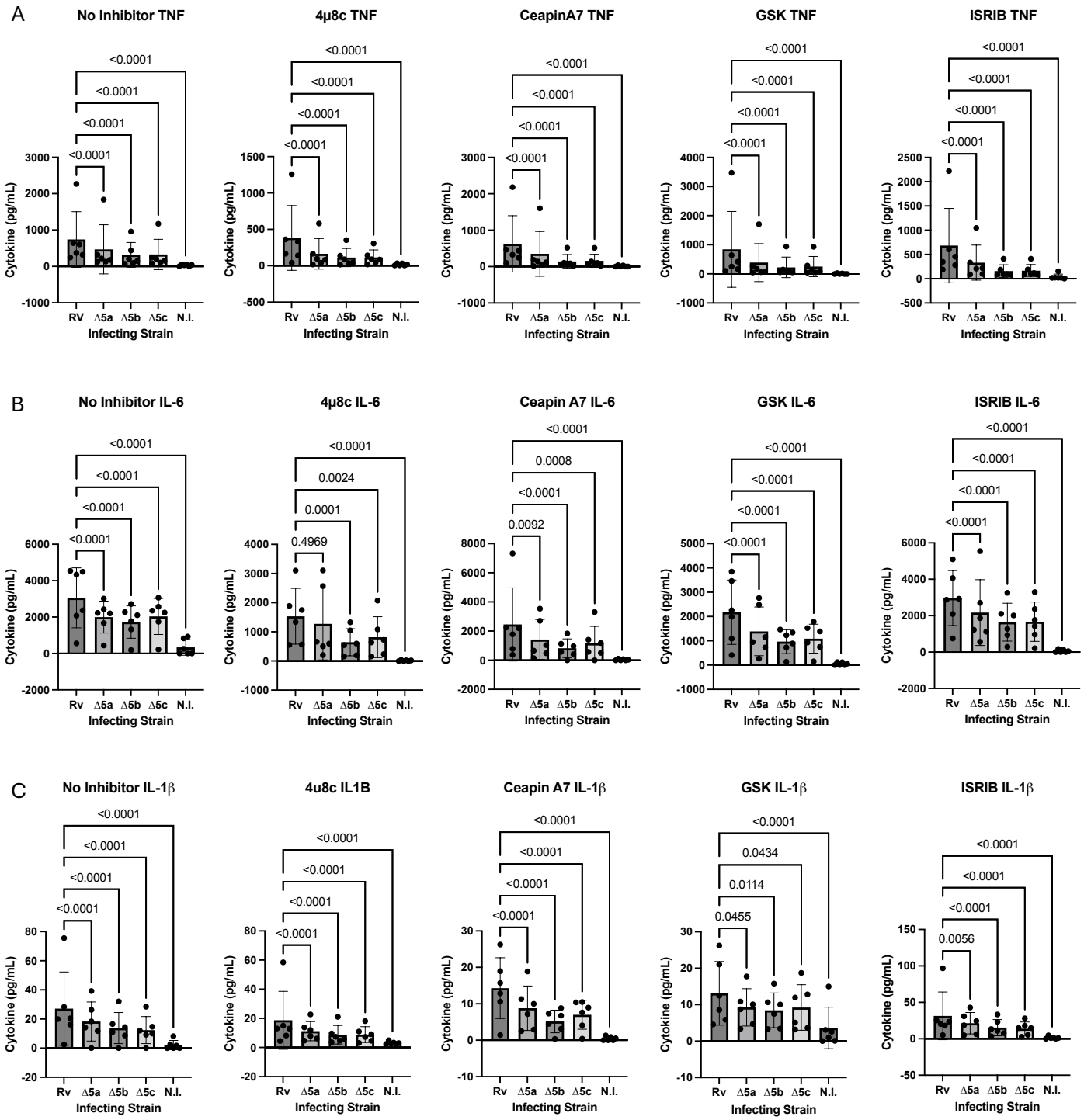

Figure 4.6 – Inhibition of UPR and ISR mediators does not rescue cytokine synthesis. 4.6A. TNF levels across cells treated with no inhibitor, 4μ8c, Ceapin A7, GSK2606414, or ISRIB respectively. 4.6B. IL-6 levels across cells treated with no inhibitor, 4μ8c, Ceapin A7, GSK2606414, or ISRIB respectively. 4.6C. IL-1β levels across cells treated with no inhibitor, 4μ8c, Ceapin A7, GSK2606414, or ISRIB respectively. 4.6A-C. Graphs depict levels of given cytokine under treatment with a respective UPR/ISR inhibitor and bacterial strain. For all graphs, y axis depicts the concentration in picograms

per milliliter while the x axis shows the strain used for infection. Titles of graphs show which inhibitor was used for respective groups. Dots within bars each represent an independent donor (N=6) run in technical triplicate. Error bars show +/- 1 standard deviation around the mean. Statistics for all analyses generated using two-way ANOVA with post-hoc T-test and Dunnett correction for multiple comparisons (95% confidence interval, $p \leq 0.05$).

4.4 Discussion

Here we have shown that small paralog deletions can have outsized impacts on the early macrophage response to infection. Specifically, we have shown that the deletion of any ESX-5 paralog (Δ5a, Δ5b, or Δ5c) elicits a robust reduction in the amount of synthesized proinflammatory cytokine. We examined numerous cellular processes to identify where these deletion mutants differentially interact with host macrophages to drive altered responses. Early during infection, phagocytosis and proinflammatory transcript induction are unchanged. Concurrently, late-stage analysis suggested there is likely a post-transcriptional or translational regulation event occurring upstream of protein synthesis. We examined global regulatory processes through micro-RNA analysis and UPR/ISR induction and did not observe differences. However, we did observe that not all cytokines are down regulated during mutant infection suggesting that target specific processes are likely at play, regulating some macrophage inflammatory factors but not all.

Classically, human macrophages respond to Mtb infection by strongly expressing proinflammatory IL-6, TNF, and IL-1β (201–203). While some cytokine responses are well described, how others shape the early cellular response to Mtb is less clear (202). It is speculated this strong inflammatory response may be beneficial to Mtb, potentiating

spread through lytic cell death and enhanced phagocytic recruitment to the site of infection(204–207). This is converse to traditional assumptions that greater inflammation is detrimental to pathogen survival, resulting in evolved mechanisms to prevent immune development (208). Our in vitro data together suggests ESX-5 effectors may actively promote cellular responses as a mechanism for potentiating inflammation and inducing bacterial spread to neighboring cells. This is not the first time this has been proposed. Others have shown that ESX-5 secreted proteins are highly immunogenic and constitute potent epitopes in MHC presentation (124,190). Our data suggests these effectors may also potently stimulate innate cell activation. This observation, paired with prior findings that attenuated innate recruitment in vivo leads to enhanced control of Mtb, suggests Mtb may have evolved to use its ESX-5 encoded proteins to potentiate infection via the activation of innate immune responses (209). We propose a model wherein an altered ESX-5 landscape via targeted deletion leads to the activation of target specific, post-transcriptional, or translational regulatory mechanisms that alter the inflammatory state of cells. This in turn leads to enhanced control via reduced immunopathology and inflammatory recruitment to the site of infection. The cellular mechanism governing this is still unclear, but our data suggests a cytokine-specific post-transcriptional or translational regulation event.

We’ve demonstrated strong initial mRNA synthesis for inflammatory gene targets, indicating intact early signaling events (210). This suggests our strains possess the correct stimulatory motifs to initiate inflammatory cascades yet lack fully formed cytokine. Notably, CCL4 and IL-8 (CXCL8) are not down regulated alongside other

inflammatory markers. The regulatory motifs driving the expression of these cytokines relative to others is not fully understood, particularly in the context of Mtb infection. However, their unaltered profile suggests a post transcriptional process that promotes their differential expression. It is well described that the cell uses many combinatory processes for regulating protein synthesis, particularly as it pertains to cytokine responses. For example, TNF, IL-6 and others possess RNA binding protein (RBP) motifs to recruit regulatory elements (211,212). Alternatively, some transcripts recruit ribosomes to upstream ORF elements (uORF) as a mechanism for regulating main ORF (mORF) translation (213). We propose under wild type conditions, the ESX-5 paralog proteins described here may inhibit these cellular regulatory elements and promote excess translation of inflammatory cytokine. However, during knockout infection these effectors are absent allowing for unabated regulatory processes to occur within infected cells, effectively curbing the inflammatory response. Although this model is highly speculative, it provides a starting framework for dissecting these regulatory processes that govern ΔESX-5 cellular responses in future studies. We propose target specific cross-linking and pulldown experiments alongside polysome profiling, to resolve the target-specific regulation events described herein while concurrently evaluating target levels of translation.

In summary, we've demonstrated the ESX-5 paralogs, ESX-5a, ESX-5b, and ESX-5c play outsized roles in driving inflammatory responses in macrophages. Previous studies on these gene clusters were limited and to our knowledge this is the first functional exploration of all three paralogs together. Our study highlights the importance of

investigating Mtb genes in the context of cellular responses to gain more complete insight into gene function across diverse environments.

4.5 Acknowledgments

We would like to extend our sincerest appreciation to Nathan Kieswetter, Aparajita Pesaladinne, Moeko Agata, and Glenna Peterson. These individuals all contributed via supporting cell maintenance, assay assistance, or sample processing, etc.

Chapter 5. In Vivo Challenge with ESX-5 Mutants Reveals Attenuation in Mouse Model of Disease

**This chapter was submitted in part as a manuscript: "ESX*-5 Deletions in *Mycobacterium tuberculosis* Alter Macrophage Cytokine Signaling, *In Vivo* Virulence, and Bacterial Heavy Metal Response" Haynes AM, et.al. 2025

5.1 Introduction

The mouse model of disease has long been used as a correlate for investigating the impacts of Mtb infection on a complete and intact mammalian immune system (64,70,75,81,201,214). The mouse immune system contains a high degree of synteny and conserved function with the human immune system, making it a tractable model for physiologically complex, high-biocontainment experiments leveraging virulent Mtb (215). By some estimates, mice and humans share ~90 percent of syntenic regions despite large physiological differences, highlighting the level of genetic conservation shared across the Mammalia class of organisms (215). As such the laboratory mouse provides a unique opportunity to explore the interaction of Mtb with a complete immune system in a cost-effective capacity. While ex vivo and in vitro monoculture of myeloid cells lines or primary antigen presenting cells (APCs) (dendritic cells, macrophages, THP-1, U937, etc.) provide large functional insight into the molecular interactions between bacterium and host, they often fail to recapitulate the complexity and unique immune microenvironments encountered in vivo (215,216).

The innate immune system comprises numerous cell types that coordinate working together to clear infections and recruit the adaptive system for target specific responses (214,217). In addition to the initial cells potentiating infection, namely the alveolar macrophage, the innate immune system is comprised of numerous tissue resident and recruited immune cells including neutrophils, peripheral macrophages, dendritic cells, etc. (74,135,217,218). The complex interplay of these cells drives a robust initial response to infection while recruitment and coordination of adaptive immunity begins to occur. Adaptive immune responses develop more slowly but allow for a targeted response to Mtb antigens that is classically believed to facilitate enhanced control of via innate coordination and participation in granuloma formation (154,214,219). However, the efficacy of this structure in restricting Mtb growth and dissemination is increasingly debated (78,79,82–84). Previously, we observed large changes to the human macrophage response to Mtb infection using our mutant strains. Despite these large alterations to the proinflammatory profile, these macrophages do not control or succumb to mutant infection more efficiently than wildtype strains. We reasoned that while altered cytokine profiles of infected macrophages might not lead to observable differences in growth kinetics, this altered effect may lead to restrictive profiles in vivo from synergistic effects of complementary cells. Previous studies have shown how tightly coordinated the cytokine response is at driving a systemic response to Mtb and as such we hypothesized that we would likely see alterations to the virulence profile of our ESX-5 paralog knockouts in vivo (153–155,214,220,221).

Herein we tested the replicative capacity of Wildtype H37Rv Mtb and ΔESX-5c Mtb in the C57BL/6 mouse model. ESX-5c has been previously suggested to be a virulence cluster promoting transmissibility, highlighting a unique opportunity to explore a previously proposed function in an in vivo model (15). We examined the CFU burden in these mice across the pulmonary compartment and disseminated locations (Spleen and Lymph nodes) to understand how these strains perform in establishing pulmonary infection, but also in how they disseminate. We analyzed both day 17 and day 35 time points to resolve the implications of an innate response early and the role adaptive immunity may play during later infection.

5.2 Methods

5.2.1 Media

Media used throughout experiments consists of RPMI-10 (RPMI 1640 medium (Gibco, Carlsbad, CA) with 10% fetal bovine serum (Atlas Biologicals, Fort Collins, CO), along with macrophage colony stimulating factor (M-CSF) (Pepro Tech, Carlsbad, CA) at 50ng/mL. For mycobacterial culture, bacteria were grown in 7H9 base medium supplemented with Glycerol, ADC, and Tween 80 at final concentrations of 0.2%, 10%, and 0.05% respectively. Sautons medium used for washing mycobacteria is a basal medium composed of 4.0 grams of L-asparagine, 0.5 grams of $MgSO_4$, 0.5 grams of K_2HPO_4, 0.1 milliliters of a 1% $ZnSO_4$, 2.0 grams of citric acid, and 0.05 grams of ferric

ammonium citrate into 1 liter of water. Tween 80 and Glycerol were added at the same concentration as for 7H9.

5.2.2 Mice

C57BL/6J (B6, #000664) mice were purchased from Jackson Laboratories (Bar Harbor, ME). Female mice between the ages of 9–12 weeks were used. All animals were housed and maintained in specific-pathogen-free conditions at Seattle Children's Research Institute (SCRI). All animal studies were performed in compliance with the SCRI Animal Care and Use Committee.

5.2.3 Mtb aerosol infections

Infections were done with stocks of H37Rv and ΔESX-5c as previously described previously(222). To perform aerosol Mtb infections, mice were placed in a Glas-Col aerosol infection chamber, and 50–100 CFU were deposited into their lungs. To confirm the infectious inoculum, two mice per infection were euthanized on the same day of infection, and their lungs were homogenized and plated onto 7H10 plates for determination of CFU.

5.2.4 Flow Cytometry of Murine Lung Cells

To generate single cell suspensions, lungs were excised and lightly homogenized in HEPES buffer containing Liberase Blendzyme 3 (70 µg/ml; Roche) and DNaseI (30 µg/ml; Sigma-Aldrich) using a GentleMACS dissociator (Miltenyi Biotec). The lungs were then incubated for 30 min at 37°C and then homogenized a second time with the GentleMACS. The homogenates were filtered through a 70 µm cell strainer, pelleted for RBC lysis with RBC lysing buffer (Thermo), and washed once with PBS. Cells were then resuspended in 50 ul of PBS containing Zombie UV viability dye (BioLegend) and incubated for 10 min at room temperature in the dark. Viability dye was quenched by the addition of 100 µl of a surface antibody cocktail diluted in 50% FACS buffer (PBS containing 2.5% FBS and 0.1% NaN3)/50% 24G2 Fc block buffer using saturating levels of antibodies (anti-CD64 PerCP-e710, anti-CD11b BV570, anti-CD11c BV711, anti-SiglecF BV421, anti-Ly6G BV605, all BioLegend). Surface staining was performed for 20 min at 4°C. Then, the cells were washed once with FACS buffer and fixed with 4% paraformaldehyde for 30 min prior to analyzing on a Symphony flow cytometer (BD Biosciences).

5.2.5 CFU plating

Target organs (Lung, pulmonary lymph node, and spleen) were homogenized in M tubes (Miltenyi) containing 1mL PBS+0.05% Tween-80 (PBS-T) using a GentleMACS machine (Miltenyi) at target time points. Homogenates were then diluted in PBS-T and plated onto 7H10 plates. Plates were incubated at 37°C for at least 21 days before quantification of CFU.

5.3 Results

5.3.1 Early Time Point Bacterial Burden and Cell Distribution Reveals Restriction of ΔESX-5c.

Despite observing no impact of these knockouts on the replicative ability within macrophages, we wanted to assess the impact that altered cellular responses may have in the context of a complete immune system. As such we designed an in vivo approach to query the restrictive capacity of B6 mice with wildtype H37Rv or our Δ5c mutant. Mice were infected using standard dosing (~50-100 CFU per mouse) of respective strains carrying a mCherry reporter plasmid. These animals were then followed for 17 and 35 days to evaluate via flow and CFU the bacterial burden in lung, spleen, and lymph node tissue. Initial flow analysis on lung homogenates at the time of harvest demonstrated a reduced mCherry signal in Δ5c infected mice indicating possible attenuation (**Figure 5.1A-B**). Delineation of different cell types within the mCherry+ fraction showed no difference for mCherry positivity by cell type indicating no altered distribution within specific cells by strain. Quantitative CFU analysis of lung, spleen, and lymph node confirmed initial findings showing a significant reduction in the lung and lymph node compartments in mice infected with the Δ5c mutant at D17 post infection (**Figure 5.1C**). Spleen also displayed a reduction in bacterial burden with 5/5

mice showing evidence of infection and bacterial burdens detectable for 2/5 mice in this tissue group.

5.3.2 Resurgence of the ΔESX-5c Strain at Later Time Points Suggests Adaptive Immune Involvement Abrogates Bacterial Restriction

The same tissues from the remaining N=5 mice were analyzed at D35 post infection. At this later time point the initial growth defect observed in Δ5c infected mice was no longer significantly different between groups (**Figure 5.1D**). CFU analysis of spleen, and lymph node from these mice confirmed findings that the observed reductions at peripheral sites (spleen and lymph node) were no longer different between strains, however lymph node differences were approaching significance (p=0.089) (**Figure 5.1D)**. Lung CFU burden at this timepoint also showed no significant difference by statistical analysis but was trending down (p=0.1905) (**Figure 5.1D**). These observations are in strong contrast with our initial observations at D17. Together these suggest early infection with Δ5c mutants results in an attenuation of these strains that is then reversed at later timepoints.

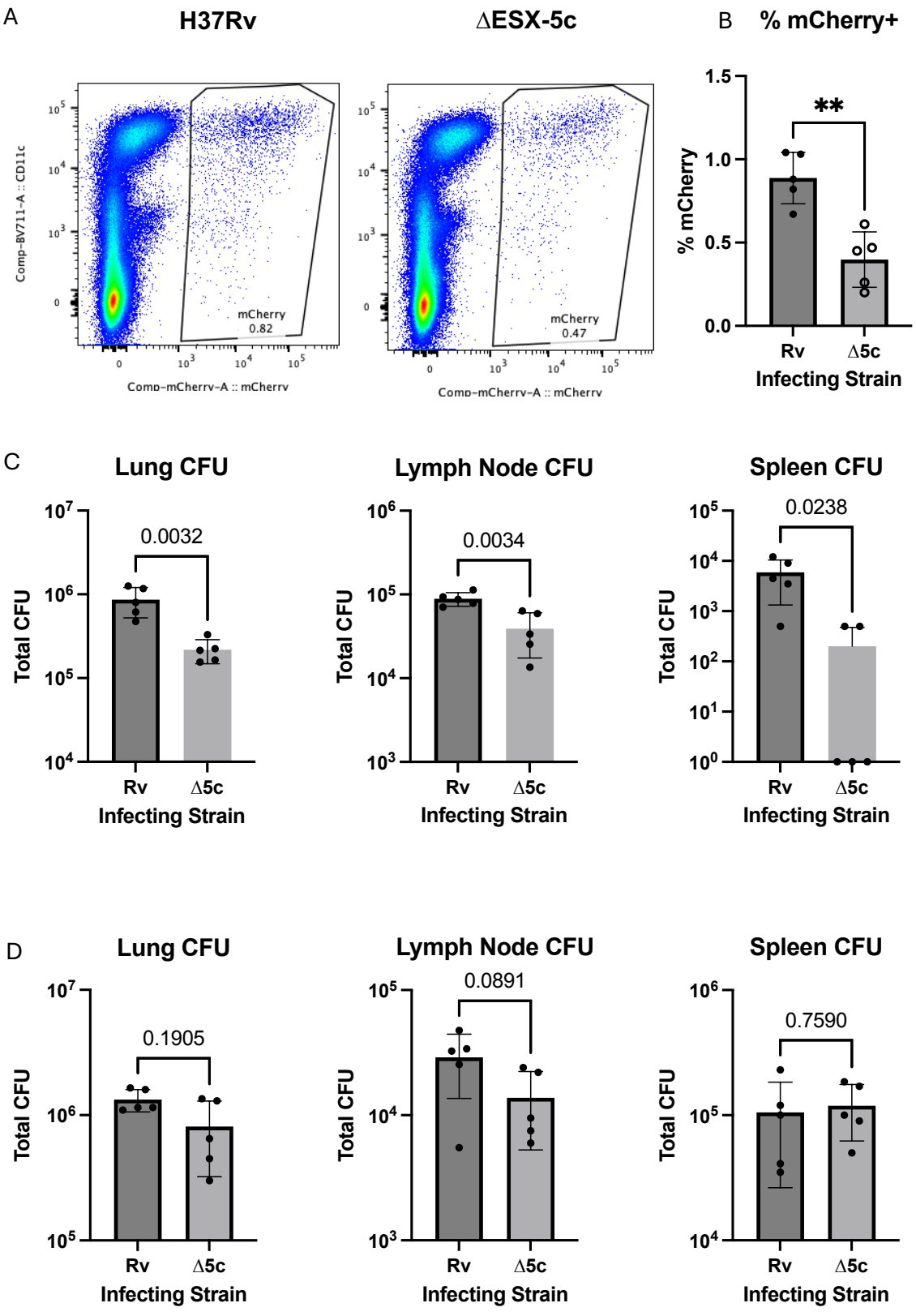

Figure 5.1 – ESX-5c paralog knockout with early attenuated survival in murine in vivo Mtb infection model. 5.1A. Flow cytometry graphs depict the mCherry positivity

signal from lung homogenates infected with either H37Rv or Δ5c, respectively. Flow plots are gated on a y axis of CD11c positivity and x axis of mCherry positivity. All mCherry signal circled in black gates. 5.1B. mCherry positivity in lung homogenates based on mCherry positive events from the flow plots over the total events measured. 5.1C. CFU day 17 post infection. 5.1D. CFU day 35 post infection. 5.1C-D. Bar charts show the total colony forming units (CFU) returned from respective tissue (lung, lymph node, and spleen) in Mtb infected mice. Y axis shows total CFU returned for respective graphs in Log10 scale while x axis shows the strain used for infection. Dots for each column represent N=5 mice tested in singlet for each respective tissue at each time point. D17 Spleen CFU shows limit of detection line (LOD) as N=3 mice were below CFU detectable limits at the dilutions used for plating. Error bars represent standard deviation from the mean value. Normality for all comparisons evaluated using Shapiro-Wilks test. Statistics for 5.1C Lung and Lymph Node, 5.1D Lymph Node and Spleen generated using unpaired, two-tailed T-test (95% confidence interval, $p \leq 0.05$). For 5.1C Spleen and 5.1D Lung, data was evaluated using Mann-Whitney analysis due to abnormal data distribution.

5.4 Discussion

Through this work we've shown that the ΔESX-5c mutant shows differential restrictive capacity in vivo. In C57BL/6 mice, we observe at day 17 post infection there is a significant reduction in bacterial burden across all tissues tested. Lung tissue shows the strongest reduction of Mtb burden; however, we also see strong reductions within disseminated sites such as the spleen and lymph nodes. At day 35 post infection, we observe a reversal of this early restriction with all tissues showing non-significant differences in burden across infections. Together these data indicate an early fitness defect in the ΔESX-5c strain that is rescued during later time point analyses.

A hallmark feature of early Mtb infection is the induction and recruitment of the early innate immune response. In the murine model, alveolar macrophages, followed by recruited peripheral cells respond and attempt to restrict bacterial growth (64). Under

standard infection (50-100 CFU) using virulent Mtb, this leads to heterogeneous outcomes influenced by mouse genotype, bacterial strain, antimicrobial processes, and immune cell recruitment (223). There is growing evidence to support the idea that heightened pulmonary pathology caused by the inflammatory recruitment of peripheral innate cells like granulocytes (neutrophils, basophils, mast cells, etc.) may also contribute to less effective control of Mtb during early innate recruitment (224,225). Integrating our human macrophage response data, we observe that these mutant strains induce an attenuated proinflammatory response, characterized by reduced TNF, IL-6, and IL-1β. Despite this, we see no difference in replicative capacity of these strains relative to wildtype in macrophage monoculture. It is interesting to speculate that we may induce a similar attenuated proinflammatory response in murine macrophages during early infection. By extension its possible this attenuated early cytokine response from professional antigen presenting cells (APCs) such as macrophages may alter the early recruitment and coordination of additional innate cells (226,227). This reduction could moderate the heightened inflammatory response of other immune cells, leading to a reduction in pulmonary immunopathology and resulting sequelae. Indeed, others have shown that the interruption of neutrophil-driven immunopathology may lead to enhanced control of Mtb during infection (81,228). This is possibly driven via the reduction of lytic cell death that promotes Mtb potentiation to naïve cells. Taken together, we hypothesize the alterations to the signaling and proinflammatory profile of infected APCs, alongside additional immune cell help, may lead to an early coordinated response that more effectively restricts ΔESX-5c.

Subsequent late-stage infection is dominated by the adaptive immune response. By day 35 post infection, CD4+ T-cells, mature B-cells, among other smaller populations of adaptive lymphocytes begin to impact the response to Mtb infection (214). Classically, this late-stage adaptive response is characterized by a strong Interferon gamma signature in mice (75,150,153,155). Interferon gamma production and stimulation amongst innate immune cells has been classically thought of as host protective but a growing body of literature suggests that the heightened inflammation and coordinated formation of the granuloma may potentiate Mtb survival and replication in some cases (78). We know that the formation of the granuloma often leads to heterogenous outcomes in bacterial clearance (76,79,83,84). Despite strong inflammatory activation via proinflammatory cytokine and the activation of antimicrobial processes like iNOS induction, granulomas may still fail to clear the bacilli and may even potentiate spread via the recruitment of other naïve immune cells (78,81). Our data suggests a putative disconnect between early and late immune responses to our ΔESX-5c mutant. The mechanism proposed herein may contribute to the resurgent growth of our ΔESX-5c strain observed during later time points. The initial restrictive innate profile is likely surmounted by a potent interferon gamma response. This may lead to restored cell-to-cell spread and subsequent loss of bacterial restriction.

Future studies examining both early innate and late adaptive immune correlates of disease would shed light on the validity of the model we propose here. Examining neutrophil infiltration during early infection would allow us to infer the role these proinflammatory potentiators of infection play during early time points. Additionally, we

propose either serum-based or flow-based analysis of the cytokine response during early infection. While there are many differences in the innate cytokine response between humans and mice, we would expect to identify significantly altered cytokine profiles in the murine model based on our human macrophage observations. These together would allow us to more confidently confirm our proposed model of early infection dynamics. Subsequent analysis of the adaptive response during late infection would allow us to confirm if recruited adaptive lymphocytes induce an interferon gamma-dominant profile and if that immune profile leads to enhanced bacterial potentiation via the recruitment of non-protective cells or increased immune-pathology. Herein we've demonstrated the importance of performing coordinated in vitro and in vivo experiments, allowing novel insights into the interactions of a complete immune system and our bacterial targets of interest.

5.5 Acknowledgments

We would like to extend our sincerest appreciation to the Urdahl lab for their help performing the animal studies described here. The Hawn lab generated the knockout strains carrying a compatible reporter plasmid. Sara Cohen, Courtney Plumlee, and Kevin Urdahl (PI) graciously expanded these bacteria, infected mice, performed all CFU analysis and reported data back to us. Without their assistance, we would not have been able to perform this study.

Chapter 6: Defining Changes in Microbial Physiology in Response to Paralog Deletions

**This chapter was submitted in part as a manuscript: "ESX-5 Deletions in Mycobacterium tuberculosis Alter Macrophage Cytokine Signaling, In Vivo Virulence, and Bacterial Heavy Metal Response" Haynes AM, et.al. 2025*

6.1 Introduction

Prokaryotic cellular process is often tightly regulated in the face of extensive environmental pressure and stimuli (229). Through the complex coordination of gene expression and protein availability, bacteria are able to adjust to environmental changes, ensuring their adaptation and survival (229–231). Concurrently with changing and dynamic gene expression, genetic modifications that arise within the genomes of bacteria add an additional layer of adaptation. These spontaneous mutations arise due to random errors in genome replication and are subject to selection (232–235). Selection on genetic variants falls into three general categories: purifying (or negative), positive, and stabilizing selection. Together, these processes select for genetic and genomic variants that are the most "fit" for a given environmental-physiological pairing (236). The large reproductive rate and quantity within prokaryotic populations often means these minor alleles are persistently coming into existence and subject to selection. To exemplify this point, we can look to the development antimicrobial resistance in bacterial populations where random chance gives rise to resistant populations, often coming with a fitness trade off (237). These bacteria would normally be purified as less fit than their parent, but under an environment containing antibiotic, the fitness tradeoff may be tolerated.

While selection within bacteria is largely due to environmental pressures such as antibiotic or host defenses (in the case of pathogens), there is often an element of physiological selection as well. The most extreme genetic variants that alter core or essential cellular processes are strongly counterbalanced against selective pressures, often being deleterious but sometimes retained in the case of strong enough stressors. For example, a reduction in membrane permeability may be purifying in a population of bacteria under rich environmental conditions but provide a selective advantage if this same population is exposed to a toxin or antimicrobial compound needing cytosolic access (238). In the case of mycobacteria, we have observed that non-pathogenic species have more permeable membranes compared to their pathogenic counterparts (239). For example, *Mycobacterium smegmatis* (Msmeg) through its MspA complex contains a relatively more permeable membrane as compared to its Mtb counterpart (239). Contrarily, pathogenic species such as Mtb, contain highly impermeable cell walls lacking classical porins (188,240). One could speculate that this lack of membrane permeability has led to the incredible success of Mtb as a human pathogen but contributes to its reduced fitness in environmental niches. In essence, the physiology of prokaryotes, especially pathogenic prokaryotes such as Mtb, is often a tightly regulated balancing act between conservation of core, essential function, and adaptation to new pressures.

This shift of mycobacteria out of environmental niches and into pathogenic niches represents a large-scale, permanent alteration in environmental pressure. This led to a

large-scale remodeling of the Mtb genome and the resulting physiological processes that enable life as an intracellular pathogen (7,14,123,241). Specifically, within Mtb, the evolution of the PE/PPE proteins have been hypothesized to be a selective expansion at the axis of membrane permeability and nutrient acquisition (185,188,240). As outlined, environmental mycobacteria such as Msmeg contain large porins that increase the permeability of the membrane and allow for the movement of aqueous substrates across the mycomembrane (239). As mycobacteria, namely the Mycobacterium tuberculosis complex (MTBC), evolved towards pathogenic niches, reductions in membrane permeability were likely required in response to the high levels of immune pressure faced by these species (242). The reduction in membrane permeability via the loss of canonical porins like MspA, likely led to the evolution of alternative processes that balance the need for exchange between the environment and the bacterial cytosol. Specifically, it is been hypothesized and preliminarily demonstrated that the PE/PPE proteins which are extensively expanded in slow growing, pathogenic, mycobacteria are responsible for the acquisition of targeted nutrients and molecules from the environment (188,240). Under the assumptions of this hypothesis, this genomic shift effectively reduced the membrane permeability of intracellular pathogens while maintaining essential nutrient exchange and bacterial survival. These genomic and environmental changes create a new tightly regulated system of cellular processes; a system we can perturb to measure bacterial responses.

The specialized adaptation and expansion of genes like the *pe/ppe* family opens the possibility for exploration using omics approaches. The outsized quantity and

hypothesized role these genes play likely indicates a tight regulation of bacterial networks that work cohesively to achieve their physiological function. Using molecular techniques, such as CRISPR interference and allelic exchange, we perturbed three putative virulence gene clusters, ESX-5a, ESX-5b, and ESX-5c. By extension, we speculate we induced detectable shifts in bacterial transcriptional profiles that we can measure to gain functional insight. To determine the role of these gene clusters at baseline in these bacteria, we examined the physiologic response within Mtb to their deletion in broth culture. Specifically, using bacterial RNA transcriptomics, we examined the gene expression within Mtb in response to these deletions. To this end, we explored how gene expression changes in response to our genomic deletions, providing possible insight into the function of these paralogs.

6.2 Methods

6.2.1 Media

Media used throughout experiments consists of RPMI-10 (RPMI 1640 medium (Gibco (Carlsbad, CA)) with 10% fetal bovine serum (Atlas Biologicals (Fort Collins, CO))), along with macrophage colony stimulating factor (M-CSF) (Pepro Tech, Carlsbad, CA) at 50ng/mL. For mycobacterial culture, bacteria were grown in 7H9 base medium supplemented with Glycerol, ADC, and Tween 80 at final concentrations of 0.2%, 10%, and 0.05% respectively. Sautons medium used for washing mycobacteria is a basal medium composed of 4.0 grams of L-asparagine, 0.5 grams of MgSO4, 0.5 grams of

K2HPO4, 0.1 milliliters of a 1% ZnSO4, 2.0 grams of citric acid, and 0.05 grams of ferric ammonium citrate into 1 liter of water. Tween 80 and Glycerol were added at the same concentration as for 7H9.

6.2.2 RNA Isolation

We resuspended bacterial targets in 1mL of Trizol and transferred to Lysing Matrix B tubes (MP Biomedicals, Santa Ana CA). We then homogenized the sample using a 6500rpm, 30 second protocol on a beadruptor (Omni International, Kennesaw GA) followed by a 30 second incubation on ice. This was repeated x3 to ensure lysis of the bacteria and RNA liberation. RNA was then isolated using the manufactures isolation protocol for Trizol to initially isolate the aqueous phase containing nucleic acids. Total RNA was then purified from the aqueous phase using an RNeasy kit with on column DNase digestion as outlined by the manufacturer (Qiagen, Hilden Germany). Isolated total RNA was subsequently quantified on a nanodrop (ThermoFisher, Waltham MA).

6.2.3 Ribosomal RNA depletion

Ribosomal RNA (rRNA) was depleted using a previously described protocol (243). In brief, biotinylated DNA probes were generated with complementarity to the ribosomal RNA sequences for Mtb. These probes target 46 different rRNA species, covering 23s, 16s, and 5s rRNA sequences (Supplemental table with probe sequences). Probes were mixed with total RNA and hybridized using a decreasing temperature gradient approach

starting at 70C and dropping by 0.1C per second until reaction reached 25C. Streptavidin magnetic beads were then added to the hybridized mixture and incubated at 50C to bind the biotin moiety on respective probes, and isolated using a magnetic separator. The supernatant containing rRNA depleted RNA was then cleaned further using AMPure XP beads (Beckman Coulter, Brea CA) to bind RNA and immobilize on a magnetic separator. Bead-bound RNA was then washed twice to remove impurities prior to elution in TE buffer.

6.2.4 Library Generation and Sequencing

Isolated mRNA was then prepared for paired end 150 base pair short read sequencing (PE150) using the NEBNext Ultra II RNA Library Prep Kit for Illumina (New England Biolabs, Ipswich, MA) according to manufacturer's instructions, and using the AMPure XP reagent (Beckman Coulter, Brea CA) for size selection and cleanup of adaptor-ligated DNA. In brief, purified mRNA was fragmented and first strand cDNA generated according to manufactures protocol. From this second strand cDNA was generated using first strand cDNA as a template. Double stranded cDNA was then purified using AMPure XP beads via magnetic isolation and serial washing. Cleaned, double stranded cDNA was end prepped and adapters ligated using standard Illumina adapter sequences followed by a subsequent AMPure XP bead cleanup. Purified, adapter ligated product was then amplified using included index specific primers for target amplification followed by a final AMPure XP cleanup. Sample ID and associated i5 and i7 indices are included in supplemental information. Amplified and purified libraries were

then submitted to Northwest Genomics Center (NWGC) sequencing core for library preliminary QC and sequencing. Library quality was assessed using a High Sensitivity DNA Assay for the Bioanalyzer 2100 (Agilent, Santa Clara CA). All libraries were then multiplexed and sequenced using an Element Aviti 300 Cycle Low Output chip totaling 2.5E8 reads (~2E7 reads per sample).

6.2.5 Transcriptomic and Bioinformatics analysis

Raw FASTQ data from the sequencing core was initially inspected using the FASTQC program to inspect read length, read quality, among other quality metrics prior to further analysis. After initial quality control, the raw sequences were run through our labs SEAsnake pipeline for RNA sequencing data processing(244). Initially, SEAsnake was setup for human sequencing analysis but was amended for Mtb sequencing inputs for the purpose of this analysis. SEAsnake was loaded and stepwise initialized. First, adapter sequences were trimmed and low-quality reads removed using the “AdapterRemoval” program. Outputted sequencing data was then run through FASTQC to ensure trimmed reads were of sufficient quality and length before proceeding. Sequences were then aligned to reference using the STAR program. Alignment filtering and output quality were assessed using samtools (flagstat). Quality assessed alignments were then input into the “Subread” package to count reads within genes, outputting a TSV file for all read quantities across the genome. Subsequent analysis was performed in R studio using the DEseq2 package to calculate differentially expressed genes across our samples, averaging experimental replicates for statistical

analysis. Differentially expressed genes were thresholded using FDR correction and log2 fold change relative to wildtype baseline. Output gene lists were intersected to identify unique and overlapping gene hits across our strains. These lists were then used in a string analysis (StringDB) to identify clustering with concurrent GSEA analysis (PantherDB) on GO processes.

6.2.6 Heavy Metal Culture

Bacterial culture with heavy metal was performed as described previously. In short bacterial cultures for all knockout and wildtype strains (4 total) were thawed from stock and grown in rich broth for ~3 days. Growth of these primary cultures were assessed via OD and back diluted to an OD of 0.1 for 48 hours of subsequent outgrowth. After outgrowth, these cultures were back diluted again into four separate rich medium cultures tubes containing heavy metal (copper, cadmium, Zinc, or Iron). Stock metal solutions were created at 1 molar concentration of the respective metal. Working concentrations of metal ranged for given experiments, dilution factors calculated based on experimental working concentration.

6.2.7 Heavy Metal Growth Curves

Growth curves were performed using OD600 collections over 5-day time span. Initially, bacterial cultures for all knockout and wildtype strains (4 total) were thawed from stock and grown in rich broth for ~3 days. Growth of these primary cultures were assessed via

OD and back diluted to an OD of 0.1 for 48 hours of subsequent outgrowth. After outgrowth, these cultures were back diluted again into four separate rich medium cultures tubes containing heavy metal (copper, cadmium, Zinc, or Iron) totaling 16 cultures. copper and cadmium cultures were treated with 100μM of the respective metal while Zinc and Iron cultures were treated with 500μM. The initial OD was calculated to 0.1 on day 0. OD measurement was then collected on day 1, 2, and 5 for all samples tested. Between OD measurements, cultures were grown shaking at 37C.

6.2.8 ESX Gene Expression Quantitation

To quantify Mtb target gene expression we performed a probe-based gene expression approach. We resuspended bacterial targets in 1mL of Trizol and transferred to Lysing Matrix B tubes (MP Biomedicals, Santa Ana CA). We then homogenized the sample using a 6500rpm, 30 second protocol on a beadruptor (Omni International, Kennesaw GA) followed by a 30 second incubation on ice. This was repeated x3 to ensure complete lysis of the bacteria and RNA liberation. RNA was then isolated using the manufactures isolation protocol for Trizol. Isolated RNA was subsequently quantified on a nanodrop. This RNA was then input into a cDNA generation protocol using a high-capacity cDNA reverse transcription kit (Life Technologies, Waltham MA). Resulting cDNA was used in a TaqMan, probe-based gene expression assay. Briefly, target probe sets were added to cDNA along with an endogenous control probe set targeting sigma factor A (SigA). Quantitative PCR (qPCR) was performed to get Ct values of each target in multiplexed samples. Relative quantitation was performed using the $\Delta\Delta$Ct method

and converted to fold change expression relative to control for the target of interest (191).

6.2.9 Macrophage Infection

Isolated macrophage infections were carried out according to our standard protocol. Cells were plated at 5E5 cells/ well of a 96 well tissue culture plate. Concurrently, bacteria were cultured as outlined. At the time of infection, bacterial culture was harvested via centrifugation (4000rpm, 5-10 min) and washed x2 with Sautons medium. The cultures were then resuspended in 2.5mL of Sautons medium and enumerated using OD600 absorbance and a standard conversion factor of 5E8 CFU/mL at OD600 of 1.0. After enumeration, necessary volumes of the bacterial suspensions were diluted into cell culture medium to achieve MOI of 5 per 100 microliters. This media was then used to exchange the media on the macrophage monolayer. To bring bacteria into contact with cells rapidly, an optional spin at 500g for 5 minutes can be performed. Macrophages were then returned to incubation for 24 hours before harvest the following day.

6.2.10 ELISA

DuoSet (R&D Systems Minneapolis MN) enzyme linked immunosorbent assay (ELISA) was performed on isolated cell fractions, either secreted or cellular. Both fractions were treated the same during the protocol. Briefly, capture antibodies for a target analyte

were plated on a ½ area 96 well plate and incubated sealed at room temp (RT) overnight to allow for antibody adherence to the plate. The following day, plates were washed using 1X PBST to remove the primary antibody solution. Reagent diluent (1%BSA PBS solution) was added to each well for one hour at RT to allow for blocking. Following blocking, plates were washed x3 with PBST then sample added to respective wells at a 1:5 dilution with reagent diluent and incubated for 2 hours at RT. Concurrently, a standard analyte was added to its respective plate to generate a standard curve. Plates were then washed x5 with PBST and detection antibody was added to all wells, including standard analyte wells which was followed by a 1-hour incubation at RT. The plate was then washed x5 with PBST and Streptavidin HRP was added to each well for 20 minutes. Following this, the plates were washed again x5 with PBST and developed with a TMB substrate for 15 minutes and stopped with a 2N sulfuric acid. Plates were immediately read at 450nm absorbance.

6.3 Results

6.3.1 Transcriptome sequencing of Paralog Knockouts Reveals Metal Responsive Gene Signature

The immunological alterations to macrophages and early attenuation of our strains in vivo prompted us to examine the underlying physiological changes in our knockouts that could impact these processes. We initially performed RNA sequencing, identifying the transcriptomic differences between our knockouts and wildtype. Using an Illumina,

short-read (PE150) platform we sequenced all mutant transcriptomes. Analysis revealed a stark downregulation of many genes (FDR ≤0.01, Log2 Fold-Change ≤-1). Specifically, 92, 88, and 85 genes were downregulated in ΔESX-5a, ΔESX-5b, and ΔESX-5c respectively (**Figure 6.1A, Supplemental Figure 6.1**). Using an informatics approach, we intersected these gene lists to identify overlaps, revealing 71 (63.2%) downregulated genes are shared between all three knockout strains. This list of 71 genes was used to generate a string network identifying connected clusters (**Figure 6.1B**). Further analysis of the clustering using gene set enrichment analysis (GSEA) via Gene Ontology (GO) revealed a strong and significant metal response gene signature (**Figure 6.1C**). Specifically, “response to cadmium ion” (FDR 2.43E-03) and “response to copper ion” (FDR 2.96E-03) were significantly enriched in our expression data (**Figure 6.1C**).

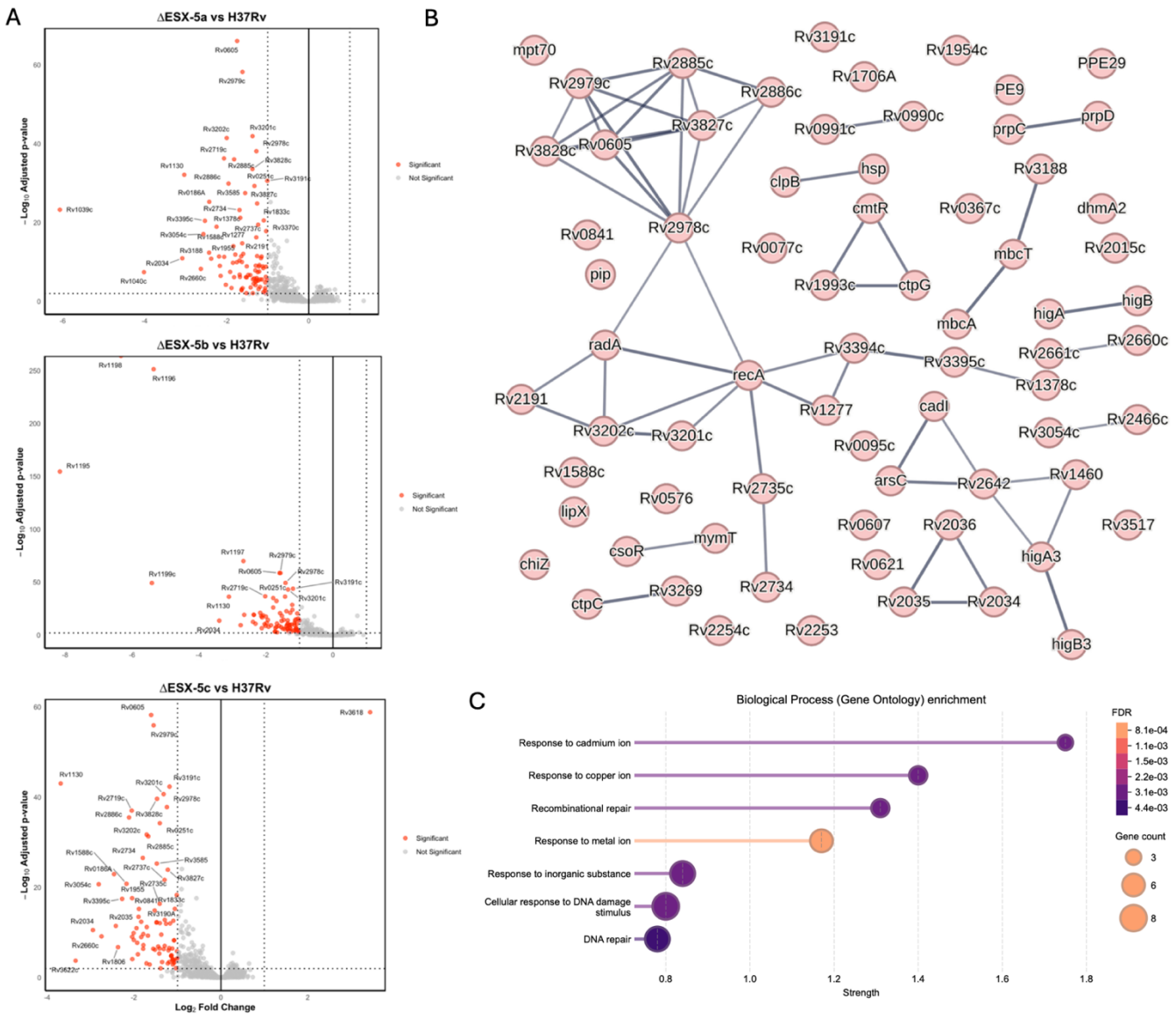

Figure 6.1 – Transcriptional analysis of ESX-5 paralog knockouts reveals metal response axis. 6.1A. Volcano plots comparing expression values of mutant relative to wildtype. All plots show respective fold change expression of the Mtb transcriptome for a given knockout strain relative to the parent wildtype strain. Title indicates which strain pair for a given graph. For all volcano plots, y axis shows the -Log10 FDR Corrected ("Adjusted") p-value, while the x axis shows the Log2 Fold Change of expression. Each dot is representative of a given Mtb gene being downregulated (-Log2 Fold Change) or upregulated (+Log2 Fold Change) relative to wildtype. Red dots denote gene expression that meets significance (FDR ≤0.01, Log2FC ≥1/≤-1), grey dots are non-significant. 6.1B. String network of overlapped down-regulated genes shared across all knockout strains. Each node represents a gene while the connecting lines represent combined string score or respective nodes (minimum string score >0.700, medium high connectivity, string-db.org). 6.1C. Functional enrichment plot of overlapping genes in gene set enrichment

analysis. Enrichment plot shows top 7 most significant gene sets based on Gene Ontology (GO) biological process gene set for Mtb H37Rv reference. Y axis of this plot shows the enriched gene set (top 7), and x axis shows the strength of the observation (Log10(observed genes/expected genes)). Size of node is proportional to the number of genes in our data belonging to a respective gene set. Color of node correlates to the FDR strength of the observation. Significance calculated using Fishers Exact test with Benjamini-Hochberg FDR correction.

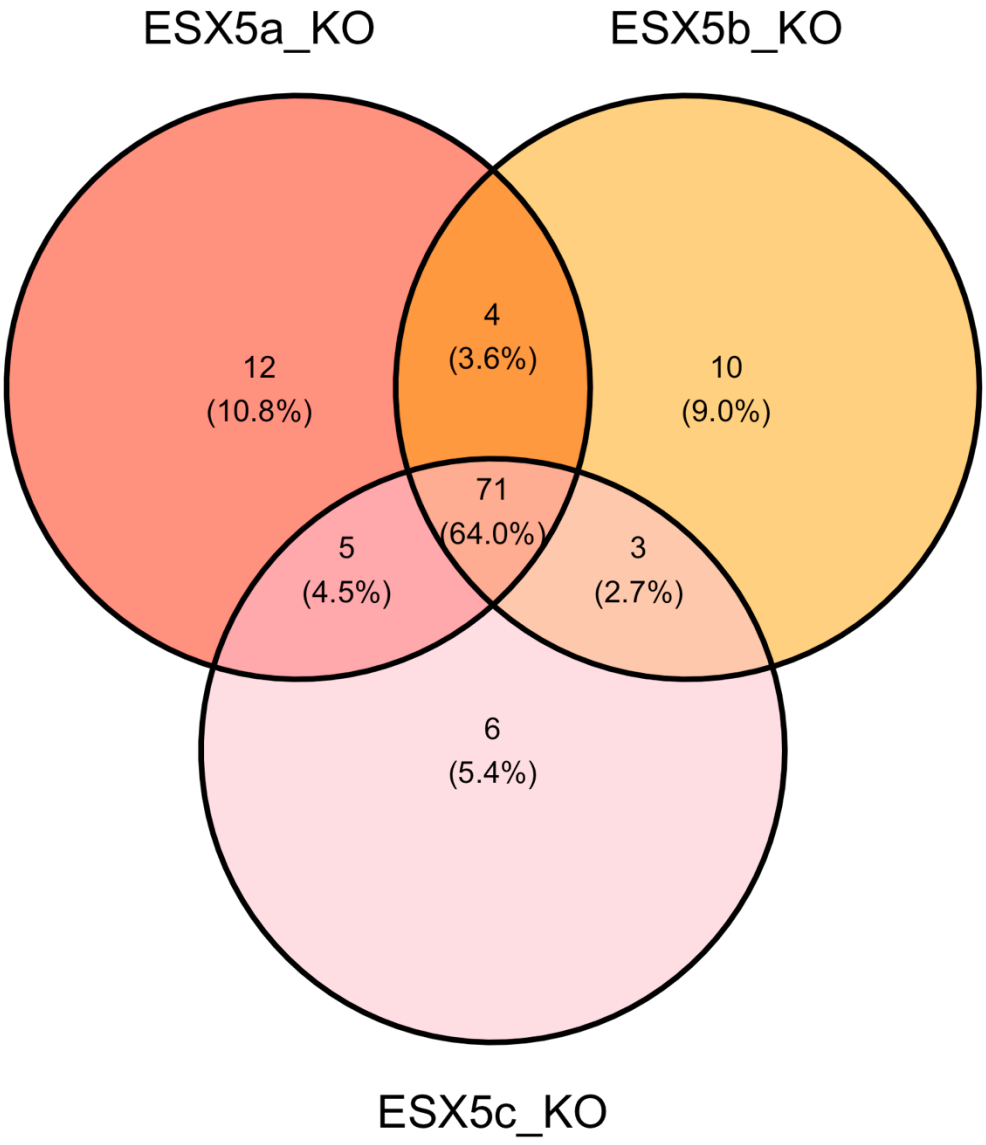

Supplemental Figure 6.1 –Venn diagram overlap of ESX-5 paralog knockout strain transcriptional profiles. SF6.1 Venn diagram shows three circles corresponding to significant gene expression for a given knockout compared to H37Rv wildtype. Gene distributions by circle and overlaps represent which genes are shared between which

mutants and which are unique within respective strains. 71 (or 64%) of all genes identified are shared.

6.3.2 Metal Treatment Does Not Differentially Affect Growth Rates of Mtb Mutants In Vitro

Based on the identification of a metal response axis in our transcriptomic data we attempted a growth curve experiment of all three knockout strains and H37Rv, treated with 100μM Cu, Cd or 500μM Fe, Zn over 5 days to determine if our knockout strains are selectively sensitive to excess environmental metals. Zn and Fe ions are imported via ESX-5 independent mechanisms and served as controls for this experiment. We collected OD600 measurements at D0, D1, D2, and D5 for 16 different conditions. After D5 collection we saw that excess Cd and Cu were growth restrictive for all strains **(Figure 6.2A, Cd & Cu)**. We also observed excess Fe and Zn ions lead to normal growth levels of ~1 doubling every 18-24 hours for all strains **(Figure 6.2A, Fe & Zn)**. Excess environmental Cd and Cu ions did not lead to any substantive differences in growth between H37Rv or any knockout strains, indicating no apparent sensitivity or resistance of our knockouts to excess heavy metal **(Figure 6.2A, Cd & Cu)**.

6.3.3 Bacterial Pretreatment with Heavy Metal Drives Upregulation of Paralog Expression

Our transcriptomic data suggested a link between the expression of ESX-5a, ESX-5b, and ESX-5c and metal response profiles. We reasoned that these clusters may be

responsive to metal treatment either directly or indirectly via inducing broad stress responses within the bacteria. To this end we grew H37Rv in the presence of high dose cadmium and copper for ~24 hours and analyzed the expression of ESX-5a, ESX-5b, and ESX-5c clusters via qPCR. We observed that excess copper can upregulate the expression of ESX-5a and ESX-5c (**Figure 6.2B**). Conversely, copper and cadmium reduced ESX-5b expression, although only copper reached significance (**Figure 6.2B).** These results suggest that ESX-5a, ESX-5b, and ESX-5c are either directly metal responsive or are indirectly responsive via bacterial stress responses under heavy metal exposure.

6.3.4 Heavy Metal Loading of Bacteria Results in Increased Cytokine Synthesis in MDMs

Our findings that heavy metal treatment affects ESX-5a, ESX-5b, and ESX-5c expression along with our MDM cytokine data suggests a putative link between paralog expression levels and cytokine expression levels in macrophages. To examine if there is a link between ESX paralog expression and the level of cytokine induction we pre-treated H37Rv Mtb for five days with either low dose copper or cadmium in rich broth. We then washed and infected macrophages to subsequently evaluate expression of TNF, IL-1β, and IL-6. As expected, the pre-treatment of Mtb with these metals did lead to the increase in cytokine production for 2/3 cytokines tested across N=5 donors (TNF, IL-6) (**Figure 6.2C**). Integrating our observations, this data indicates the presence of heavy metals likely upregulates gene expression for tolerating metal stress, including

the ESX-5a and ESX-5c clusters. The upregulation of these stress responses in Mtb then leads to subsequent cytokine responsiveness in macrophages. This is in agreement with our overexpression complementation results (**Supplemental Figure 4.1**), adding a robust link between the level of paralog expression and the amount of cytokine synthesis.

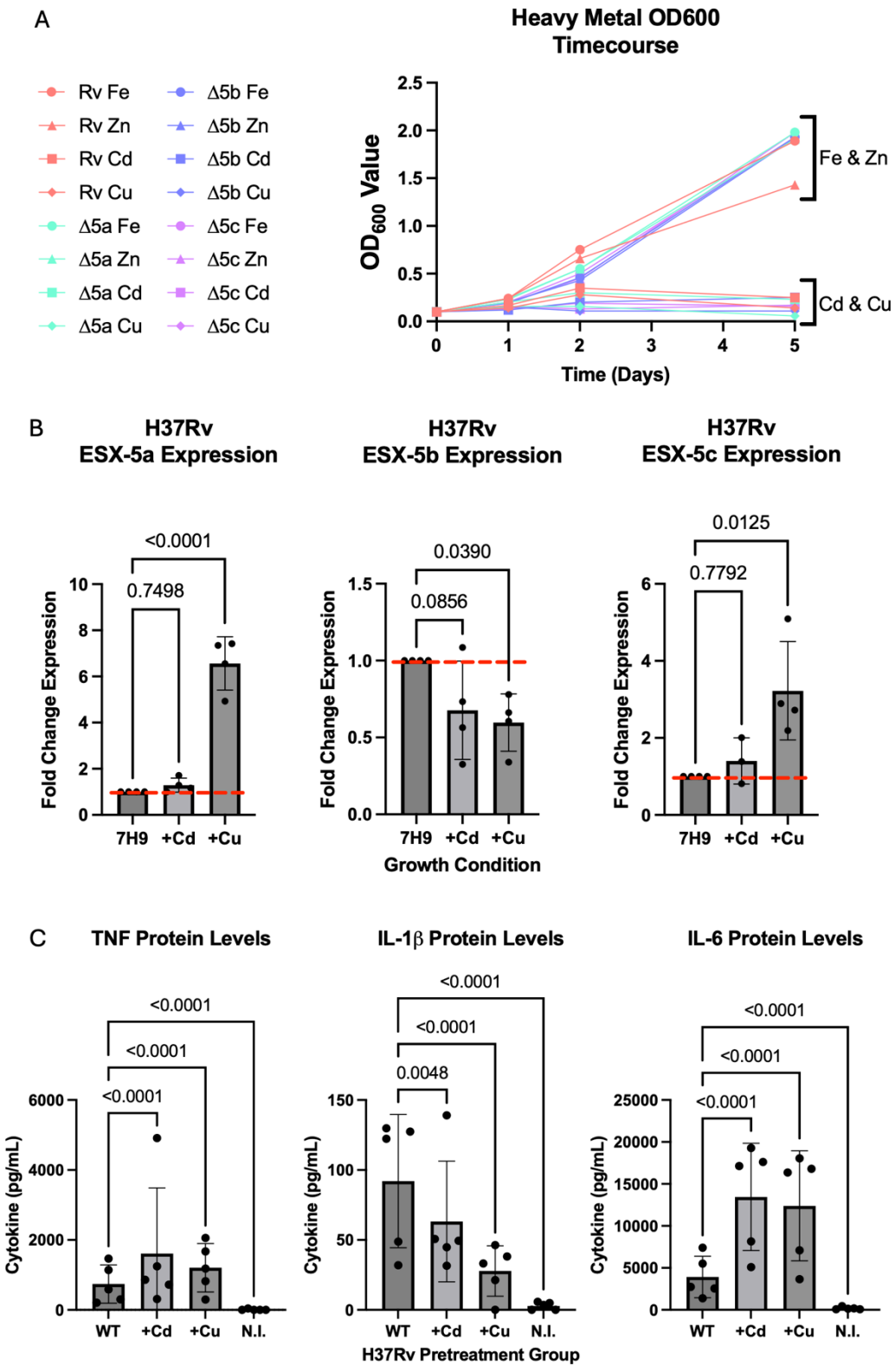

Figure 6.2 – Bacterial heavy metal treatment leads to differential paralog expression and increased cytokine output in macrophages. 6.2A. Time course growth curve for heavy metal treated strains. Graph depicts data from 16 different optical

density (OD) growth curves performed, each strain (H37Rv = red, ∆5a = teal, ∆5b = blue, and ∆5c = pink) were grown in Fe, Zn, Cu, or Cd (500μM, 500μM, 100μM, and 100μM respectively) for 5 days starting at on OD of 0.1 on day 0. Each metal correlates with a dot shape (Fe = circle, Zn = Triangle, Square = Cd, Diamond = Cu). Y axis denotes the optical density (OD600) value while x axis shows time in days. Brackets on graph depict clustering of metal groups, upper bracket shows Iron and Zinc treated strains while lower bracket shows copper and cadmium treated strains. 6.2B. Esx paralog gene expression in H37Rv under metal stimulus. Bar charts show expression of a respective Esx gene cluster within H37Rv wildtype under different stimulation conditions. Y axis shows the "Fold Change Expression" of the target relative to untreated. X axis shows the stimulus condition for each column, 7H9 denotes the untreated control grown in rich broth. Red dotted line indicates baseline expression of respective gene cluster in untreated bacteria. Dots represent individual RNA harvests and gene quantitation experiments. 6.2C. Metal pre-treatment leads to increased cytokine expression in macrophages. Bar charts show the relative abundance of a given target (TNF, IL-1β, and IL-6) from cells infected with metal pre-treated H37Rv. Y axis for all graphs depicts the concentration (picograms/milliliter) for a given target. X axis depicts the H37Rv pretreatment group used to infect macrophages. "WT" is untreated bacteria, Cd is cadmium treated, Cu is copper treated, and NI is the "not infected" cellular control. Each dot on a column represents a biological donor (N=5) run in minimum technical quadruplicate. 6.2B-C. Statistics for all analyses generated using two-way ANOVA with post-hoc T-test and Dunnett correction for multiple comparisons (95% confidence interval, $p \leq 0.05$). Error bars show standard deviation of the mean.

6.4 Discussion

In summary we've leveraged small changes to the bacterial genome to resolve large underlying responses in bacterial physiological networks. Using bacterial transcriptomics, we've identified a shared metal response axis between all three ESX-5 paralogs. Subsequently, we've shown that we can modulate ESX-5 paralog expression in H37Rv using heavy metals, confirming this link. By modulating ESX paralog expression using heavy metal stimulation, we are also able to alter the level of cytokine secretion in infected macrophages.

There is a growing body of literature that suggests the PE/PPE proteins play a large role in nutrient import and homeostasis of biologically critical ions (109,188,240). Interestingly, our data seems to suggest a complex interplay of all three gene clusters in the homeostasis of heavy metals such as copper and cadmium. To our knowledge, this is the first time ESX-5a, ESX-5b, and ESX-5c clusters have been implicated in heavy metal homeostasis. It is interesting to speculate that the co-regulation of the ESX-5 paralog encoded PE/PPE and Esx heterodimers may have evolved due to the localization of Mtb in the phagosome and the need for response to metal intoxication (231,245,246). Integrating our cellular microbiologic observations, we hypothesize that metal stress in the phagosome may lead to differential regulation of the ESX-5 paralogs. This in turn leads to the expression of the PE/PPE heterodimers which work directly to stabilize metal stress. In addition to our data here, others have shown PE/PPE proteins transcriptionally respond to metal stress, supporting this hypothesis(240). In tandem, the co-transcribed Esx heterodimers are expressed, driving inflammatory responses that may potentiate cell spread. In support of this model, our overexpression mutants and metal pre-treated bacteria (which both upregulate these gene clusters) demonstrate increased cytokine elicitation within infected MDMs. This supports our earlier model suggesting paralog expression levels are directly tied to the cytokine response and by extension paralog expression is a response to antimicrobial stress encountered in phagocytes.

Our study has many limitations and will be better served by future investigations. While we have provided strong evidence for the role of these gene clusters in responding to

metal stress, we have not identified how these clusters specifically interact with cellular metal balance; that being efflux, import, or alternative processes. Additionally, there are larger questions to answer regarding the direct role of these clusters in metal response. Specifically, do these paralogs respond directly to metal stress or secondary stress stimuli downstream in the metal signaling response. Future work will focus on understanding the regulatory network that drives the expression of these gene clusters and whether they are primary responders to metal stress or secondary responders.

In conclusion we have demonstrated that small alterations to the bacterial genome can lead to large changes in bacterial physiological processes. Specifically, we have shown that the ESX-5a, ESX-5b, and ESX-5c gene clusters not only play a role in the early stages of the innate immune response, but also the PE/PPE proteins encoded within may contribute in the response to heavy metal stimulus or heavy metal acquisition. Through this data we've added to the growing body of literature that hypothesizes a role of the PE/PPE genes in facilitating specialized nutrient acquisition and possibly identified novel importers or exporters of copper and cadmium through the mycomembrane.

6.5 Acknowledgments

We would like to extend our sincerest appreciation to the Sherman lab for their assistance performing the studies described here. Specifically, we would like to thank Jessica Assadi, Ella Lamont, and David Sherman (PI). They provided consumable

resources we did not have access to for performing this approach, in addition to providing technical insight into library preparation for successful Mtb transcriptome sequencing.

Chapter 7. Concluding Remarks and Future Directions

Future Directions

This body of work reveals novel insights into how host genetic background and bacterial effector repertoires converge to shape the trajectory of *Mycobacterium tuberculosis* (Mtb) infection from its earliest moments (**Figure 7.1**). However, this work also surfaces new, pressing questions that warrant further investigation. One major area of opportunity lies in the upstream determinants of the distinct alveolar macrophage (AM) responses observed between individuals with tuberculosis infection (LTBI) and those categorized as resisters (RSTR). While prior work focused largely on peripheral blood monocytes, our data demonstrate that AMs carry distinct, potentially pre-programmed transcriptional profiles in RSTR individuals, which become even more divergent upon Mtb exposure. Notably, RSTR AMs show robust activation of inflammatory gene sets including TNF, IL-1β, and ROS-generating pathways, alongside enhanced responsiveness to IFNγ and IFNα. Future functional studies including restriction assays and cytokine response profiling will be essential to determine whether these differences drive measurable response differences on a donor-by-donor basis.

On the bacterial side, our work underscores the importance of subtle genetic elements, specifically the ESX-5 paralog clusters, in modulating macrophage response. While deletion of individual paralogs does not impair bacterial replication in vitro, these strains elicit a significantly attenuated cytokine response from macrophages, specifically reducing levels of IL-6, TNF, and IL-1β. Intriguingly, this reduction is not observed at the

level of transcription, pointing to a post-transcriptional or translational bottleneck in cytokine production. Future experiments further resolving the underpinning cellular mechanisms responsible could prove valuable for future therapeutic host-directed targets for modulating disease, improving outcomes. By extension, our in vivo experiments suggest that ESX-5 paralog deletions confer a transient fitness cost to Mtb early during infection. In C57BL/6 mice, we observed significantly reduced bacterial burdens at day 17 post-infection, particularly in the lung. This in vivo observation suggests there may be ESX-5-host interaction axes we can target using both bacterial and host directed therapeutics to enhance host control of infection. A more complete, temporal understanding of immune recruitment alongside specific cellular and cytokine responses in vivo could prove to be a highly valuable future direction to query. Specifically, assessing neutrophil recruitment, cytokine milieu, and lymphocyte effector functions may shed light on how the immune system's initial response to these mutants governs enhanced control early during infection.

Finally, we uncovered a novel and compelling link between ESX-5 paralogs and bacterial response to heavy metal stress. Through transcriptomics and functional assays, we demonstrated that copper and cadmium can modulate ESX-5 paralog expression in wildtype Mtb, and that metal pre-exposure of bacteria enhances proinflammatory cytokine production in infected macrophages. This observation opens a new line of inquiry into the role of the ESX-5 system in bacterial nutrient acquisition and intracellular stress adaptation. The PE/PPE proteins secreted by ESX-5 have been increasingly implicated in nutrient homeostasis, and our data suggest a coordinated system where Mtb detects and responds to phagosomal metal intoxication by

modulating both nutrient scavenging and immune engagement. Future studies will need to determine whether these paralogs directly transport metals or simply co-regulate with metal efflux/import machinery.

Conclusions

Together, these findings highlight the nuance and complexity of Mtb infection. While we've known since the discovery of the TB bacillus how complex and challenging this organism is, molecular queries like this expose just how heterogeneous this infection can be. Through the interplay of host and bacterial genetics, spatial, and temporal heterogeneity, TB infection has revealed itself to be highly dynamic in which both sides modulate their behavior. We hope this highlights the essentiality of studying the pair together and the value of insights we can resolve in these lines of inquiry.

While this work has answered key questions, it has also raised many more. What is the full suite of host receptors and signaling nodes that respond to ESX-5 paralog expression? How do different human genotypes, including those related to IFN signaling, influence this response? Do ESX-5 paralogs function similarly in diverse clinical Mtb strains, or is their effect strain-specific? Can their expression be modulated therapeutically to enhance early immune recognition? Can the RSTR phenotype be induced in susceptible individuals via vaccines or airway-targeted immune modulation?

These open questions are a testament to the complexity of TB pathogenesis and to the importance of dissecting it at the molecular level. This dissertation offers one framework for how subtle genetic variation, both human and microbial, can meaningfully influence infection outcomes. As the global health community continues to pursue better TB diagnostics, vaccines, and therapies, studies like this offer an optimistic outlook: we possess the knowledge and technology to deeply dissect complicated interactions and generate meaningful insights, moving us closer to a world without TB.

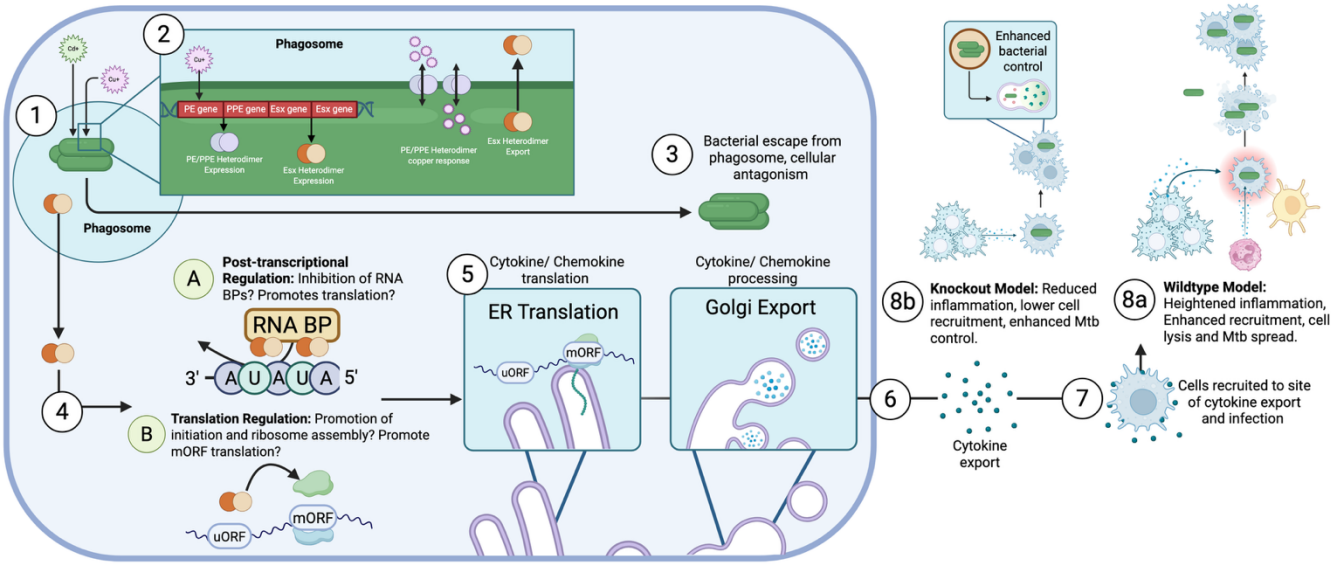

Figure 7.1 – Diagram conceptualizes the integration of our observations across experimental models and findings. Early on during infection Mtb is phagocytosed, initiating inflammatory and antimicrobial processes to respond to infection (1). Bacteria respond to phagosomal stress, including heavy metal intoxication, by upregulating stress response and virulence effectors such as the ESX-5 paralogs (2). Concurrently, Mtb escapes the phagosome and translocates to the cytosol while also releasing virulence effectors like the Esx heterodimers (3). The released Esx heterodimers then antagonize inflammatory regulatory processes such as RNA binding proteins or translation initiation inhibition to promote the translation of proinflammatory cytokines and chemokines (4A-4B, 5). Inflammatory markers are then exported where they recruit additional immune cells (6,7). Under wildtype infection, unrestricted cytokine induction leads to heightened inflammation, enhanced cellular recruitment and immunopathology, subsequent cell lysis and bacterial spread (8a). Conversely, mutant infection results in lower inflammatory cytokine output, damping cellular recruitment and inflammation resulting in enhanced Mtb control (8b). Created in BioRender. Altman, M. (2026) https://BioRender.com/3kkdwdd.

References

1. Chiaradia L, Lefebvre C, Parra J, Marcoux J, Burlet-Schiltz O, Etienne G, et al. Dissecting the mycobacterial cell envelope and defining the composition of the native mycomembrane. Sci Rep. 2017 Oct 9;7(1):12807.

2. Mycobacteria - an overview | ScienceDirect Topics [Internet]. 2021 [cited 2021 July 8]. Available from: https://www.sciencedirect.com/topics/immunology-and-microbiology/mycobacteria

3. Vilchèze C, Kremer L. Acid-Fast Positive and Acid-Fast Negative Mycobacterium tuberculosis: The Koch Paradox. Microbiol Spectr. 2017 Mar 24;5(2):10.1128/microbiolspec.tbtb2-0003–2015.

4. Honda JR, Virdi R, Chan ED. Global Environmental Nontuberculous Mycobacteria and Their Contemporaneous Man-Made and Natural Niches. Front Microbiol [Internet]. 2018 [cited 2021 July 8];9. Available from: https://www.frontiersin.org/articles/10.3389/fmicb.2018.02029/full#h4

5. Walsh CM, Gebert MJ, Delgado-Baquerizo M, Maestre FT, Fierer N. A Global Survey of Mycobacterial Diversity in Soil. Appl Environ Microbiol. 2021 July 8;85(17):e01180-19.

6. Meehan CJ, Barco RA, Loh YHE, Cogneau S, Rigouts L. Reconstituting the genus Mycobacterium. Int J Syst Evol Microbiol [Internet]. 2021 Oct 1 [cited 2025 May 8];71(9). Available from: https://www.microbiologyresearch.org/content/journal/ijsem/10.1099/ijsem.0.004922

7. Gagneux S. Ecology and evolution of Mycobacterium tuberculosis. Nat Rev Microbiol. 2018 Apr;16(4):202–13.

8. Comas I, Coscolla M, Luo T, Borrell S, Holt KE, Kato-Maeda M, et al. Out-of-Africa migration and Neolithic co-expansion of Mycobacterium tuberculosis with modern humans. Nat Genet. 2013 Oct;45(10):1176–82.

9. Barbier M, Wirth T. The Evolutionary History, Demography, and Spread of the Mycobacterium tuberculosis Complex. Microbiol Spectr. 2016 Aug 12;4(4):10.1128/microbiolspec.tbtb2-0008–2016.

10. Jia X, Yang L, Dong M, Chen S, Lv L, Cao D, et al. The Bioinformatics Analysis of Comparative Genomics of Mycobacterium tuberculosis Complex (MTBC) Provides Insight into Dissimilarities between Intraspecific Groups Differing in Host Association, Virulence, and Epitope Diversity. Front Cell Infect Microbiol [Internet]. 2017 Mar 21 [cited 2023 July 19];7. Available from: http://journal.frontiersin.org/article/10.3389/fcimb.2017.00088/full

11. Firdessa R, Berg S, Hailu E, Schelling E, Gumi B, Erenso G, et al. Mycobacterial Lineages Causing Pulmonary and Extrapulmonary Tuberculosis, Ethiopia. Emerg Infect Dis. 2013 Mar;19(3):460–3.

12. Coscolla M, Gagneux S, Menardo F, Loiseau C, Ruiz-Rodriguez P, Borrell S, et al. Phylogenomics of Mycobacterium africanum reveals a new lineage and a complex evolutionary history. Microb Genomics. 2021 Feb 8;7(2):000477.

13. Hershkovitz I, Donoghue HD, Minnikin DE, May H, Lee OYC, Feldman M, et al. Tuberculosis origin: The Neolithic scenario. Tuberculosis. 2015 June 1;95:S122–6.

14. Bottai D, Frigui W, Sayes F, Di Luca M, Spadoni D, Pawlik A, et al. TbD1 deletion as a driver of the evolutionary success of modern epidemic Mycobacterium tuberculosis lineages. Nat Commun. 2020 Dec;11(1):684.

15. Holt KE, McAdam P, Thai PVK, Thuong NTT, Ha DTM, Lan NN, et al. Frequent transmission of the Mycobacterium tuberculosis Beijing lineage and positive selection for the EsxW Beijing variant in Vietnam. Nat Genet. 2018 June;50(6):849–56.

16. McHenry ML, Bartlett J, Igo RP, Wampande EM, Benchek P, Mayanja-Kizza H, et al. Interaction between host genes and Mycobacterium tuberculosis lineage can affect tuberculosis severity: Evidence for coevolution? Schurr E, editor. PLOS Genet. 2020 Apr 30;16(4):e1008728.

17. Goletti D, Meintjes G, Andrade BB, Zumla A, Lee SS. Insights from the 2024 WHO Global Tuberculosis Report – More Comprehensive Action, Innovation, and Investments required for achieving WHO End TB goals. Int J Infect Dis [Internet]. 2025 Jan 1 [cited 2025 May 1];150. Available from: https://www.ijidonline.com/article/S1201-9712%2824%2900400-4/fulltext

18. Glaziou P, Sismanidis C, Floyd K, Raviglione M. Global Epidemiology of Tuberculosis. Cold Spring Harb Perspect Med. 2015 Feb;5(2):a017798.

19. Chakaya J, Khan M, Ntoumi F, Aklillu E, Fatima R, Mwaba P, et al. Global Tuberculosis Report 2020 – Reflections on the Global TB burden, treatment and prevention efforts. Int J Infect Dis. 2021 Dec;113:S7–12.

20. Tobin EH, Tristram D. Tuberculosis Overview. In: StatPearls [Internet]. Treasure Island (FL): StatPearls Publishing; 2025 [cited 2025 Aug 11]. Available from: http://www.ncbi.nlm.nih.gov/books/NBK441916/

21. Global Tuberculosis Report 2024. 1st ed. Geneva: World Health Organization; 2024. 1 p.

22. Lin PL, Flynn JL. Understanding Latent Tuberculosis: A Moving Target. J Immunol Baltim Md 1950. 2010 July 1;185(1):15–22.

23. Al Khatib A, Hassanein S, Almari M, Koubar M, Fakhreddine S. Tuberculosis morbidity and mortality during the COVID-19 pandemic: a life-threatening complex challenge. Front Cell Infect Microbiol. 2024 Oct 1;14:1423081.

24. Sun M, Phan JM, Kieswetter NS, Huang H, Yu KKQ, Smith MT, et al. Specific CD4+ T cell phenotypes associate with bacterial control in people who 'resist' infection with Mycobacterium tuberculosis. Nat Immunol. 2024 Aug;25(8):1411–21.

25. Simmons JD, Stein CM, Seshadri C, Campo M, Alter G, Fortune S, et al. Immunological mechanisms of human resistance to persistent Mycobacterium tuberculosis infection. Nat Rev Immunol. 2018 Sept;18(9):575–89.

26. Dill-McFarland KA, Simmons JD, Peterson GJ, Nguyen FK, Campo M, Benchek P, et al. Epigenetic programming of host lipid metabolism associated with resistance to TST/IGRA conversion after exposure to *Mycobacterium tuberculosis*. Oliveira PH, editor. mSystems. 2024 Sept 17;9(9):e00628-24.

27. Dallmann-Sauer M, Fava VM, Malherbe ST, MacDonald CE, Orlova M, Kroon EE, et al. Mycobacterium tuberculosis resisters despite HIV exhibit activated T cells and macrophages in their pulmonary alveoli. J Clin Invest [Internet]. 2025 Jan 21 [cited 2025 Mar 12]; Available from: http://www.jci.org/articles/view/188016

28. Gutierrez J, Kroon EE, Möller M, Stein CM. Phenotype Definition for "Resisters" to Mycobacterium tuberculosis Infection in the Literature—A Review and Recommendations. Front Immunol. 2021 Feb 25;12:619988.

29. Stein CM, Nsereko M, Malone LL, Okware B, Kisingo H, Nalukwago S, et al. Long-term Stability of Resistance to Latent Mycobacterium tuberculosis Infection in Highly Exposed Tuberculosis Household Contacts in Kampala, Uganda. Clin Infect Dis. 2019 May 2;68(10):1705–12.

30. Stein CM, Zalwango S, Malone LL, Thiel B, Mupere E, Nsereko M, et al. Resistance and Susceptibility to Mycobacterium tuberculosis Infection and Disease in Tuberculosis Households in Kampala, Uganda. Am J Epidemiol. 2018 July 1;187(7):1477–89.

31. Chandra P, Grigsby SJ, Philips JA. Immune evasion and provocation by Mycobacterium tuberculosis. Nat Rev Microbiol. 2022 Dec;20(12):750–66.

32. Pal R, Bisht MK, Mukhopadhyay S. Secretory proteins of *Mycobacterium tuberculosis* and their roles in modulation of host immune responses: focus on therapeutic targets. FEBS J. 2022 July;289(14):4146–71.

33. Saelens JW, Viswanathan G, Tobin DM. Mycobacterial Evolution Intersects With Host Tolerance. Front Immunol. 2019 Mar 22;10:528.

34. Gagneux S. Ecology and evolution of Mycobacterium tuberculosis. Nat Rev Microbiol. 2018 Apr;16(4):202–13.

35. McHenry ML, Bartlett J, Igo RP, Wampande EM, Benchek P, Mayanja-Kizza H, et al. Interaction between host genes and Mycobacterium tuberculosis lineage can affect tuberculosis severity: Evidence for coevolution? Schurr E, editor. PLOS Genet. 2020 Apr 30;16(4):e1008728.

36. Zhang Y, Zhou G, Shi W, Shi W, Hu M, Kong D, et al. Comparing the diagnostic performance of QuantiFERON-TB Gold Plus with QFT-GIT, T-SPOT.TB and TST: a systematic review and meta-analysis. BMC Infect Dis. 2023 Jan 20;23(1):40.

37. Simmons JD, Dill-McFarland KA, Stein CM, Van PT, Chihota V, Ntshiqa T, et al. Monocyte Transcriptional Responses to Mycobacterium tuberculosis Associate with Resistance to Tuberculin Skin Test and Interferon Gamma Release Assay Conversion. D'Orazio SEF, editor. mSphere. 2022 June 29;7(3):e00159-22.

38. Cross DL, Layton ED, Yu KKQ, Smith MT, Aguilar MS, Li S, et al. MR1-restricted T cell clonotypes are associated with "resistance" to Mycobacterium tuberculosis infection. JCI Insight. 2024 May 8;9(9):e166505.

39. Setiabudiawan TP, Apriani L, Verrall AJ, Utami F, Schneider M, Indrati AR, et al. Immune correlates of early clearance of Mycobacterium tuberculosis among tuberculosis household contacts in Indonesia. Nat Commun. 2025 Jan 2;16(1):309.

40. Weiner J, Domaszewska T, Donkor S, Kaufmann SHE, Hill PC, Sutherland JS. Changes in Transcript, Metabolite, and Antibody Reactivity During the Early Protective Immune Response in Humans to Mycobacterium tuberculosis Infection. Clin Infect Dis. 2020 June 24;71(1):30–40.

41. McHenry ML, Benchek P, Malone L, Nsereko M, Mayanja-Kizza H, Boom WH, et al. Resistance to TST/IGRA conversion in Uganda: Heritability and Genome-Wide Association Study. eBioMedicine. 2021 Dec;74:103727.

42. Hong H, Dill-McFarland KA, Simmons JD, Peterson GJ, Benchek P, Mayanja-Kizza H, et al. Mycobacterium tuberculosis-dependent monocyte expression quantitative trait loci, cytokine production, and TB pathogenesis. Front Immunol. 2024 Mar 7;15:1359178.

43. Treatment of Tuberculosis American Thoracic Society, CDC, and Infectious Diseases Society of America [Internet]. [cited 2025 May 9]. Available from: https://www.cdc.gov/mmwr/preview/mmwrhtml/rr5211a1.htm#tab16

44. CDC. Tuberculosis (TB). 2025 [cited 2025 July 29]. Treatment for Drug-Susceptible Tuberculosis Disease. Available from: https://www.cdc.gov/tb/hcp/treatment/tuberculosis-disease.html

45. Saukkonen JJ, Duarte R, Munsiff SS, Winston CA, Mammen MJ, Abubakar I, et al. Updates on the Treatment of Drug-Susceptible and Drug-Resistant Tuberculosis: An Official ATS/CDC/ERS/IDSA Clinical Practice Guideline. Am J Respir Crit Care Med. 2025 Jan;211(1):15–33.

46. Sotgiu G, Centis R, D'ambrosio L, Migliori GB. Tuberculosis Treatment and Drug Regimens. Cold Spring Harb Perspect Med. 2015 May 1;5(5):a017822–a017822.

47. Andersen P, Doherty TM. The success and failure of BCG — implications for a novel tuberculosis vaccine. Nat Rev Microbiol. 2005 Aug;3(8):656–62.

48. Brandt L, Feino Cunha J, Weinreich Olsen A, Chilima B, Hirsch P, Appelberg R, et al. Failure of the Mycobacterium bovis BCG Vaccine: Some Species of Environmental Mycobacteria Block Multiplication of BCG and Induction of Protective Immunity to Tuberculosis. Infect Immun. 2002 Feb;70(2):672–8.

49. Bukula L, Chengalroyen MD, Omollo C, Moseki RM. Factors influencing the efficacy of Bacille Calmette-Guérin (BCG) vaccine. The Microbe. 2025 Mar 1;6:100230.

50. Carpenter SM, Boom WH. To BCG or Not Two BCG. N Engl J Med. 2025 May 7;392(18):1860–2.

51. Fine PEM. Variation in protection by BCG: implications of and for heterologous immunity. The Lancet. 1995 Nov 18;346(8986):1339–45.

52. Hatherill M, Cobelens F. Infant BCG vaccination is beneficial, but not sufficient. Lancet Glob Health. 2022 Sept 1;10(9):e1220–1.

53. Martinez L, Cords O, Liu Q, Acuna-Villaorduna C, Bonnet M, Fox GJ, et al. Infant BCG vaccination and risk of pulmonary and extrapulmonary tuberculosis throughout the life course: a systematic review and individual participant data meta-analysis. Lancet Glob Health. 2022 Sept;10(9):e1307–16.

54. Randhawa AK, Shey MS, Keyser A, Peixoto B, Wells RD, de Kock M, et al. Association of Human TLR1 and TLR6 Deficiency with Altered Immune Responses to BCG Vaccination in South African Infants. Rubin EJ, editor. PLoS Pathog. 2011 Aug 11;7(8):e1002174.

55. O'Neill LAJ, Netea MG. BCG-induced trained immunity: can it offer protection against COVID-19? Nat Rev Immunol. 2020 June;20(6):335–7.

56. Schmidt AC, Fairlie L, Hellström E, Kany ALK, Middelkoop K, Naidoo K, et al. BCG Revaccination for the Prevention of Mycobacterium tuberculosis Infection. N Engl J Med. 2025 May 7;392(18):1789–800.

57. Bagcchi S. WHO's Global Tuberculosis Report 2022. Lancet Microbe. 2023 Jan;4(1):e20.

58. The end TB strategy [Internet]. [cited 2025 May 9]. Available from: https://www.who.int/publications/i/item/WHO-HTM-TB-2015.19

59. Gunsaru V, Henrion MYR, McQuaid CF. The impact of the COVID-19 pandemic on tuberculosis treatment outcomes in 49 high burden countries. BMC Med. 2024 July 29;22(1):312.

60. Kyu HH, Ledesma JR. What is the impact of the COVID-19 pandemic on tuberculosis? Lancet Glob Health. 2023 Sept 1;11(9):e1323–4.

61. Dartois VA, Rubin EJ. Anti-tuberculosis treatment strategies and drug development: challenges and priorities. Nat Rev Microbiol. 2022 Nov;20(11):685–701.

62. Lai R, Ogunsola AF, Rakib T, Behar SM. Key advances in vaccine development for tuberculosis—success and challenges. Npj Vaccines. 2023 Oct 13;8(1):1–10.

63. Zhuang L, Ye Z, Li L, Yang L, Gong W. Next-Generation TB Vaccines: Progress, Challenges, and Prospects. Vaccines. 2023 July 31;11(8):1304.

64. Cohen SB, Gern BH, Delahaye JL, Adams KN, Plumlee CR, Winkler JK, et al. Alveolar Macrophages Provide an Early Mycobacterium tuberculosis Niche and Initiate Dissemination. Cell Host Microbe. 2018 Sept;24(3):439-446.e4.

65. Thiel BA, Worodria W, Nalukwago S, Nsereko M, Sanyu I, Rejani L, et al. Immune cells in bronchoalveolar lavage fluid of Ugandan adults who resist versus those who develop latent Mycobacterium tuberculosis infection. Subbian S, editor. PLOS ONE. 2021 Apr 9;16(4):e0249477.

66. Sikkema L, Ramírez-Suástegui C, Strobl DC, Gillett TE, Zappia L, Madissoon E, et al. An integrated cell atlas of the lung in health and disease. Nat Med. 2023 June;29(6):1563–77.

67. Stanzel F. Bronchoalveolar Lavage. Princ Pract Interv Pulmonol. 2012 May 22;165–76.

68. Balcewicz-Sablinska MK, Keane J, Kornfeld H, Remold HG. Pathogenic Mycobacterium tuberculosis Evades Apoptosis of Host Macrophages by Release of TNF-R2, Resulting in Inactivation of TNF-α1. J Immunol. 1998 Sept 1;161(5):2636–41.

69. Malainou C, Abdin SM, Lachmann N, Matt U, Herold S. Alveolar macrophages in tissue homeostasis, inflammation, and infection: evolving concepts of therapeutic targeting. J Clin Invest. 2023 Oct 2;133(19):e170501.

70. Huang L, Nazarova EV, Tan S, Liu Y, Russell DG. Growth of *Mycobacterium tuberculosis* in vivo segregates with host macrophage metabolism and ontogeny. J Exp Med. 2018 Apr 2;215(4):1135–52.

71. Rothchild AC, Olson GS, Nemeth J, Amon LM, Mai D, Gold ES, et al. Alveolar macrophages generate a noncanonical NRF2-driven transcriptional response *to Mycobacterium tuberculosis* in vivo. Sci Immunol. 2019 July 5;4(37):eaaw6693.

72. Matucci A, Maggi E, Vultaggio A. Cellular and Humoral Immune Responses During Tuberculosis Infection: Useful Knowledge in the Era of Biological Agents. J Rheumatol Suppl. 2014 May 1;91:17–23.

73. Cooper AM, Dalton DK, Stewart TA, Griffin JP, Russell DG, Orme IM. Disseminated tuberculosis in interferon gamma gene-disrupted mice. J Exp Med. 1993 Dec 1;178(6):2243–7.

74. Campo M, Dill-McFarland KA, Peterson GJ, Benson B, Skerrett SJ, Hawn TR. Human Alveolar and Monocyte-Derived Human Macrophage Responses to *Mycobacterium tuberculosis*. J Immunol. 2024 July 15;213(2):161–9.

75. Flynn JL, Chan J, Triebold KJ, Dalton DK, Stewart TA, Bloom BR. An essential role for interferon gamma in resistance to Mycobacterium tuberculosis infection. J Exp Med. 1993 Dec 1;178(6):2249–54.

76. Silva Miranda M, Breiman A, Allain S, Deknuydt F, Altare F. The Tuberculous Granuloma: An Unsuccessful Host Defence Mechanism Providing a Safety Shelter for the Bacteria? Clin Dev Immunol. 2012;2012:139127.

77. Flynn JL, Chan J, Lin PL. Macrophages and control of granulomatous inflammation in tuberculosis. Mucosal Immunol. 2011 May;4(3):271–8.

78. Shaler CR, Horvath C, Jeyanathan M, Xing Z. Within the Enemy's Camp: contribution of the granuloma to the dissemination, persistence and transmission of Mycobacterium tuberculosis. Front Immunol [Internet]. 2013 Feb 14 [cited 2025 May 9];4. Available from: https://www.frontiersin.orghttps://www.frontiersin.org/journals/immunology/articles/10.3389/fimmu.2013.00030/full

79. Rubin EJ. The Granuloma in Tuberculosis — Friend or Foe? N Engl J Med. 2009 June 4;360(23):2471–3.

80. Qualls JE, Murray PJ. Immunometabolism within the tuberculosis granuloma: amino acids, hypoxia, and cellular respiration. Semin Immunopathol. 2016 Mar;38(2):139–52.

81. Gern BH, Adams KN, Plumlee CR, Stoltzfus CR, Shehata L, Moguche AO, et al. TGFβ restricts expansion, survival, and function of T cells within the tuberculous granuloma. Cell Host Microbe. 2021 Apr 14;29(4):594-606.e6.

82. Gideon HP, Hughes TK, Tzouanas CN, Wadsworth MH, Tu AA, Gierahn TM, et al. Multimodal profiling of lung granulomas in macaques reveals cellular correlates of tuberculosis control. Immunity. 2022 May;55(5):827-846.e10.

83. Lin PL, Ford CB, Coleman MT, Myers AJ, Gawande R, Ioerger T, et al. Sterilization of granulomas is common in both active and latent tuberculosis despite extensive within-host variability in bacterial killing. Nat Med. 2014 Jan;20(1):75–9.

84. Reece ST, Kaufmann SH. Floating between the poles of pathology and protection: can we pin down the granuloma in tuberculosis? Curr Opin Microbiol. 2012 Feb;15(1):63–70.

85. Flynn JL, Chan J. Tuberculosis: Latency and Reactivation. Infect Immun. 2001 July;69(7):4195–201.

86. Dale KD, Karmakar M, Snow KJ, Menzies D, Trauer JM, Denholm JT. Quantifying the rates of late reactivation tuberculosis: a systematic review. Lancet Infect Dis. 2021 Oct 1;21(10):e303–17.

87. Correia-Neves M, Nigou J, Mousavian Z, Sundling C, Källenius G. Immunological hyporesponsiveness in tuberculosis: The role of mycobacterial glycolipids. Front Immunol [Internet]. 2022 Dec 2 [cited 2025 June 6];13. Available from: https://www.frontiersin.org/journals/immunology/articles/10.3389/fimmu.2022.1035122/full

88. Rodriguez-Rodriguez L, Gillet L, Machiels B. Shaping of the alveolar landscape by respiratory infections and long-term consequences for lung immunity. Front Immunol [Internet]. 2023 Apr 4 [cited 2025 June 6];14. Available from: https://www.frontiersin.org/journals/immunology/articles/10.3389/fimmu.2023.1149015/full

89. Chandra P, Grigsby SJ, Philips JA. Immune evasion and provocation by Mycobacterium tuberculosis. Nat Rev Microbiol. 2022 Dec;20(12):750–66.

90. Chai Q, Wang L, Liu CH, Ge B. New insights into the evasion of host innate immunity by Mycobacterium tuberculosis. Cell Mol Immunol. 2020 Sept;17(9):901–13.

91. Fernandez-Soto P, Bruce AJE, Fielding AJ, Cavet JS, Tabernero L. Mechanism of catalysis and inhibition of Mycobacterium tuberculosis SapM, implications for the development of novel antivirulence drugs. Sci Rep. 2019 Dec;9(1):10315.

92. Wong D, Bach H, Sun J, Hmama Z, Av-Gay Y. *Mycobacterium tuberculosis* protein tyrosine phosphatase (PtpA) excludes host vacuolar-H^+–ATPase to inhibit phagosome acidification. Proc Natl Acad Sci. 2011 Nov 29;108(48):19371–6.

93. Izquierdo Lafuente B, Ummels R, Kuijl C, Bitter W, Speer A. Mycobacterium tuberculosis Toxin CpnT Is an ESX-5 Substrate and Requires Three Type VII Secretion Systems for Intracellular Secretion. mBio. 2021 Apr 27;12(2):e02983-20.

94. Pajuelo D, Tak U, Zhang L, Danilchanka O, Tischler AD, Niederweis M. Toxin secretion and trafficking by Mycobacterium tuberculosis. Nat Commun. 2021 Dec;12(1):6592.

95. Quigley J, Hughitt VK, Velikovsky CA, Mariuzza RA, El-Sayed NM, Briken V. The Cell Wall Lipid PDIM Contributes to Phagosomal Escape and Host Cell Exit of *Mycobacterium tuberculosis*. Kaufmann SHE, editor. mBio. 2017 May 3;8(2):e00148-17.

96. Bao Y, Wang L, Sun J. A Small Protein but with Diverse Roles: A Review of EsxA in Mycobacterium–Host Interaction. Cells. 2021 June 30;10(7):1645.

97. Osman MM, Shanahan JK, Chu F, Takaki KK, Pinckert ML, Pagán AJ, et al. The C terminus of the mycobacterium ESX-1 secretion system substrate ESAT-6 is required for phagosomal membrane damage and virulence. Proc Natl Acad Sci. 2022 Mar 15;119(11):e2122161119.

98. Trivedi A, Gosai J, Nakane D, Shrivastava A. Design Principles of the Rotary Type 9 Secretion System. Front Microbiol. 2022 May 10;13:845563.

99. Green ER, Mecsas J. Bacterial Secretion Systems: An Overview. Microbiol Spectr. 2016 Feb 26;4(1):10.1128/microbiolspec.vmbf-0012–2015.

100. Miller BK, Zulauf KE, Braunstein M. The Sec Pathways and Exportomes of Mycobacterium tuberculosis. Microbiol Spectr. 2017 Apr 7;5(2):10.1128/microbiolspec.tbtb2-0013–2016.

101. Rivera-Calzada A, Famelis N, Llorca O, Geibel S. Type VII secretion systems: structure, functions and transport models. Nat Rev Microbiol. 2021 Sept;19(9):567–84.

102. Famelis N, Geibel S, Tol D van. Mycobacterial type VII secretion systems. Biol Chem. 2023 June 1;404(7):691–702.

103. Bunduc CM, Fahrenkamp D, Wald J, Ummels R, Bitter W, Houben ENG, et al. Structure and dynamics of a mycobacterial type VII secretion system. Nature. 2021 May 20;593(7859):445–8.

104. Newton-Foot M, Warren RM, Sampson SL, van Helden PD, Gey van Pittius NC. The plasmid-mediated evolution of the mycobacterial ESX (Type VII) secretion systems. BMC Evol Biol. 2016 Mar 15;16(1):62.

105. Coros A, Callahan B, Battaglioli E, Derbyshire KM. The Specialized secretory apparatus ESX-1 is essential for DNA transfer in Mycobacterium smegmatis. Mol Microbiol. 2008 Aug;69(4):794–808.

106. Gey van Pittius NC, Gamieldien J, Hide W, Brown GD, Siezen RJ, Beyers AD. The ESAT-6 gene cluster of Mycobacterium tuberculosis and other high G+C Gram-positive bacteria. Genome Biol. 2001 Sept 19;2(10):research0044.1.

107. Houben ENG, Korotkov KV, Bitter W. Take five — Type VII secretion systems of *Mycobacteria*. Biochim Biophys Acta BBA - Mol Cell Res. 2014 Aug 1;1843(8):1707–16.

108. Gröschel MI, Sayes F, Simeone R, Majlessi L, Brosch R. ESX secretion systems: mycobacterial evolution to counter host immunity. Nat Rev Microbiol. 2016 Nov;14(11):677–91.

109. Tufariello JM, Chapman JR, Kerantzas CA, Wong KW, Vilchèze C, Jones CM, et al. Separable roles for Mycobacterium tuberculosis ESX-3 effectors in iron acquisition and virulence. Proc Natl Acad Sci U S A. 2016 Jan 19;113(3):E348–57.

110. Qian J, Chen R, Wang H, Zhang X. Role of the PE/PPE Family in Host–Pathogen Interactions and Prospects for Anti-Tuberculosis Vaccine and Diagnostic Tool Design. Front Cell Infect Microbiol [Internet]. 2020 Nov 26 [cited 2025 June 4];10. Available from: https://www.frontiersin.org/journals/cellular-and-infection-microbiology/articles/10.3389/fcimb.2020.594288/full

111. Saelens JW, Sweeney MI, Viswanathan G, Xet-Mull AM, Jurcic Smith KL, Sisk DM, et al. An ancestral mycobacterial effector promotes dissemination of infection. Cell. 2022 Nov;S0092867422013617.

112. Ates LS, Sayes F, Frigui W, Ummels R, Damen MPM, Bottai D, et al. RD5-mediated lack of PE_PGRS and PPE-MPTR export in BCG vaccine strains results in strong reduction of antigenic repertoire but little impact on protection. PLOS Pathog. 2018 June 18;14(6):e1007139.

113. Ates LS, Ummels R, Commandeur S, van der Weerd R, Sparrius M, Weerdenburg E, et al. Essential Role of the ESX-5 Secretion System in Outer Membrane Permeability of Pathogenic Mycobacteria. Viollier PH, editor. PLOS Genet. 2015 May 4;11(5):e1005190.

114. Di Luca M, Bottai D, Batoni G, Orgeur M, Aulicino A, Counoupas C, et al. The ESX-5 Associated eccB5-eccC5 Locus Is Essential for Mycobacterium tuberculosis Viability. Manganelli R, editor. PLoS ONE. 2012 Dec 17;7(12):e52059.

115. Bottai D, Di Luca M, Majlessi L, Frigui W, Simeone R, Sayes F, et al. Disruption of the ESX-5 system of Mycobacterium tuberculosis causes loss of PPE protein secretion, reduction of cell wall integrity and strong attenuation: ESX-5 of M. tuberculosis. Mol Microbiol. 2012 Mar;83(6):1195–209.

116. Ates LS, van der Woude AD, Bestebroer J, van Stempvoort G, Musters RJP, Garcia-Vallejo JJ, et al. The ESX-5 System of Pathogenic Mycobacteria Is Involved In Capsule Integrity and Virulence through Its Substrate PPE10. Behr MA, editor. PLOS Pathog. 2016 June 9;12(6):e1005696.

117. Shah S, Cannon JR, Fenselau C, Briken V. A Duplicated ESAT-6 Region of ESX-5 Is Involved in Protein Export and Virulence of Mycobacteria. Infect Immun. 2015 Nov;83(11):4349–61.

118. Abdallah AM, Savage NDL, van Zon M, Wilson L, Vandenbroucke-Grauls CMJE, van der Wel NN, et al. The ESX-5 Secretion System of *Mycobacterium marinum* Modulates the Macrophage Response. J Immunol. 2008 Nov 15;181(10):7166–75.

119. Elliott SR, White DW, Tischler AD. Mycobacterium tuberculosis Requires Regulation of ESX-5 Secretion for Virulence in Irgm1-Deficient Mice. Ehrt S, editor. Infect Immun [Internet]. 2019 Feb [cited 2021 June 25];87(2). Available from: https://journals.asm.org/doi/10.1128/IAI.00660-18

120. Sayes F, Sun L, Di Luca M, Simeone R, Degaiffier N, Fiette L, et al. Strong Immunogenicity and Cross-Reactivity of Mycobacterium tuberculosis ESX-5 Type VII Secretion -Encoded PE-PPE Proteins Predicts Vaccine Potential. Cell Host Microbe. 2012 Apr;11(4):352–63.

121. Beckham KSH, Ciccarelli L, Bunduc CM, Mertens HDT, Ummels R, Lugmayr W, et al. Structure of the mycobacterial ESX-5 type VII secretion system membrane complex by single-particle analysis. Nat Microbiol. 2017 June;2(6):17047.

122. Ates LS, Dippenaar A, Ummels R, Piersma SR, Van Der Woude AD, Van Der Kuij K, et al. Mutations in ppe38 block PE_PGRS secretion and increase virulence of Mycobacterium tuberculosis. Nat Microbiol. 2018 Jan 15;3(2):181–8.

123. Shah S, Briken V. Modular Organization of the ESX-5 Secretion System in Mycobacterium tuberculosis. Front Cell Infect Microbiol. 2016;6:49.

124. Stylianou E, Pinpathomrat N, Sampson O, Richard A, Korompis M, McShane H. A five-antigen Esx-5a fusion delivered as a prime-boost regimen protects against M.tb challenge. Front Immunol. 2023 Oct 5;14:1263457.

125. Houben RMGJ, Dodd PJ. The Global Burden of Latent Tuberculosis Infection: A Re-estimation Using Mathematical Modelling. Metcalfe JZ, editor. PLOS Med. 2016 Oct 25;13(10):e1002152.

126. Global Tuberculosis Report 2023. Geneva: World Health Organization; 2023.

127. Chakaya J, Khan M, Ntoumi F, Aklillu E, Fatima R, Mwaba P, et al. Global Tuberculosis Report 2020 – Reflections on the Global TB burden, treatment and prevention efforts. Int J Infect Dis. 2021 Dec;113:S7–12.

128. Pai M, Behr MA, Dowdy D, Dheda K, Divangahi M, Boehme CC, et al. Tuberculosis. Nat Rev Dis Primer. 2016 Dec 22;2(1):16076.

129. Wong D, Bach H, Sun J, Hmama Z, Av-Gay Y. *Mycobacterium tuberculosis* protein tyrosine phosphatase (PtpA) excludes host vacuolar-H^+–ATPase to inhibit phagosome acidification. Proc Natl Acad Sci. 2011 Nov 29;108(48):19371–6.

130. Fernandez-Soto P, Bruce AJE, Fielding AJ, Cavet JS, Tabernero L. Mechanism of catalysis and inhibition of Mycobacterium tuberculosis SapM, implications for the development of novel antivirulence drugs. Sci Rep. 2019 Dec;9(1):10315.

131. Forrellad MA, Klepp LI, Gioffré A, Sabio y García J, Morbidoni HR, Santangelo M de la P, et al. Virulence factors of the Mycobacterium tuberculosis complex. Virulence. 2013 Jan 1;4(1):3–66.

132. Healy C, Golby P, MacHugh DE, Gordon SV. The MarR family transcription factor Rv1404 coordinates adaptation of Mycobacterium tuberculosis to acid stress via controlled expression of Rv1405c, a virulence-associated methyltransferase. Tuberculosis. 2016 Mar 1;97:154–62.

133. Osman MM, Shanahan JK, Chu F, Takaki KK, Pinckert ML, Pagán AJ, et al. The C terminus of the mycobacterium ESX-1 secretion system substrate ESAT-6 is required for phagosomal membrane damage and virulence. Proc Natl Acad Sci. 2022 Mar 15;119(11):e2122161119.

134. Smith I. Mycobacterium tuberculosis Pathogenesis and Molecular Determinants of Virulence. Clin Microbiol Rev. 2003 July;16(3):463–96.

135. Cohen SB, Gern BH, Delahaye JL, Adams KN, Plumlee CR, Winkler JK, et al. Alveolar Macrophages Provide an Early Mycobacterium tuberculosis Niche and Initiate Dissemination. Cell Host Microbe. 2018 Sept;24(3):439-446.e4.

136. Thiel BA, Worodria W, Nalukwago S, Nsereko M, Sanyu I, Rejani L, et al. Immune cells in bronchoalveolar lavage fluid of Ugandan adults who resist versus those who develop latent Mycobacterium tuberculosis infection. Subbian S, editor. PLOS ONE. 2021 Apr 9;16(4):e0249477.

137. Hussell T, Bell TJ. Alveolar macrophages: plasticity in a tissue-specific context. Nat Rev Immunol. 2014 Feb;14(2):81–93.

138. Morales-Nebreda L, Misharin AV, Perlman H, Budinger GRS. The heterogeneity of lung macrophages in the susceptibility to disease. Eur Respir Rev. 2015 Sept;24(137):505–9.

139. Malainou C, Abdin SM, Lachmann N, Matt U, Herold S. Alveolar macrophages in tissue homeostasis, inflammation, and infection: evolving concepts of therapeutic targeting. J Clin Invest. 2023 Oct 2;133(19):e170501.

140. Rothchild AC, Olson GS, Nemeth J, Amon LM, Mai D, Gold ES, et al. Alveolar macrophages generate a noncanonical NRF2-driven transcriptional response *to Mycobacterium tuberculosis* in vivo. Sci Immunol. 2019 July 5;4(37):eaaw6693.

141. Campo M, Dill-McFarland KA, Peterson GJ, Benson B, Skerrett SJ, Hawn TR. Human Alveolar and Monocyte-Derived Human Macrophage Responses to *Mycobacterium tuberculosis*. J Immunol. 2024 July 15;213(2):161–9.

142. Papp AC, Azad AK, Pietrzak M, Williams A, Handelman SK, Igo RP, et al. AmpliSeq transcriptome analysis of human alveolar and monocyte-derived macrophages over time in response to Mycobacterium tuberculosis infection. Neyrolles O, editor. PLOS ONE. 2018 May 30;13(5):e0198221.

143. Simmons JD, Van PT, Stein CM, Chihota V, Ntshiqa T, Maenetje P, et al. Monocyte metabolic transcriptional programs associate with resistance to tuberculin skin test/interferon-γ release assay conversion. J Clin Invest. 2021 July 15;131(14):e140073.

144. Ma N, Zalwango S, Malone LL, Nsereko M, Wampande EM, Thiel BA, et al. Clinical and epidemiological characteristics of individuals resistant to M. tuberculosis infection in a longitudinal TB household contact study in Kampala, Uganda. BMC Infect Dis. 2014 Dec;14(1):352.

145. Subramanian A, Tamayo P, Mootha VK, Mukherjee S, Ebert BL, Gillette MA, et al. Gene set enrichment analysis: A knowledge-based approach for interpreting genome-wide expression profiles. Proc Natl Acad Sci. 2005 Oct 25;102(43):15545–50.

146. Mubarak RA, Roberts N, Mason RJ, Alper S, Chu HW. Comparison of pro- and anti-inflammatory responses in paired human primary airway epithelial cells and alveolar macrophages. Respir Res. 2018 Dec;19(1):126.

147. Marino S, Sud D, Plessner H, Lin PL, Chan J, Flynn JL, et al. Differences in Reactivation of Tuberculosis Induced from Anti-TNF Treatments Are Based on Bioavailability in Granulomatous Tissue. Wodarz D, editor. PLoS Comput Biol. 2007 Oct 19;3(10):e194.

148. Kulsantiwong P, Pudla M, Srisaowakarn C, Boondit J, Utaisincharoen P. Pam2CSK4 and Pam3CSK4 induce iNOS expression via TBK1 and MyD88 molecules in mouse macrophage cell line RAW264.7. Inflamm Res. 2017 Oct;66(10):843–53.

149. Fang FC. Antimicrobial reactive oxygen and nitrogen species: concepts and controversies. Nat Rev Microbiol. 2004 Oct;2(10):820–32.

150. Desvignes L, Wolf AJ, Ernst JD. Dynamic Roles of Type I and Type II IFNs in Early Infection with *Mycobacterium tuberculosis*. J Immunol. 2012 June 15;188(12):6205–15.

151. Karimi Y, Giles EC, Vahedi F, Chew MV, Nham T, Loukov D, et al. IFN- **β** signalling regulates RAW 264.7 macrophage activation, cytokine production, and killing activity. Innate Immun. 2020 Apr;26(3):172–82.

152. Bohlen J, Zhou Q, Philippot Q, Ogishi M, Rinchai D, Nieminen T, et al. Human MCTS1-dependent translation of JAK2 is essential for IFN-γ immunity to mycobacteria. Cell. 2023 Nov;186(23):5114-5134.e27.

153. Cooper AM, Dalton DK, Stewart TA, Griffin JP, Russell DG, Orme IM. Disseminated tuberculosis in interferon gamma gene-disrupted mice. J Exp Med. 1993 Dec 1;178(6):2243–7.

154. Flynn JL, Chan J, Triebold KJ, Dalton DK, Stewart TA, Bloom BR. An essential role for interferon gamma in resistance to Mycobacterium tuberculosis infection. J Exp Med. 1993 Dec 1;178(6):2249–54.

155. Herbst S, Schaible UE, Schneider BE. Interferon Gamma Activated Macrophages Kill Mycobacteria by Nitric Oxide Induced Apoptosis. Tailleux L, editor. PLoS ONE. 2011 May 2;6(5):e19105.

156. Hoerter A, Petrucciani A, Bonifacio J, Arnett E, Schlesinger LS, Pienaar E. Timing matters in macrophage/CD4+ T cell interactions: an agent-based model comparing *Mycobacterium tuberculosis* host-pathogen interactions between latently infected and naïve individuals. Bartko A, editor. mSystems. 2025 Feb 7;e01290-24.

157. Thiel BA, Lundberg KC, Schlatzer D, Jarvela J, Li Q, Shaw R, et al. Human alveolar macrophages display marked hypo-responsiveness to IFN-γ in both proteomic and gene expression analysis. Barik S, editor. PLOS ONE. 2024 Feb 1;19(2):e0295312.

158. Meermeier EW, Zheng CL, Tran JG, Soma S, Worley AH, Weiss DI, et al. Human lung-resident mucosal-associated invariant T cells are abundant, express antimicrobial proteins, and are cytokine responsive. Commun Biol. 2022 Sept 9;5(1):942.

159. Jeong D, Woo YD, Chung DH. Invariant natural killer T cells in lung diseases. Exp Mol Med. 2023 Sept 11;55(9):1885–94.

160. Van Kaer L, Postoak JL, Song W, Wu L. Innate and Innate-like Effector Lymphocytes in Health and Disease. J Immunol. 2022 July 15;209(2):199–207.

161. Arkatkar T, Davé V, Cruz Talavera I, Graham JB, Swarts JL, Hughes SM, et al. Memory T cells possess an innate-like function in local protection from mucosal infection. J Clin Invest. 2023 May 15;133(10):e162800.

162. Borger JG, Lau M, Hibbs ML. The Influence of Innate Lymphoid Cells and Unconventional T Cells in Chronic Inflammatory Lung Disease. Front Immunol. 2019 July 11;10:1597.

163. Hsu AT, Gottschalk TA, Tsantikos E, Hibbs ML. The Role of Innate Lymphoid Cells in Chronic Respiratory Diseases. Front Immunol. 2021 Sept 22;12:733324.

164. DeGregori J, Leone G, Miron A, Jakoi L, Nevins JR. Distinct roles for E2F proteins in cell growth control and apoptosis. Proc Natl Acad Sci U S A. 1997 July 8;94(14):7245–50.

165. Ginsberg D. E2F1 pathways to apoptosis. FEBS Lett. 2002 Oct 2;529(1):122–5.

166. Iaquinta PJ, Lees JA. Life and death decisions by the E2F transcription factors. Curr Opin Cell Biol. 2007 Dec;19(6):649–57.

167. Gan H, Lee J, Ren F, Chen M, Kornfeld H, Remold HG. Mycobacterium tuberculosis blocks crosslinking of annexin-1 and apoptotic envelope formation on infected macrophages to maintain virulence. Nat Immunol. 2008 Oct;9(10):1189–97.

168. Butler RE, Brodin P, Jang J, Jang MS, Robertson BD, Gicquel B, et al. The Balance of Apoptotic and Necrotic Cell Death in Mycobacterium tuberculosis Infected Macrophages Is Not Dependent on Bacterial Virulence. Briken V, editor. PLoS ONE. 2012 Oct 30;7(10):e47573.

169. Toossi Z, Wu M, Rojas R, Kalsdorf B, Aung H, Hirsch CS, et al. Induction of Serine Protease Inhibitor 9 by Mycobacterium tuberculosis Inhibits Apoptosis and Promotes Survival of Infected Macrophages. J Infect Dis. 2012 Jan 1;205(1):144–51.

170. Gutierrez C, Somoskovi A. Human Pathogenic Mycobacteria. In: Reference Module in Biomedical Sciences [Internet]. Elsevier; 2014 [cited 2021 July 8]. Available from: https://www.sciencedirect.com/science/article/pii/B9780128012383001379

171. Pai M, Behr MA, Dowdy D, Dheda K, Divangahi M, Boehme CC, et al. Tuberculosis. Nat Rev Dis Primer. 2016 Dec 22;2(1):16076.

172. Kinchen JM, Ravichandran KS. Phagosome maturation: going through the acid test. Nat Rev Mol Cell Biol. 2008 Oct;9(10):781–95.

173. Sontyana B, Shrivastava R, Battu S, Ghosh S, Mukhopadhyay S. Phagosome maturation and modulation of macrophage effector function by intracellular pathogens: target for therapeutics. Future Microbiol. 2022 Jan;17(1):59–76.

174. Buter J, Cheng TY, Ghanem M, Grootemaat AE, Raman S, Feng X, et al. Mycobacterium tuberculosis releases an antacid that remodels phagosomes. Nat Chem Biol. 2019 Sept;15(9):889–99.

175. Tak U, Dokland T, Niederweis M. Pore-forming Esx proteins mediate toxin secretion by Mycobacterium tuberculosis. Nat Commun. 2021 Dec;12(1):394.

176. Chai Q, Yu S, Zhong Y, Lu Z, Qiu C, Yu Y, et al. A bacterial phospholipid phosphatase inhibits host pyroptosis by hijacking ubiquitin. Science. 2022 Oct 14;378(6616):eabq0132.

177. Forrellad MA, Klepp LI, Gioffré A, Sabio y García J, Morbidoni HR, Santangelo M de la P, et al. Virulence factors of the Mycobacterium tuberculosis complex. Virulence. 2013 Jan 1;4(1):3–66.

178. Feltcher ME, Sullivan JT, Braunstein M. Protein export systems of Mycobacterium tuberculosis: novel targets for drug development? Future Microbiol. 2010 Oct;5:1581–97.

179. Cole ST, Brosch R, Parkhill J, Garnier T, Churcher C, Harris D, et al. Deciphering the biology of Mycobacterium tuberculosis from the complete genome sequence. Nature. 1998 June;393(6685):537–44.

180. Stoop EJM, Bitter W, Sar AM van der. Tubercle bacilli rely on a type VII army for pathogenicity. Trends Microbiol. 2012 Oct 1;20(10):477–84.

181. Chen X, Cheng H fu, Zhou J, Chan C yeung, Lau K fai, Tsui SK wing, et al. Structural basis of the PE–PPE protein interaction in Mycobacterium tuberculosis. J Biol Chem. 2017 Oct 13;292(41):16880–90.

182. Pathak SK, Basu S, Basu KK, Banerjee A, Pathak S, Bhattacharyya A, et al. Direct extracellular interaction between the early secreted antigen ESAT-6 of Mycobacterium tuberculosis and TLR2 inhibits TLR signaling in macrophages. Nat Immunol. 2007 June;8(6):610–8.

183. Stanley SA, Johndrow JE, Manzanillo P, Cox JS. The Type I IFN Response to Infection with *Mycobacterium tuberculosis* Requires ESX-1-Mediated Secretion and Contributes to Pathogenesis. J Immunol. 2007 Mar 1;178(5):3143–52.

184. Abdallah AM, Verboom T, Weerdenburg EM, Gey van Pittius NC, Mahasha PW, Jiménez C, et al. PPE and PE_PGRS proteins of *Mycobacterium marinum* are transported via the type VII secretion system ESX-5. Mol Microbiol. 2009 Aug;73(3):329–40.

185. Bunduc CM, Ding Y, Kuijl C, Marlovits TC, Bitter W, Houben ENG. Reconstitution of a minimal ESX-5 type VII secretion system suggests a role for PPE proteins in the outer

membrane transport of proteins. Ellermeier CD, editor. mSphere. 2023 Oct 24;8(5):e00402-23.

186. De Maio F, Berisio R, Manganelli R, Delogu G. PE_PGRS proteins of Mycobacterium tuberculosis: A specialized molecular task force at the forefront of host–pathogen interaction. Virulence. 11(1):898–915.

187. Ates LS. New insights into the mycobacterial PE and PPE proteins provide a framework for future research. Mol Microbiol. 2020 Jan;113(1):4–21.

188. Wang Q, Boshoff HIM, Harrison JR, Ray PC, Green SR, Wyatt PG, et al. PE/PPE proteins mediate nutrient transport across the outer membrane of Mycobacterium tuberculosis. Science. 2020 Mar 6;367(6482):1147–51.

189. Dong D, Wang D, Li M, Wang H, Yu J, Wang C, et al. PPE38 Modulates the Innate Immune Response and Is Required for Mycobacterium marinum Virulence. Flynn JL, editor. Infect Immun. 2012 Jan;80(1):43–54.

190. Stylianou E, Harrington-Kandt R, Beglov J, Bull N, Pinpathomrat N, Swarbrick GM, et al. Identification and Evaluation of Novel Protective Antigens for the Development of a Candidate Tuberculosis Subunit Vaccine. Ehrt S, editor. Infect Immun. 2018 July;86(7):e00014-18.

191. Livak KJ, Schmittgen TD. Analysis of relative gene expression data using real-time quantitative PCR and the 2(-Delta Delta C(T)) Method. Methods San Diego Calif. 2001 Dec;25(4):402–8.

192. Joffe AM, Bakalar MH, Fletcher DA. Macrophage phagocytosis assay with reconstituted target particles. Nat Protoc. 2020 July;15(7):2230–46.

193. Baron L, Paatero AO, Morel JD, Impens F, Guenin-Macé L, Saint-Auret S, et al. Mycolactone subverts immunity by selectively blocking the Sec61 translocon. J Exp Med. 2016 Dec 12;213(13):2885–96.

194. Hall BS, Hill K, McKenna M, Ogbechi J, High S, Willis AE, et al. The Pathogenic Mechanism of the Mycobacterium ulcerans Virulence Factor, Mycolactone, Depends on Blockade of Protein Translocation into the ER. Deretic V, editor. PLoS Pathog. 2014 Apr 3;10(4):e1004061.

195. Hall BS, Hsieh LTH, Sacre S, Simmonds RE. The One That Got Away: How Macrophage-Derived IL-1β Escapes the Mycolactone-Dependent Sec61 Blockade in Buruli Ulcer. Front Immunol. 2022 Jan 26;12:788146.

196. Jiang P, Zhang Y, Ru B, Yang Y, Vu T, Paul R, et al. Systematic Investigation of Cytokine Signaling Activity at the Tissue and Single-Cell Level. Nat Methods. 2021 Oct;18(10):1181–91.

197. Hart PH, Vitti GF, Burgess DR, Whitty GA, Piccoli DS, Hamilton JA. Potential antiinflammatory effects of interleukin 4: suppression of human monocyte tumor necrosis factor alpha, interleukin 1, and prostaglandin E2. Proc Natl Acad Sci. 1989 May;86(10):3803–7.

198. Tokunaga R, Zhang W, Naseem M, Puccini A, Berger MD, Soni S, et al. CXCL9, CXCL10, CXCL11/CXCR3 axis for immune activation – A target for novel cancer therapy. Cancer Treat Rev. 2018 Feb 1;63:40–7.

199. Kawka M, Płocińska R, Płociński P, Pawełczyk J, Słomka M, Gatkowska J, et al. The functional response of human monocyte-derived macrophages to serum amyloid A and Mycobacterium tuberculosis infection. Front Immunol. 2023 Sept 15;14:1238132.

200. Nakamura A, Rampersaud YR, Sharma A, Lewis SJ, Wu B, Datta P, et al. Identification of microRNA-181a-5p and microRNA-4454 as mediators of facet cartilage degeneration. JCI Insight [Internet]. 2016 Aug 4 [cited 2025 May 15];1(12). Available from: https://insight.jci.org/articles/view/86820?utm_source=chatgpt.com#SEC2

201. Marino S, Sud D, Plessner H, Lin PL, Chan J, Flynn JL, et al. Differences in Reactivation of Tuberculosis Induced from Anti-TNF Treatments Are Based on Bioavailability in Granulomatous Tissue. Wodarz D, editor. PLoS Comput Biol. 2007 Oct 19;3(10):e194.

202. Martinez AN, Mehra S, Kaushal D. Role of Interleukin 6 in Innate Immunity to Mycobacterium tuberculosis Infection. J Infect Dis. 2013 Apr 15;207(8):1253–61.

203. Silvério D, Gonçalves R, Appelberg R, Saraiva M. Advances on the Role and Applications of Interleukin-1 in Tuberculosis. mBio. 12(6):e03134-21.

204. Beckwith KS, Beckwith MS, Ullmann S, Sætra RS, Kim H, Marstad A, et al. Plasma membrane damage causes NLRP3 activation and pyroptosis during Mycobacterium tuberculosis infection. Nat Commun. 2020 May 8;11(1):2270.

205. Abdallah AM, Bestebroer J, Savage NDL, de Punder K, van Zon M, Wilson L, et al. Mycobacterial Secretion Systems ESX-1 and ESX-5 Play Distinct Roles in Host Cell Death and Inflammasome Activation. J Immunol. 2011 Nov 1;187(9):4744–53.

206. Afriyie-Asante A, Dabla A, Dagenais A, Berton S, Smyth R, Sun J. Mycobacterium tuberculosis Exploits Focal Adhesion Kinase to Induce Necrotic Cell Death and Inhibit Reactive Oxygen Species Production. Front Immunol. 2021 Oct 20;12:742370.

207. Butler RE, Brodin P, Jang J, Jang MS, Robertson BD, Gicquel B, et al. The Balance of Apoptotic and Necrotic Cell Death in Mycobacterium tuberculosis Infected Macrophages Is Not Dependent on Bacterial Virulence. Briken V, editor. PLoS ONE. 2012 Oct 30;7(10):e47573.

208. Hornef MW, Wick MJ, Rhen M, Normark S. Bacterial strategies for overcoming host innate and adaptive immune responses. Nat Immunol. 2002 Nov;3(11):1033–40.

209. Gern BH, Klas JM, Foster KA, Cohen SB, Plumlee CR, Duffy FJ, et al. CD4-mediated immunity shapes neutrophil-driven tuberculous pathology. BioRxiv Prepr Serv Biol. 2024 Apr 15;2024.04.12.589315.

210. Chen S, Saeed AFUH, Liu Q, Jiang Q, Xu H, Xiao GG, et al. Macrophages in immunoregulation and therapeutics. Signal Transduct Target Ther. 2023 May 22;8(1):207.

211. Cook ME, Bradstreet TR, Webber AM, Kim J, Santeford A, Harris KM, et al. The ZFP36 family of RNA binding proteins regulates homeostatic and autoreactive T cell responses. Sci Immunol. 2022 Oct 28;7(76):eabo0981.

212. Otsuka H, Fukao A, Funakami Y, Duncan KE, Fujiwara T. Emerging Evidence of Translational Control by AU-Rich Element-Binding Proteins. Front Genet [Internet]. 2019 May 2 [cited 2025 July 21];10. Available from: https://www.frontiersin.org/journals/genetics/articles/10.3389/fgene.2019.00332/full

213. Zhong Z, Li Y, Sun Q, Chen D. Tiny but mighty: Diverse functions of uORFs that regulate gene expression. Comput Struct Biotechnol J. 2024 Dec;23:3771–9.

214. Mayer-Barber KD, Barber DL. Innate and Adaptive Cellular Immune Responses to Mycobacterium tuberculosis Infection. Cold Spring Harb Perspect Med. 2015 Dec;5(12):a018424.

215. Breschi A, Gingeras TR, Guigó R. Comparative transcriptomics in human and mouse. Nat Rev Genet. 2017 July;18(7):425–40.

216. Chanput W, Mes JJ, Wichers HJ. THP-1 cell line: An in vitro cell model for immune modulation approach. Int Immunopharmacol. 2014 Nov 1;23(1):37–45.

217. Clark R, Kupper T. Old Meets New: The Interaction Between Innate and Adaptive Immunity. J Invest Dermatol. 2005 Oct 1;125(4):629–37.

218. Pieters J. Mycobacterium tuberculosis and the Macrophage: Maintaining a Balance. Cell Host Microbe. 2008 June 12;3(6):399–407.

219. Co DO, Hogan LH, Il-Kim S, Sandor M. T cell contributions to the different phases of granuloma formation. Immunol Lett. 2004 Mar 29;92(1):135–42.

220. Cooper A. Role of innate cytokines in mycobacterial infection.

221. Hong H, Dill-McFarland KA, Simmons JD, Peterson GJ, Benchek P, Mayanja-Kizza H, et al. Mycobacterium tuberculosis-dependent monocyte expression quantitative trait loci, cytokine production, and TB pathogenesis. Front Immunol. 2024 Mar 7;15:1359178.

222. Urdahl KB, Liggitt D, Bevan MJ. CD8+ T Cells Accumulate in the Lungs of Mycobacterium tuberculosis-Infected Kb−/−Db−/− Mice, But Provide Minimal Protection 1. J Immunol. 2003 Feb 15;170(4):1987–94.

223. Cooper AM. Mouse Model of Tuberculosis. Cold Spring Harb Perspect Med. 2015 Feb;5(2):a018556.

224. Yeremeev V, Linge I, Kondratieva T, Apt A. Neutrophils exacerbate tuberculosis infection in genetically susceptible mice. Tuberculosis. 2015 July 1;95(4):447–51.

225. Eruslanov EB, Lyadova IV, Kondratieva TK, Majorov KB, Scheglov IV, Orlova MO, et al. Neutrophil Responses to Mycobacterium tuberculosis Infection in Genetically Susceptible and Resistant Mice. Infect Immun. 2005 Mar;73(3):1744–53.

226. De Filippo K, Henderson RB, Laschinger M, Hogg N. Neutrophil chemokines KC and macrophage-inflammatory protein-2 are newly synthesized by tissue macrophages using distinct TLR signaling pathways. J Immunol Baltim Md 1950. 2008 Mar 15;180(6):4308–15.

227. De Filippo K, Dudeck A, Hasenberg M, Nye E, van Rooijen N, Hartmann K, et al. Mast cell and macrophage chemokines CXCL1/CXCL2 control the early stage of neutrophil recruitment during tissue inflammation. Blood. 2013 June 13;121(24):4930–7.

228. Liu D, Mai D, Jahn AN, Murray TA, Aitchison JD, Gern BH, et al. APOE Protects Against Severe Infection with Mycobacterium tuberculosis by Restraining Production of Neutrophil Extracellular Traps. BioRxiv Prepr Serv Biol. 2024 Oct 4;2024.10.04.616580.

229. Guan N, Li J, Shin H dong, Du G, Chen J, Liu L. Microbial response to environmental stresses: from fundamental mechanisms to practical applications. Appl Microbiol Biotechnol. 2017 May 1;101(10):3991–4008.

230. Jacob-Dubuisson F, Mechaly A, Betton JM, Antoine R. Structural insights into the signalling mechanisms of two-component systems. Nat Rev Microbiol. 2018 Oct;16(10):585–93.

231. Frando A, Boradia V, Gritsenko M, Beltejar C, Day L, Sherman DR, et al. The Mycobacterium tuberculosis protein O-phosphorylation landscape. Nat Microbiol. 2023 Mar;8(3):548–61.

232. Wei W, Ho WC, Behringer MG, Miller SF, Bcharah G, Lynch M. Rapid evolution of mutation rate and spectrum in response to environmental and population-genetic challenges. Nat Commun. 2022 Aug 13;13(1):4752.

233. Saumaa S, Tarassova K, Tark M, Tover A, Tegova R, Kivisaar M. Involvement of DNA mismatch repair in stationary-phase mutagenesis during prolonged starvation of *Pseudomonas putida*. DNA Repair. 2006 Apr 8;5(4):505–14.

234. Nguyen D, Joshi-Datar A, Lepine F, Bauerle E, Olakanmi O, Beer K, et al. Active Starvation Responses Mediate Antibiotic Tolerance in Biofilms and Nutrient-Limited Bacteria. Science. 2011 Nov 18;334(6058):982–6.

235. Long H, Miller SF, Strauss C, Zhao C, Cheng L, Ye Z, et al. Antibiotic treatment enhances the genome-wide mutation rate of target cells. Proc Natl Acad Sci. 2016 May 3;113(18):E2498–505.

236. Charlesworth B. Stabilizing Selection, Purifying Selection, and Mutational Bias in Finite Populations. Genetics. 2013 Aug;194(4):955–71.

237. Basra P, Alsaadi A, Bernal-Astrain G, O'Sullivan ML, Hazlett B, Clarke LM, et al. Fitness Tradeoffs of Antibiotic Resistance in Extraintestinal Pathogenic Escherichia coli. Genome Biol Evol. 2018 Feb 7;10(2):667–79.

238. Phan K, Ferenci T. The fitness costs and trade-off shapes associated with the exclusion of nine antibiotics by OmpF porin channels. ISME J. 2017 June;11(6):1472–82.

239. Stahl C, Kubetzko S, Kaps I, Seeber S, Engelhardt H, Niederweis M. MspA provides the main hydrophilic pathway through the cell wall of Mycobacterium smegmatis. Mol Microbiol. 2001 Apr;40(2):451–64.

240. Boradia V, Frando A, Grundner C. The Mycobacterium tuberculosis PE15/PPE20 complex transports calcium across the outer membrane. PLOS Biol. 2022 Nov 28;20(11):e3001906.

241. Orgeur M, Sous C, Madacki J, Brosch R. Evolution and emergence of Mycobacterium tuberculosis. FEMS Microbiol Rev. 2024 Mar 1;48(2):fuae006.

242. Jacobo-Delgado YM, Rodríguez-Carlos A, Serrano CJ, Rivas-Santiago B. Mycobacterium tuberculosis cell-wall and antimicrobial peptides: a mission impossible? Front Immunol. 2023 May 17;14:1194923.

243. Culviner PH, Guegler CK, Laub MT. A Simple, Cost-Effective, and Robust Method for rRNA Depletion in RNA-Sequencing Studies. Cooper VS, editor. mBio. 2020 Apr 28;11(2):e00010-20.

244. Dill-McFarland K, Benson B, rmsegnitz. BIGslu/SEAsnake: v1.1 [Internet]. Zenodo; 2024 [cited 2025 June 22]. Available from: https://zenodo.org/records/11646755

245. Sheldon JR, Skaar EP. Metals as phagocyte antimicrobial effectors. Curr Opin Immunol. 2019 Oct;60:1–9.

246. Parish T. Two-Component Regulatory Systems of Mycobacteria. Microbiol Spectr. 2014 Jan 31;2(1):10.1128/microbiolspec.mgm2-0010–2013.